Imaging and therapy in multiple sclerosis

James William Lyle Brown

Peterhouse

University of Cambridge

December 2019

This dissertation is submitted for the degree of Doctor of Philosophy.

Personal Declaration

This dissertation is the result of my own work and includes nothing which is the outcome of work done in collaboration except as declared in the text under the Methods section of each project (p. 59-77).

It is not substantially the same as any that I have submitted, or, is being concurrently submitted for a degree or diploma or other qualification at the University of Cambridge or any other University or similar institution except as declared in the Preface and specified in the text. I further state that no substantial part of my dissertation has already been submitted, or, is being concurrently submitted for any such degree, diploma or other qualification at the University of Cambridge or any other University or similar institution except as declared in the Preface and specified in the text.

It does not exceed the prescribed word limit for the relevant Degree Committee.

Imaging and therapy in multiple sclerosis

James William Lyle Brown

Abstract

Multiple sclerosis (MS) is a common, debilitating autoimmune disorder of the central nervous system (CNS). The most visible element of MS pathology is white matter (WM) lesions. However, extra-lesional abnormalities are recognised and appear most marked at the outer (subpial) brain surfaces at post-mortem. Magnetisation transfer ratio (MTR) is a non-conventional MRI sequence that correlates with myelin density and axonal count, and has recently uncovered reductions in the innermost (periventricular) layers and outermost (cortical) layers of patients with longstanding MS. These abnormalities are termed "outside-in" changes. The cause, extent, evolution and treatment-responsiveness of these outside-in gradients is unknown.

Most patients present with relapsing-remitting (RR) MS for which numerous immunomodulatory disease-modifying therapies (DMTs) are licensed. However, after approximately 20 years most convert to secondary progressive (SP) MS where immunomodulatory therapies have little if any effect. Whether DMTs delay or prevent this transition remains unclear.

During this PhD I examined whether outside-in MTR gradients occur in different disease stages, their clinical associations and predictive capabilities, and (for periventricular gradients) their response to a potent immunomodulatory DMT. In a separate project, I used real-world data to explore whether DMT use is associated with a lower risk of conversion to SPMS.

Outside-in MTR gradients of tissue damage were seen in periventricular and cortical regions at all stages of relapse-onset MS and primary-progressive MS. The periventricular MTR gradient was reversed by peripheral immunomodulation and independently predicted subsequent relapse

activity on and off DMTs. The underlying process(es) remain unknown but appear at least partially distinct from those underlying lesion formation; a CSF-mediated process – secondary to meningeal inflammation or primarily degenerative – might explain both periventricular and cortical gradients.

Among patients with RRMS, initial treatment with fingolimod, natalizumab or alemtuzumab was associated with a lower risk of conversion to SPMS compared to initial treatment with glatiramer acetate or interferon beta over a median 5.8 years of follow-up. A lower risk of conversion was also associated with early (versus late) commencement of glatiramer acetate or interferon beta; and with early escalation from these therapies to fingolimod, natalizumab or alemtuzumab compared to late escalation. These findings, considered along with these therapies' risks, may help inform decisions about DMT selection.

For Claire

Supervisors

Alasdair Coles (Principal)

University of Cambridge

Declan Chard

University College London

Tomas Kalincik

University of Melbourne

Contents

Publications arising from PhD

Brown JW, Chard DT. The role of MRI in the evaluation of secondary progressive multiple sclerosis. Expert review of neurotherapeutics 2016; 16(2): 157-71.

Brown JW*, Pardini M*, Brownlee WJ, Fernando K, Samson RS, Prados Carrasco F, et al. An abnormal periventricular magnetization transfer ratio gradient occurs early in multiple sclerosis. Brain : a journal of neurology 2017; 140(Pt 2): 387-98.

Kalincik T, Brown JW, Robertson N, Willis M, Scolding N, Rice CM, et al. Treatment effectiveness of alemtuzumab compared with natalizumab, fingolimod, and interferon beta in relapsing-remitting multiple sclerosis: a cohort study. The Lancet Neurology 2017. 16(4): 271-81.

Brown JW*, Coles AJ*, Horakova D, Havrdova E, Izquierdo G, Prat A, et al. Association of initial disease-modifying therapy with later conversion to secondary progressive multiple sclerosis. JAMA 2019; 321(2): 175-87.

Brown JW*, Prados F*, Eshaghi A, Sudre C, Button T, Pardini M, et al. Periventricular magnetisation transfer ratio abnormalities in multiple sclerosis improve after alemtuzumab. Multiple Sclerosis Journal. [Accepted; In Press]

Brown JW*, Chowdhury A*, Kanber B, Prados F, Eshaghi A, Sudre C, et al. Magnetisation transfer ratio abnormalities in primary and secondary progressive multiple sclerosis. Multiple Sclerosis Journal. [Accepted; In Press] ** = Joint first author*

Foreword

I am interested in multiple sclerosis (MS). I use magnetic resonance imaging (MRI) to explore MS disease effects, particularly their differential regional variability, and – within the limitations of the tool – potential reasons behind this. More recently, I have become interested in using large-scale real-world data to examine associations between clinical outcomes and exposures, particularly disease-modifying therapies.

As an introduction, I will briefly examine our current understanding of the aetiology and pathogenesis of MS, and then discuss disease classification, diagnosis and therapeutic strategies. Next, the role of MRI and its contributions to disease understanding will be explored, with special emphasis placed on regional variation and potential explanations. This will lead into the key objectives for the thesis. The methods and results of each project will be presented in turn. The discussion incorporates separate sections for each project. However, as Projects 1-3 explore different facets of the same topic (regional variability in disease effects on MRI), the biological interpretation – and advances in the field contemporaneous to this PhD - have been apportioned an additional section of the Discussion. The fourth project explores a very different research question using a different tool. It does not seamlessly link to the previous projects but I felt it sufficiently important to include.

Chapter 1. Introduction

The aetiology and pathology of multiple sclerosis

The precise aetiology of MS is unknown, though it appears to be triggered by environmental factors in genetically susceptible individuals. Genetic variation accounts for about one third of the overall disease risk (Harkiolaki *et al.*, 2009; International Multiple Sclerosis Genetics *et al.*, 2013), yet identified loci account for only a quarter of this heritability - a further quarter is likely to reflect undiscovered risk alleles (Zuk *et al.*, 2012), and the remaining half from hitherto-undefined interactions between risk factors (International Multiple Sclerosis Genetics *et al.*, 2010).

The immunopathogenesis of multiple sclerosis

Immune system dysregulation outside the central nervous system

In health, the majority of autoreactive T cells are removed within the thymus as part of central tolerance. Some escape into the periphery, but peripheral tolerance mechanisms keep these cells at bay. In MS, reduced regulatory T-cell (T_{reg}) activity or effector T/B-cell resistance to suppressive mechanisms, causes peripheral autoreactive T cells to trigger CNS-directed autoreactive T/B cells to become aggressive effector cells (CD8+ T cells, differentiated CD4+ T helper (T_H1 and T_H17 cells), B cells and innate immune cells), which in turn infiltrate the CNS (Viglietta *et al.*, 2004).

Immune system dysregulation within the central nervous system

Peripheral lymphocytes and monocytes access the CNS through the blood-brain barrier (BBB) or blood-CSF barrier. The identification of veins/venules within MS plaques - first described by Charcot (1880), and shortly afterwards attributed to vascular inflammation by Babinski (1885) – can now be observed *in vivo* with clinical-grade MRI scanners (for example (Samaraweera *et al.*, 2017)). Plaques comprise perivascular inflammation dominated by CD8+ cell infiltrates, and cluster around the lateral ventricles, juxtacortical tissues, the infratentorial region, spinal cord and optic nerves. Inflammatory demyelination and neurodegeneration appear to result from multiple mechanisms: direct cytotoxicity of CD8-positive T cells directed against an antigen expressed on oligodendrocytes (Saxena *et al.*, 2008); activation of microglia by cytokines secreted from CD4 cells and subsequent microglial attack of the oligodendrocyte-myelin unit (for example (Zajicek *et al.*, 1992; Felts *et al.*, 2005)); and demyelinating antibody production (Linington *et al.*, 1988). Axonal injury within lesions is seen from the earliest clinical stage of the disease and correlates with the extent of T-cell and microglial infiltration (Ferguson *et al.*, 1997; Trapp *et al.*, 1998; Kuhlmann *et al.*, 2002). There is also evidence of inflammation, demyelination and neuroaxonal loss in the normal—appearing white matter (NAWM) and grey matter (NAGM) (Kutzelnigg *et al.*, 2005), including early in the disease course (Lucchinetti *et al.*, 2011).

The pathology of progressive multiple sclerosis

Inflammation and neurodegeneration are both present throughout the disease course. However, the inflammatory demyelinating processes that dominate the early disease course gradually yield to more neurodegenerative mechanisms and diffuse changes in later disease (Frischer *et al.*, 2009). Potential mechanisms underlying neuronal death in progressive disease - chronic oxidative injury, axonal mitochondrial damage, microglial activation and age-related iron-

accumulation – will be sequentially discussed, though the precise cascade and their interrelations remain unclear.

The most prominent pathological feature of progressive disease is brain atrophy (Bermel and Bakshi, 2006), although this is seen at the very earliest stages of the disease (Chard *et al.*, 2002). Atrophy reflects irreversible axonal and neuronal loss and occurs in both lesions and normal-appearing tissue (for example (Evangelou *et al.*, 2005)).

Degeneration of chronically demyelinated axons within lesions leads to shrinkage of lesions (even those with a border of advancing myelin and axonal destruction decrease in relative size (Kutzelnigg *et al.*, 2005)). The degree of axonal loss is clinically relevant: in the most disabled patients, chronic WM lesions have lost up to 70% of their axons (Bjartmar *et al.*, 2000). Mouse models suggest a degree of compensatory reserve: loss of less than 38% of spinal axons was not associated with permanent disability (Wujek *et al.*, 2002). Exhaustion of this axonal functional reserve – in combination with the below mechanisms - may represent a pathological tipping point culminating in the neurodegenerative cascade underlying progressive disease.

There is increasing evidence of abnormality in the NAWM and grey matter which worsen with disease duration. Cortical demyelination and diffuse NAWM axonal injury are predominantly seen in progressive disease and are accompanied by pronounced microglial activation (Kutzelnigg *et al.*, 2005). These appear at least partially distinct from the processes underlying lesion genesis: WM lesion load does not correlate with the extent of cortical demyelination, diffuse NAWM axonal injury nor cortical volume (De Stefano *et al.*, 2003; Kutzelnigg *et al.*, 2005). In the spinal cord - where atrophy has been reported in the absence of white matter plaques (Evangelou *et al.*, 2005) - the degree of axonal loss appears influenced by T-cell infiltration from the meninges (Androdias *et al.*, 2010). Taken together, these data point to one or more processes distinct from

lesion genesis causing clinically relevant tissue damage throughout the central nervous system. Potential processes are explored later.

While the overall extent of inflammation is clearly lower in progressive disease (Frischer *et al.*, 2009), there is increasing evidence of its presence and importance. For example, in progressive MS, neurodegeneration is only seen in patients with pronounced inflammation (quantified by levels of B-cells, T-cells, plasma-cells, HLA-D positive macrophages and microglia); while in very late progressive disease (where the degree of brain T-cell / B-cell infiltration matches age-matched controls) the rate of neurodegeneration in patients matches that seen in controls (Frischer *et al.*, 2009). The marked reduction (or absence) of contrast-enhancing lesions on MRI (indicating BBB breakdown) in progressive MS should also not be construed as a lack of inflammation: parenchymal and perivascular inflammation are still seen despite absent protein leakage from blood vessels (Hochmeister *et al.*, 2006), implying a 'trapped' inflammatory process, no longer reliant on peripheral inflammation, no longer indicated by contrast-enhancement on MRI and no-longer accessible to disease-modifying therapies that cannot cross the BBB (Mahad *et al.*, 2015).

Such compartmentalised inflammation is also seen in the meninges. Meningeal inflammation is reported in all stages of relapse-onset (Magliozzi *et al.*, 2010; Howell *et al.*, 2011; Lucchinetti *et al.*, 2011) and primary progressive (Choi *et al.*, 2012) MS, with the most severe form – lymph follicle-like structures – reported in a subset of SPMS patients with early-onset disease, rapid progression and early death (Magliozzi *et al.*, 2007). In PPMS (Choi *et al.*, 2012) and SPMS (Howell *et al.*, 2011), the degree of demyelination and neurodegeneration in cortical lesions directly correlates with the degree of meningeal inflammation. In fact, a gradient of cortical axonal loss was seen in the NAGM surrounding meningeal aggregates in the ~40% of SPMS patients found to have lymph follicle-like aggregates (Magliozzi *et al.*, 2010). This is discussed further on p. 51.

While the mechanisms underlying active demyelination and neuronal degeneration are varied in early disease (Lucchinetti *et al.*, 2000), they are invariably associated with microglial activation in progressive disease (Prineas *et al.*, 2001; Fischer *et al.*, 2013). However, as inflammation is a physiological process, microglial activation may simply reflect the inflammatory response to tissue damage (clearing up myelin debris for example), rather than an inflammatory driver itself resulting in oligodendrocyte or neuronal death. While disentangling these microglial functions is difficult, their presence in NAWM, WM lesions and normal appearing grey matter (NAGM) – where they express molecules involved in reactive oxygen species production – imply at least some destructive role (Prineas *et al.*, 2001; Gray *et al.*, 2008; Fischer *et al.*, 2012).

There is also growing interest in the role of mitochondria in MS progression, abnormalities of which have been found in progressive disease in the absence of meningeal inflammation (Campbell *et al.*, 2011). For multiple reasons – not the least difficulties in mitochondrial distribution resulting from the elongated shape of the neuron-axon unit – axons are highly susceptible to mitochondrial dysfunction. A cascade of events leading from mitochondrial dysfunction to axonal degeneration has been hypothesized: during the relapsing phase of MS, mitochondrial injury occurs through inflammation-induced dysfunction of cytochrome c oxidase-1 and mitochondrial DNA deletions in both WM and GM, culminating in energy deficiency. With increasing age and disease duration abnormal mitochondria in cell bodies of neurones are amplified and, when distributed around the axon, result in further energy deficiency and further production of reactive oxygen species which amplify oxidative injury (Mahad *et al.*, 2015). The resultant state of reduced oxygen consumption and energy failure despite normal blood and oxygen supply (known as histotoxic hypoxia) couple with the increased oxygen demands posed by perivascular inflammation such that – if this occurs in areas of lower blood flow (for example the boundary zones between cerebral arteries (watershed areas)) – the oxygen tension might

drop below a critical threshold (Davies *et al.*, 2013). This in turn may account for the increased density of WM lesions, demyelination and neurodegeneration in the watershed areas in progressive MS (Brownell and Hughes, 1962; Holland *et al.*, 2012; Haider *et al.*, 2016).

Iron builds up in the human brain with age and is stored (as the non-toxic Fe^{3+} form) in myelin, oligodendrocytes and microglia (Hallgren and Sourander, 1958). However, following their damage, iron is converted to the divalent – and highly toxic – Fe2+ form, which convert hydrogen peroxide into highly reactive hydroxyl molecules resulting in intensified oxidative injury (Hametner *et al.*, 2013).

The final major pathological change seen in progressive MS is failure of endogenous remyelination. Following inflammatory demyelination, lesions undergo varying degrees of endogenous remyelination (Schmierer *et al.*, 2004; Patrikios *et al.*, 2006; Patani *et al.*, 2007). This process has two principal benefits. First, it re-enables saltatory conduction (Smith *et al.*, 1979) facilitating improvement in symptoms and function after a relapse (Jeffery and Blakemore, 1997). Second, and arguably more importantly, remyelination protects the underlying axon, thereby reducing axonal loss. This assumption reflects an increasing body of evidence showing that myelin directly supports the underlying axon: myelinating glia sequester ineffective axonal organelles (Spencer and Thomas, 1974) and transfer trophic factors to the axon (Novotny, 1984; Kramer-Albers *et al.*, 2007); oligodendrocytes release growth factors for neurons *in-vitro* (Wilkins *et al.*, 2003); fast axonal transport is focally impaired beneath biochemically deficient myelin in a mouse model (Edgar *et al.*, 2004); and oligodendrocytes may exert a metabolic role through conveying glycolytic products to fuel oxidative phosphorylation (Nave, 2010) and even increase axonal calibre (Witt and Brady, 2000).

Endogenous remyelination does not seem to arise from existing oligodendrocytes; instead oligodendrocyte precursor cells (OPCs) divide, migrate and differentiate into myelinating

oligodendrocytes that ensheath the axons with new myelin (Franklin and Ffrench-Constant, 2008). Much effort has been channelled into identifying why endogenous remyelination fails in the hope that therapeutic manipulation might enhance remyelination and in so doing prevent axonal loss (De Stefano et al., 1998; Franklin, 2002; Franklin et al., 2012).

At post-mortem, OPCs are found within the majority of demyelinated lesions (Wolswijk, 1998; Chang *et al.*, 2002) suggesting that – in a large proportion of patients - the limiting step in endogenous remyelination is OPC differentiation (Franklin *et al.*, 2012). Much work has focused on the pathways regulating OPC differentiation into myelinating oligodendrocytes. These have been recently reviewed elsewhere (Kremer *et al.*, 2015) but include two negative regulators of OPC differentiation (LINGO-1(Mi *et al.*, 2005) and the Wnt signaling pathway (Fancy *et al.*, 2009)), inhibition of which have both been shown to promote remyelination in animal models of MS (Mi *et al.*, 2007; Preisner *et al.*, 2015). The retinoid acid receptor RXR-γ is a positive regulator of endogenous OPC differentiation, which, when stimulated, increased axonal remyelination in animal models (Huang *et al.*, 2011).

In a far smaller proportion of patients, endogenous remyelination failure reflects inadequate OPC recruitment to lesions (Niehaus *et al.*, 2000); in such situations the therapeutic promotion of endogenous OPC differentiation would be fruitless (Franklin, 2002), and exogenous therapy – transplantation of oligodendrocytes or OPCs – would ostensibly be more helpful. Distinguishing patients who would benefit from each therapeutic approach is a major unmet need, fore mostly necessitating the development and validation of in-vivo imaging markers of OPCs.

The aetiology of multiple sclerosis

Genetic predisposition

Numerous genome-wide association studies (GWAS) have uncovered more than 200 different loci associated with multiple sclerosis. These variants almost invariably implicate genes associated with immunological processes, are predominantly found in regulatory (non-coding) regions and often colocalise with gene enhancers or repressors in immune cells (International Multiple Sclerosis Genetics *et al.*, 2011; Farh *et al.*, 2015). Thirty-seven percent either influence the risk of other autoimmune diseases or are in linkage disequilibrium with other autoimmune-disease-associated variants (International Multiple Sclerosis Genetics *et al.*, 2011). The functional implications for most identified loci however remain unknown. We know most about HLA-DRB1*15:01 (the main risk allele for multiple sclerosis, odds ratio (OR) 3.10), the protective allele HLA-A*02:01 and the genes encoding IL-2Rα and IL-7Rα (Gregersen *et al.*, 2006; Gregory *et al.*, 2007; Friese *et al.*, 2008; International Multiple Sclerosis Genetics *et al.*, 2011; Hartmann *et al.*, 2014).

Despite this progress, MS genetics must be interpreted carefully. The HLA-DRB1*15:01 allele, for example, is present in 13.3% of the UK population (International Multiple Sclerosis Genetics *et al.*, 2011), yet less than 0.3% of people carrying it develop MS; and a significant number of patients without the allele will develop the disease. Further, genetic factors only account for a third of the overall disease risk (International Multiple Sclerosis Genetics *et al.*, 2013). Genetic risk factors should therefore be viewed as insufficient alone to cause multiple sclerosis but definitively contribute to the risk of its development.

Environmental factors

Numerous environmental and lifestyle factors increase the risk of MS including tobacco smoke exposure, Epstein-Barr virus (EBV) infection, low vitamin D levels, adolescent obesity and organic solvents. All environmental risk factors for MS can, like MS risk alleles, influence adaptive and / or innate immunity.

One of the most convincing arguments for the environment's role in MS centre around the latitude gradient. A recent meta-analysis of 321 peer-reviewed studies (Simpson *et al.*, 2011), found a positive association between latitude and the prevalence of MS (change in prevalence per degree 1.04, $p < 0.001$), which persisted after adjusting for HLA-DRB1 allele frequency. Perhaps most compellingly, individuals migrating from low to high risk areas before adolescence acquire the same high risk as those who are born and grow up in the high-risk area (Gale and Martyn, 1995).

The commonly reported risk factors are discussed below.

Smoking and organic solvents

Smoking tobacco results in a dose-dependent increase in the risk of (i) developing MS (Hernan *et al.*, 2001); (ii) developing neutralising antibodies against two of the most frequently used DMTs (natalizumab (Hedstrom *et al.*, 2014a) and interferon-beta (Hedstrom *et al.*, 2014c)); and (iii) a worse disease course (for example (Manouchehrinia *et al.*, 2013)), though this may be ameliorated through smoking cessation (for example, patients that quit smoking converted to SPMS 8 years later than in those that continued (Ramanujam *et al.*, 2015)).

EBV

Clinically-overt infectious mononucleosis carries more than a two-fold increase in the risk of developing MS (Martyn *et al.*, 1993), though this only appears the case with infection during adolescence, not childhood (Makhani *et al.*, 2016). The vast majority of patients with infectious mononucleosis do not, however, go on to develop MS. Markedly higher levels of antibodies against EBV nuclear antigen 1 (EBNA1) are found in patients with MS, and almost all EBNA1-negative individuals serologically convert to being EBNA1 positive prior to MS onset (Levin *et al.*, 2010). Infectious mononucleosis may act in synergy with HLA DRB1*15:01 to increase the risk of MS (Nielsen *et al.*, 2009); while the precise mechanisms are debated, molecular mimicry appears a prominent candidate.

Ultraviolet radiation and vitamin D

Both ultraviolet radiation exposure and vitamin D levels inversely correlate with the risk of MS (Lucas *et al.*, 2015). Production of the active metabolite of vitamin D requires ultraviolet radiation, so distinguishing the protective effect of each is challenging. Even so, both animal work and human studies appear to show that ultraviolet radiation confers a protective effect independent of vitamin D levels (Becklund *et al.*, 2010; Baarnhielm *et al.*, 2012). The mechanism however remains elusive. Animal models have shown reduced inflammation in the periphery (Rana *et al.*, 2011) and CNS (Becklund *et al.*, 2010) following ultraviolet radiation which appear to be mediated through increased T_{reg} activation.

Low vitamin D levels are associated with (i) a greater risk of developing MS (particularly low levels in childhood and adolescence (Munger *et al.*, 2006)); (ii) higher subsequent rates of relapses, new lesion accrual, lesion growth and disability accumulation when measured after a clinically isolated syndrome (Ascherio *et al.*, 2014); and (iii) increased neurofilament light chain levels in

the CSF, indicating greater axonal damage (Sandberg *et al.*, 2016). However, despite a reduction in lesion accrual on MRI (Soilu-Hanninen *et al.*, 2012) and increased oligodendrocyte production *in vitro* (de la Fuente *et al.*, 2015), vitamin D supplementation has thus far not led to improved clinical outcomes in small (n<100) clinical trials (Kampman *et al.*, 2012; Soilu-Hanninen *et al.*, 2012)), and larger studies (e.g. NCT01490502) are eagerly awaited. How vitamin D influences the development and activity of MS is not clear; however numerous effects that follow supplementation in humans – T_{reg} stimulation, for example (Muris *et al.*, 2016) – broadly point to improved immunomodulation.

Obesity

Adolescent obesity carries an adjusted two-fold risk of subsequently developing MS compared to a normal adolescent body mass index, though obesity at the time of onset has no influence (Hedstrom *et al.*, 2014b). The higher risk may reflect an interaction with HLA variants (particularly HLA-DRB1*15:01 and A*02 (Hedstrom *et al.*, 2014b)), release of pro-inflammatory mediators from the low-grade inflammation found in obesity (Lumeng *et al.*, 2007), elevated levels of the proinflammatory mediator leptin (Matarese *et al.*, 2005) and or decreased vitamin D bioavailability (Wortsman *et al.*, 2000).

Types of MS

About 85% of people with MS initially have relapsing-remitting (RR) disease (Confavreux *et al.*, 2000) characterised by acute or subacute episodes of neurological dysfunction (relapses) followed by at least partial resolution (remissions). The first such episode is termed a clinically isolated syndrome (CIS), and 63% of patients with a CIS will experience a further episode over 20 years (Fisniku *et al.*, 2008), thus realising the diagnosis clinically definite multiple sclerosis (CDMS). Eventually, most people with MS develop progressive disease: ~80% of people with CDMS will eventually accrue progressive neurological deficits (SPMS) and ~15% develop progressive impairments without ever having had relapses (known as primary progressive (PP) MS (Weinshenker *et al.*, 1989; Confavreux *et al.*, 2000; Kremenchutzky *et al.*, 2006). While incomplete recovery from relapses causes persistent neurological deficits, most disability accumulates in people with progressive disease (Confavreux *et al.*, 2000; Confavreux *et al.*, 2003). Once progression has started, its rate does not appear to be strongly influenced by previous relapses (Confavreux *et al.*, 2003).

Most literature on progressive MS reports on findings from people with SPMS. There is on-going debate about whether PPMS and SPMS are essentially the same disease or fundamentally different. For example the age at onset and rate of progression is similar in both (Gayou *et al.*, 1997; Confavreux *et al.*, 2000) but lesions appear to be less extensive and less inflammatory in PPMS compared with SPMS (Revesz *et al.*, 1994; Lucchinetti *et al.*, 2011). It should therefore not be assumed that findings in PPMS and SPMS are interchangeable.

Diagnosis and prognostication

Diagnosing and predicting RRMS

Attaining the diagnosis of RRMS requires evidence of dissemination in time and space (DIT and DIS), traditionally requiring, after the first episode, a further clinical episode reflecting an anatomically distinct region of the CNS (CDMS). Numerous revisions to diagnostic criteria have enabled earlier, more sensitive and more specific diagnosis (Brownlee *et al.*, 2017) through the use of paraclinical tests, particularly MRI. The 2010 revisions enable multiple sclerosis to be diagnosed after a single attack in the presence of radiological evidence of dissemination in time (simultaneous asymptomatic gadolinium-enhancing and unenhancing lesions on the same scan; or new T2 lesions on a follow-up scan) and dissemination in space (>1 T2 lesion in at least 2 MS-typical regions: periventricular, juxtacortical, infratentorial or spinal cord) (Polman *et al.*, 2011). Dissemination in space may also be achieved by examination findings suggesting a lesion in a region distinct to that of the CIS. In the most recent 2017 McDonald Criteria, dissemination in time may also be attained through the presence of CSF-specific oligoclonal bands; and cortical lesions may be used to demonstrate dissemination in space (Thompson *et al.*, 2017).

An MRI scan acquired soon after a CIS also provides significant prognostic information: the presence of asymptomatic WM lesions is associated with an ~80% risk of developing CDMS over the following 20 years, while in their absence the risk is ~20% (Fisniku *et al.*, 2008). It also has a well-defined role in clinical trials. In RRMS, WM lesion measures are now an accepted outcome measure in early phase immunomodulatory treatment trials (Sormani and Bruzzi, 2013), while in SPMS brain atrophy measures are increasingly used (for example (Kapoor *et al.*, 2010)).

Diagnosing and predicting SPMS

While the definition of SPMS is clear - "a history of gradual worsening after an initial relapsing disease course, with or without acute exacerbations" (Lublin *et al.*, 2014) - making the diagnosis is challenging. Clinical manifestations occur slowly, often requiring years of gradual deterioration for confident recognition by neurologists (Sand *et al.*, 2014). Relapses further complicate the situation in SPMS, and it can be very difficult to distinguish the residual effects of relapses from underlying symptom progression. Relapses are not unusual in people with SPMS: for example, in one recent treatment trial in SPMS about half those in the placebo arm had a relapse over the two years of the study (Hayton *et al.*, 2012). In contrast to PPMS, for which the current McDonald criteria require at least one year of disease progression (Thompson *et al.*, 2017), the guidelines contain no agreed criteria on the duration of disease progression necessary before a diagnosis of SPMS can be made. One study found that on average three years elapsed after the possibility of progressive disease was first raised before a confident diagnosis of SPMS was made (Sand *et al.*, 2014), and some recent SPMS treatment trials have required at least two years of progression as an inclusion criterion (Kapoor *et al.*, 2010; Chataway *et al.*, 2014). This uncertainty in clinical diagnosis means that studies looking for markers predicting the onset of SPMS, or recognizing it once it has begun, need to be sufficiently long-term for the diagnosis to be certain in the majority of cases. Fortunately, recent work has compared the performance of more than 500 potential definitions of SPMS, concluding that the best performing definition required an expanded disability status scale (EDSS) increase (if the EDSS score was 5.5 or less, an increase of 1 point was required; if the EDSS score was over 5.5 an increase of 0.5 points was required), in the absence of a relapse, achieving a minimum EDSS score of 4, with confirmation of EDSS progression at least 3 months later (Lorscheider *et al.*, 2016).

Given the difficulty in identifying the onset of SPMS, it is perhaps unsurprising that predicting the onset of SPMS is also challenging. The strongest clinical predictor for developing SPMS is the total disease duration - more than half of those with RRMS will have developed SPMS 15 years after symptom onset (Vukusic and Confavreux, 2003; Scalfari *et al.*, 2014) - but, this is impractical for short-term predictive purposes as there is a modest effect per year (odds ratio 1.07 for each additional year, p<0.001 (Scalfari *et al.*, 2014)). Males are also at greater risk of developing secondary progression (hazard ratio 1.41, p<0.001 (Scalfari *et al.*, 2014)), as are smokers (hazard ratio 1.49 (95% CI 1.18-1.86 (Manouchehrinia *et al.*, 2013))), although again these features do not allow reliable prediction of SPMS onset on an individual basis. The advent of an evidence-based, validated SPMS definition (Lorscheider *et al.*, 2016) might finally facilitate the robust examination of risk factors for conversion; and help answer the controversial question as to whether immunosuppressive drugs influence conversion to SPMS (Signori *et al.*, 2016).

Notwithstanding this, clinical measures are the standard against which any predictive measures (for example MRI) are compared. The most commonly used outcome measure is the EDSS, which ranges from 0 (normal neurological examination) to 10 (death due to MS) in 0.5 point increments (Kurtzke, 1983). However it has several significant limitations (Hobart *et al.*, 2000). First, while MS commonly affects motor, sensory and cognitive functions (Compston and Coles, 2002), EDSS scores above 3.5 are almost entirely determined by the person's walking ability. MRI measures that correlate with non-ambulatory functions may therefore be undervalued based on their association with EDSS scores (Meyer-Moock *et al.*, 2014). Secondly, the reproducibility of EDSS scores between assessors and over time is limited when compared with MRI measures such as brain atrophy (Noseworthy *et al.*, 1990) particularly at lower EDSS scores (Goodkin *et al.*, 1992), and this limits the maximum correlation possible between MRI measures and EDSS scores. This

might lead us to erroneously underestimate how clinically relevant an MRI measure is. Thirdly, the EDSS score is neither cardinal nor linear: a person with MS will tend to traverse some parts of the scale more rapidly than others (Weinshenker *et al.*, 1991). This means that correlations between EDSS scores and MRI measures may vary along the EDSS.

Other MS clinical measures have been developed to address these limitations, including the MS functional composite (MSFC) score (Fischer *et al.*, 1999). Rather than relying on the distance a person can walk, the MSFC combines measures of walking speed, arm function and cognitive performance, and scores are calculated relative to normative values. The MSFC may be more reproducible and sensitive to change than the EDSS (Cutter *et al.*, 1999; Meyer-Moock *et al.*, 2014), but by combining functions that may be unrelated within a single score, associations between specific clinical and MRI measures may be diluted. The MSFC is also vulnerable to learning effects, i.e. improved scores with practice (Meyer-Moock *et al.*, 2014). As such there is increasing interest in using multiple separate clinical outcome measures rather than composite functional scores.

The management of multiple sclerosis

Patients with MS should be managed in multi-disciplinary teams. The pharmacological management presently comprises three facets: (i) management of a relapse (for patients with relapse-onset disease); (ii) disease-modifying treatments; and (iii) symptomatic therapies.

Management of a relapse

In patients with RRMS or SPMS, a relapse may be indicated by the acute or subacute onset of new neurological symptoms or worsening or pre-existing symptoms. The clinician's first priority – particularly in the latter scenario – is to exclude a systemic illness that might mimic a relapse (termed a "pseudo-relapse"), for example fever from a urinary tract infection resulting in Uhthoff's phenomena. Then, if the symptoms are particularly disabling or unpleasant, a short course of corticosteroids (typically 0.5-1g oral or intravenous methylprednisolone for 3-5 days) is offered. Corticosteroids reduce the relapse duration but have no bearing on the extent of symptomatic improvement following a relapse nor future disease course (Miller *et al.*, 2000). Up to 42% of steroid-resistant relapses may improve with plasma exchange administered within 1 month of relapse onset, though this too has no bearing on future disease activity (Weinshenker *et al.*, 1999).

Disease modifying treatments (DMTs)

At the time of writing, 13 DMTs were licensed for patients with RRMS or a CIS internationally (Table 1). Comparisons of drug efficacy between trials is precluded by markedly different trial inclusion criteria and methodologies, particularly whether the comparator was placebo or an injectable therapy (interferon or glatiramer acetate). Many drug comparisons therefore rely on

meta-analyses, observational cohort studies and independent clinical trials. For example, rigorous examination of real-world data has identified similar effects on relapses between alemtuzumab and natalizumab, which both appear superior to fingolimod (Kalincik *et al.*, 2017a); and cladribine has shown similar efficacy to fingolimod but inferior efficacy to natalizumab (Kalincik *et al.*, 2017b). There is insufficient evidence to know whether DMT prescription should follow an escalation strategy (beginning with a moderate efficacy therapy with better safety profile then escalating to more effective (and toxic) therapies if required) or an induction strategy (beginning with a highly-effective therapy such as natalizumab). Comparisons of disability data are even more challenging due to multiple disability scales, differing definitions of worsening or improvement, variable durations of disability change required between studies and short trial durations (Brown and Chard, 2016). Perhaps more relevant than disability 'event'-driven outcomes is whether DMTs in RRMS have any bearing on (i) the timing of conversion to SPMS (where most disability accumulates); and (ii) the rate of disability accumulation after conversion to SPMS.

Generic name	Mechanism of action	Reduction in relapse rate*	Side effects
Interferon-ß-1a (5 preparations)	Reduced antigen presentation and T cell proliferation, alters cytokine expression, restores suppressor function	30-34% (vs placebo)	**Common:** Influenza-like symptoms, injection site reactions and deranged liver function tests (LFTs) **Less common:** Liver toxicity

Glatiramer acetate	Alters T-cell differentiation which induces proliferation of anti-inflammatory lymphocytes	29% (vs placebo)	**Common:** Injection-site reactions, lipoatrophy, post-injection general reaction.
Dimethyl fumarate	Reduces release of inflammatory cytokines and activates antioxidant pathways	51% (vs placebo)	**Common:** Flushing, gastrointestinal symptoms, lymphopenia **Less common:** Progressive multifocal leukoencephalopathy (PML) (1:50,000)
Teriflunomide	Inhibits proliferation of autoreactive B and T cells and induces shift to anti-inflammatory profile	31% (vs placebo)	**Common:** Nausea, diarrhea, hair-thinning, rash. **Less common:** Teratogenicity.
Fingolimod	Syphingosine-1-phosphate receptor antagonist, thereby inhibiting the egress of lymphocytes from lymph nodes and their recirculation	45% (vs interferon)	**Common:** Bradycardia, heart block, infections, lymphopenia, liver dysfunction **Less common:** PML (1:12,000), macular oedema, varicella zoster virus infection, herpes encephalitis
Natalizumab	Humanised monoclonal antibody which blocks α-4 integrin, preventing	68% (vs placebo)	**Common:** Dizziness, nausea, itchy skin, rash, shivering, increased risk infection.

	lymphocyte entry to CNS across the BBB		**Less common:** PML (4-19/1,000), hypersensitivity reactions
Cladribine	Deoxyadenosine analogue which depletes B & T lymphocytes	58% (vs placebo)	**Common:** Lymphopenia, increased risk of infection, headache. **Less common:** Possibly teratogenic, pulmonary TB, PML (in hairy cell leukaemia at a different dose), malignancy
Alemtuzumab	Anti-CD52 humanised monoclonal antibody, leading to profound B and T cell lymphopenia	52% (vs interferon)	**Common:** Infusion reactions, viral infection, thyroid disease (especially hyperthyroid) in up to 40% of patients. **Less common:** idiopathic thrombocytopenic purpura, Goodpasture's, listeria meningitis.
Ocrelizumab	Anti-CD20 (B-cells) humanised monoclonal antibody	47% (vs interferon)	**Common:** Infusion reactions, chest infections, herpes infection **Less common:** Six cases of PML (5 post natalizumab, 1 post fingolimod), possible increased risk of malignancy (particularly breast) though longer follow-up needed

*Table 1: Licensed disease-modifying therapies in RRMS. *Comparison between trials precluded by markedly different trial inclusion criteria and methodologies, particularly whether the comparator was placebo or an injectable therapy (interferon or glatiramer acetate).*

These therapies principally target inflammation, though some may have modest indirect effects on neurodegeneration. Ocrelizumab is the only drug shown to slow progression in PPMS, although subgroup analyses demonstrated the greatest benefit in those with enhancing T1 lesions on MRI (Montalban *et al.*, 2017).

Remyelination trials

Clinical trial results have been mixed. The RENEW study compared the LINGO1 antagonist opicinumab with placebo in patients with a clinically-isolated optic neuritis, using visual-evoked potentials (VEPs) as the primary outcome measure. While a (pre-specified) subpopulation analysis showed an improvement in VEPs favouring opicinumab (53% normalisation in the opicinumab group versus 26% normalisation in controls), the primary outcome and clinical measures were negative (Cadavid *et al.*, 2017). The SYNERGY study also found no clinically-significant improvements between the same molecule and placebo in patients with RRMS and SPMS (Cadavid *et al.*, 2019). The ReBUILD study compared the anticholinergic agent clemastine with placebo in patients with chronic demyelinating optic neuropathy from RRMS (Green *et al.*, 2017). Although no significant improvements in clinical outcomes were seen, the study did identify a statistically significant reduction in the primary outcome measure (mean reduction in the P100 latency by 1.7ms/eye on VEP), and thus the first positive trial of a putatively remyelinating agent. A phase IIa trial of the RXR-agonist bexarotene will report shortly.

MRI in multiple sclerosis

Field strength

Nearly all current clinical and research MRI scanners operate at 1.5 or 3 Tesla (T), although higher fields strengths (for example 7T) are available in specialised research centres. With increasing field strength comes a greater signal to noise ratio, and so potentially higher resolution. This is well illustrated with GM lesion detection. In people with long-standing SPMS, GM lesions are at least as extensive as those in WM (Calabrese *et al.*, 2010) and most GM lesions occur adjacent to the outer (subpial) surface of the brain (Mainero *et al.*, 2009). However, GM lesions are difficult to detect using 3T MRI systems even with sequences that have been tuned for this (see below). At 7T, not only are significantly more GM lesions seen, but subpial lesions - which are very rarely seen in 3T MRI scans - can be detected (Mainero *et al.*, 2009). At present few in vivo studies have assessed the associations between GM lesions and clinical outcomes in MS, despite this being a substantial component of MS pathology. Increasing sensitivity to lesions with higher magnetic field strengths may reflect both the higher resolution and differences in the contrast between normal and abnormal tissues (Kreidstein *et al.*, 1997; Kollia *et al.*, 2009). With higher field strengths more energy can be deposited in tissues, which itself can lead to heating, limiting the clinical utility. As such, scanning methods developed at 1.5T or 3T may need to be significantly modified before running at higher field strengths, and so reduce the potential signal to noise gains. In addition, with higher field strengths it becomes increasingly difficult to achieve an even magnetic field throughout the brain or spinal cord, leading to noticeable changes in tissue intensity towards the edge of MRI scans. However, the main field strength is not the only factor that affects image quality. For example, the design of the coils that send and receive the radio-

frequency signals used by MRI can significantly effect signal to noise, and the strength and accuracy of a scanner's magnetic gradients also effects scan quality.

MRI methods

The MRI toolkit can be broadly divided into techniques assessing macrostructure, microstructure, metabolism and neural function. Macrostructural techniques are the best established and include measures of WM and GM lesion counts and volumes, and brain and spinal cord atrophy. Microstructural techniques, such as magnetisation transfer imaging (MTI) and diffusion tensor imaging (DTI), can provide some information about neuronal and axonal damage, and demyelination. Of the metabolic MRI methods, to date proton spectroscopy has been the most used technique, and can provide relatively cell specific information.

White matter lesions

White matter lesions are the most visible abnormality on MRI in people with MS. They are usually identified on T2-weighted, T1-weighted and fluid-attenuated inversion recovery (FLAIR) scans (Figure 1). At 1.5T, about 60% of histopathologically confirmed WM lesions are seen on T2-weighted scans, and 70% on FLAIR (Geurts *et al.*, 2005a). Lesions seen on T2-weighted scans are not pathologically specific, and may exhibit different degrees of inflammation, axonal loss, demyelination (Miller *et al.*, 1998) and remyelination (Barkhof *et al.*, 2003). A subset of lesions seen on T2-weighted and FLAIR scans are also seen on T1-weighted scans (Figure 2), termed 'black holes' due to their hypointensity relative to surrounding WM, and these are thought to represent more destructive lesions with greater myelin (Bitsch *et al.*, 2001) and axonal loss (van Walderveen *et al.*, 1998; Bitsch *et al.*, 2001). The BBB is normally impermeable, but during acute inflammation this is breached, and acute WM lesions may be seen to enhance when gadolinium-

based MRI contrast agents are given intravenously. On average new WM lesions enhance for about four weeks (Silver *et al.*, 1999). The additional information gained through contrast administration must be weighed against the potential risks. Contrast-induced nephrogenic systemic fibrosis (NSF) has been largely eradicated through pre-administration screening for renal disease and avoidance of agents with a higher risk of NSF, but dose-dependent retention of gadolinium-based contrast agents within the brain is seen on T1 scans (Kanda *et al.*, 2014) and at post-mortem (McDonald *et al.*, 2015). The consequences remain unclear and no pathologic nor clinical sequelae have been confirmed.

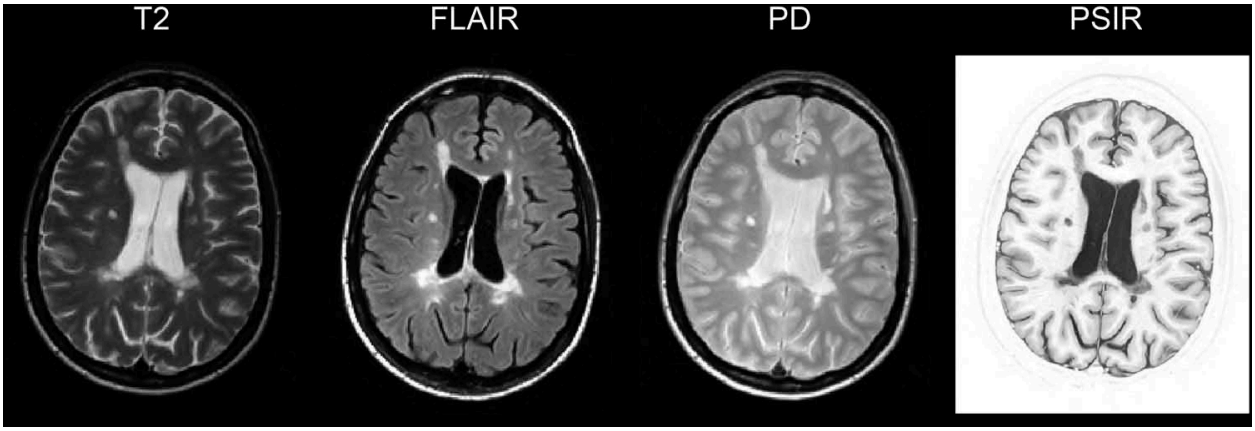

Figure 1: Axial MRI scan showing lesions in the same slice from the same patient with relapsing-remitting multiple sclerosis. FLAIR: fluid attenuated inversion recovery. PD: proton density. PSIR: phase sensitive inversion recovery. Figure from (Brown and Chard, 2016)

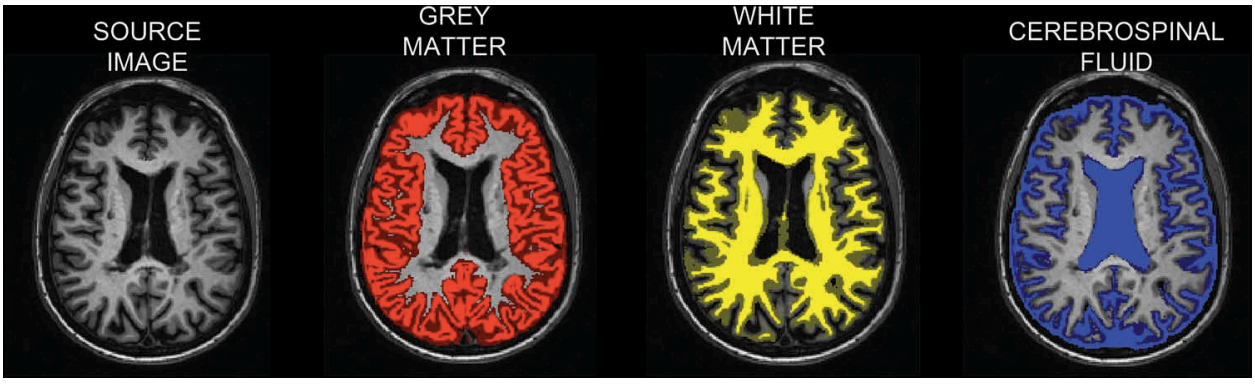

Figure 2: 3D T1-weighted MRI scan from a patient with relapsing remitting multiple sclerosis (same slice, time point and patient as Figure 1). Periventricular T1 hypointense lesions ('black holes') evident on source image. Remaining images show automated segmentation of the 3DT1 scan into grey matter (red), white matter (yellow) and cerebrospinal fluid (blue). Figure from (Brown and Chard, 2016)

Grey matter lesions

In long-standing MS, lesions account for 26% of cortical GM compared to 6% of the WM (Bo *et al.*, 2003). GM lesions are seen in the spinal cord (Fog, 1950); deep GM (where they occur most frequently in the inner layers closest to the ventricles (Haider *et al.*, 2014)); and cortical GM (where they occur most frequently in the outermost (subpial) layer (Kutzelnigg *et al.*, 2005)). Subpial lesions are evident early (Calabrese *et al.*, 2007; Lucchinetti *et al.*, 2011) but become more prevalent in progressive disease (Kutzelnigg *et al.*, 2005) where they account for two thirds of all cortical lesions (Bo *et al.*, 2003). Subpial lesions are not perivenous. If active, subpial lesions are found close to focal areas of meningeal inflammation (Howell *et al.*, 2011) which predominantly occur in cortical sulci (Magliozzi *et al.*, 2007; Haider *et al.*, 2016), suggesting that these lesions might arise from a soluble factor released by meningeal inflammation, which diffuses across the CSF and causes tissue damage (perhaps via microglial activation) (Kutzelnigg *et al.*, 2005; Howell *et al.*, 2011).

When compared with WM, GM lesion detection using MRI is poor: at 1.5T only ~5% of GM lesions confined to the cortex (intracortical GM lesions), ~40% of mixed cortical GM-WM lesions, and ~40% of deep GM lesions are identified, (Geurts *et al.*, 2005a)) so sequences tuned to detect them have been developed. Double inversion recovery (DIR) more than doubles the detection of intracortical GM lesions when compared with FLAIR (Geurts *et al.*, 2005b). Another sequence, phase sensitive inversion recovery (PSIR) may improve on this further, and when compared in vivo with DIR, two to three times more cortical GM lesions are seen (Sethi *et al.*, 2013). However, even at 7T, no more than 35% of cortical lesions are seen with any sequence (while at 7T T2 and FLAIR detect 75% and 88% of histopathologically-confirmed WM lesions respectively) (Kilsdonk *et al.*, 2016). Defining NAGM using MRI is therefore less robust as apparent extralesional abnormalities could reflect occult lesions.

Atrophy

Brain and spinal cord atrophy are thought to reflect irreversible neuronal and axonal loss (Evangelou *et al.*, 2005); brain atrophy is evident from the CIS stage (Chard *et al.*, 2002). In the brain, atrophy appears to occur more in GM than WM (Dalton *et al.*, 2004; Fisher *et al.*, 2008; Perez-Miralles *et al.*, 2013) and accelerates as a person transits from RRMS to SPMS (Dalton *et al.*, 2006; Fisher *et al.*, 2008). Brain atrophy is most often assessed using high-resolution (usually 1x1x1mm) T1-weighted scans, and can be measured using a variety of automated or semi-automated methods, for example SIENA/SIENAX (Smith *et al.*, 2002), FreeSurfer (Dale *et al.*, 1999) and SPM [SPM; Wellcome Trust Centre for Neuroimaging, London, UK; www.fil.ion.ucl.ac.uk/]. When measuring brain atrophy on T1-weighted scans, a complicating issue in MS is the presence of lesions. WM lesions can have similar signal intensities to GM on a T1-weighted scan, and so may erroneously be counted as part of the GM. It is now increasingly usual to account for this either by filling WM lesions with simulated normal-appearing WM (NAWM) before segmentation (for example (Chard et al., 2010)) or by correcting segmentations before measuring tissue volumes.

Spinal cord atrophy is usually measured in the upper cervical spine, as a mean cross-sectional area or volume over a fixed length of the cord. It can be measured on T2-weighted sequences (Horsfield et al., 2010), T1-weighted sequences (including those acquired for brain atrophy measures (Liu et al., 2014)), and more recently PSIR scans (Kearney et al., 2014). Semi-automated methods that require minimal operator input are now most commonly used for these measurements (Horsfield et al., 2010).

Diffusion-tensor imaging (DTI)

DTI assesses the movement of water molecules in tissues, providing information about tissue microstructure. In MS, it has mostly been used to assess WM rather than GM. Fractional anisotropy (FA) is a measure of the directionality of water movement, i.e. whether it occurs evenly in all directions (low anisotropy) or mostly in one direction (high anisotropy), and is usually high in WM and lower in GM (Basser and Pierpaoli, 1996). Mean diffusivity (MD) measures the mean distance water travels in any direction, and is usually low in WM and higher in GM (Basser and Pierpaoli, 1996). Combined MRI and histopathology studies have shown that both of these measures are affected by myelin content and, to a lesser degree, axonal count in post mortem WM brain tissue (Table 2) (Schmierer *et al.*, 2007b).

Magnetization transfer imaging

Conventional MRI techniques are largely based on signals derived from protons in water, so protons bound to macromolecular structures (such as myelin and cell membranes) go relatively undetected. However, this bound pool may be seen indirectly using magnetization transfer imaging. Magnetization transfer is often expressed as a ratio (magnetization transfer ratio (MTR)), which provides a semi-quantitative measure of the proportion of protons bound to macromolecular structures relative to those that are in free water. Combined MRI and histopathology studies in post mortem MS brains have demonstrated correlations between WM MTR and myelin content, and to a lesser degree, axonal and glial densities (Table 2) (Schmierer *et al.*, 2004). In the cortex myelin content is also significantly correlated with MTR (Schmierer et al., 2010; Chen et al., 2013).

		Histopathological feature		
		Myelin density†	Axonal density	Glial density†
MRI feature	MTR	-0.84**	0.66**	0.13^{NS}
	DTI: FA	-0.79**	0.70**	0.50*
	DTI: MD	0.68**	-0.66**	-0.55*
	qMT: f_B	-0.80**	0.72**	0.41*

*Table 2: Pearson r correlations coefficients of MTR, DTI and qMT with histopathological features. Modified from (Schmierer et al., 2007b) and (Schmierer et al., 2004) and (Schmierer et al., 2007a). †Myelin and glial density estimated by light transmittance through stained tissues rather than absolute measures (thus the negative correlations). Axonal density measured as counts over a standardised stereological grid. MTR = magnetization transfer ratio. DTI = diffusion tensor imaging. FA = fractional anisotropy. MD = mean diffusivity. qMT = quantitative magnetisation transfer. f_B = fraction of macromolecular protons. NS = non-significant *p ≤ 0.01 **p ≤ 0.001*

Quantitative magnetisation transfer

MTR is also reduced by oedema (Dousset *et al.*, 1992), and is affected by sequence-dependent factors such as the saturation pulse frequency (Henkelman *et al.*, 2001). Quantitative MT (qMT) measures (e.g. the fraction of macromolecular protons, f_B) are absolute measures so may be less dependent on the MRI system used. Overall, no combined MRI-histopathological study has shown any greater sensitivity for myelin in comparison to MTR (Table 2). F_B is thought to reflect protons in the macromolecular pool only, while MTR reflects both the macromolecular and bound pools. In-vivo and at post-mortem, the significantly lower lesional f_B (43-46% of the surrounding NAWM f_B) compared to the lesional MTR (69-75% of the surrounding NAWM MTR) is thought to reflect attenuation of the MTR by oedema and may suggest f_B's greater specificity for myelin (Schmierer *et al.*, 2007a; Giacomini *et al.*, 2009). However, although decreasing, the longer acquisition times and complex modelling necessary have thus far precluded widespread use in clinics or remyelination trials.

Myelin water fraction

Multi-component T_2 relaxometry exploits the distinct proton relaxation characteristics of water trapped in myelin bilayers ("myelin water", with short T_2 relaxation times), intracellular and extracellular water (medium T_2 relaxation times) and CSF (long T_2 relaxation times) (MacKay *et al.*, 1994). Myelin water fraction (MWF) – the ratio of the short to the total water signal – correlates with myelin content (Laule *et al.*, 2006), but again requires long acquisition times and suffers limited brain coverage. These concerns have, to some extent, been addressed with newer techniques such as 3D-GRASE (Prasloski *et al.*, 2012), mcDESPOT (Deoni *et al.*, 2008), FAST-T2 (Vargas *et al.*, 2015) and T2prep 3D SPIRAL (Nguyen *et al.*, 2012), though acquisition times still exceed those of MTR and histopathological evidence of greater specificity or sensitivity compared to MTR are lacking.

Non-MRI methods - Positron-emission tomography (PET)

The limited specificity of MRI can to some extent be ameliorated with PET, which uses various radio-labelled tracers to target specific cells or tissues. In MS, PET has been used to explore changes in myelin content, inflammation and neuronal damage (though data in the latter is awaited).

Multiple PET tracers have been used to study myelin, particularly the amyloid tracer 2-(4'-methylaminophenyl)-6-hydroxybenzothiazole, also known as Pittsburgh Compound B ([11C]PIB) (Stankoff *et al.*, 2011). [11C]PIB (and therefore myelin) concentration is lowest in black holes with ascending values seen in T2 lesions, perilesional WM and gadolinium-enhancing lesions, all of which show significantly lower uptake than in NAWM (Bodini *et al.*, 2016). This pattern has been

replicated using 18F florbetapir which has a longer half-life (Carotenuto, 2018). [11C]PIB decreases (reflecting demyelination) and increases (reflecting remyelination) can be explored on a voxel-level with repeated scans. This has uncovered significant heterogeneity in the extent of remyelination between patients, heterogeneity within individual lesions (with some parts continuing to demyelinate and others remyelinating) and strong correlations between derived remyelination indices and clinical indices (for example EDSS (*B* = -0.67, p=0.006) (Bodini *et al.*, 2016). [11C]PIB is not myelin-specific though – it is also used to detect fibrillary β-amyloid deposits in neurodegenerative conditions such as Alzheimer's disease, blurring assessments of those with such comorbidities (particularly the elderly).

For exploring innate inflammation, the most widely used target is the translocator protein (TSPO) which is found on the mitochondrial membranes of microglia, macrophages and astroglia. While not specific, it's expression is principally driven by activation of microglia and macrophages. Using numerous tracers, significant heterogeneity has been identified in-vivo. For example, uptake of 11C-PK11195 is (i) increased in lesions, the NAWM and grey matter of patients with SPMS, in-keeping with pathological studies showing widespread microglial activation; and (ii) markedly increased in the perilesional NAWM of more than half of chronic T1 lesions in patients with SPMS consistent with the post-mortem findings of chronic active lesions (Prineas *et al.*, 2001; Kutzelnigg *et al.*, 2005; Rissanen *et al.*, 2014). WM lesional and perilesional [18F]DPA-714 uptake correlated with severe disability worsening in the period preceding imaging, but has also highlighted that a far greater proportion of lesions exhibit active inflammation (37%) than is shown with gadolinium-enhanced MRI sequences (<2%) (Stankoff *et al.*, 2018). Increased 11C-OBR28 has been shown in cortical lesions, the extent of which – like WM lesions – correlated with clinical outcomes (Herranz *et al.*, 2019). Limitations include many tracers' inability to distinguishing microglial subtypes (and therefore discriminate their protective and

proinflammatory effects); and that microglial activation occurs in diseases other than MS including degenerative conditions, stroke and brain injury (Tronel *et al.*, 2017).

While PET offers significantly greater specificity and superior serialization of in-vivo pathophysiological changes compared to MRI, the comparatively lower resolution hampers visualization of lesions or small areas (Catana, 2017). Furthermore, the unknown effects of repeated exposure to ionizing radiation, the need to produce the radioisotopes near to the scanner (due to their short half-life) and the limited number of available PET scanners currently limit PET to the research setting (Preziosa *et al.*, 2019).

Heterogeneity in normal-appearing tissues.

Normal-appearing grey matter (NAGM)

MRI's aforementioned poor detection of GM lesions (Kilsdonk *et al.*, 2016) means that apparent NAGM abnormalities could reflect occult lesions. This problem is circumvented in histopathological studies. Extralesional cortical and thalamic GM show significant axonal loss compared to healthy controls (Cifelli *et al.*, 2002; Choi *et al.*, 2012; Bevan *et al.*, 2018). Neuronal loss appears relatively independent of demyelination (Magliozzi et al., 2010): no differences in axonal density were seen between demyelinating cortical lesions and NAGM (Klaver *et al.*, 2015). Cortical demyelination has typically been quantified in terms of demyelinating lesions, but reductions in NAGM myelin density are seen, in part reflecting areas of remyelination (Albert *et al.*, 2007).

However, the extent of NAGM damage is not uniform. Significantly greater neuronal loss is seen in the outermost cortical layers in some patients with SPMS, and the extent of cortical demyelinating lesions is also greatest in the outer cortical layers in both SPMS and PPMS (Choi *et al.*, 2012). These abnormalities are associated, both in location and extent, with the degree of

meningeal inflammation, so a cytotoxic factor, released into the CSF by meningeal inflammation, has been postulated to be driving this outside-in cortical pathology (Magliozzi *et al.*, 2010). The most striking form, meningeal lymphoid aggregates, have only been seen in SPMS, not PPMS (Magliozzi *et al.*, 2007; Magliozzi *et al.*, 2010). Such post-mortem studies are, by definition, biased towards those with end-stage MS, and due to the relatively young age at death of many participants, these two studies may be additionally biased towards those with more meningeal inflammation (which is associated with more rapid clinical disease progression and death (Howell *et al.*, 2011)). Whether this outside-in gradient occurs earlier in disease, or is even detectable in-vivo, prompted a search in-vivo using MRI. Using MTR, Samson and colleagues found that in both SPMS and RRMS the MTR was lowest (most abnormal) in comparison to healthy controls at the outer cortical surface with smaller MTR reductions visible within inner cortical layers (Samson *et al.*, 2014). However, no such outside-in cortical gradient was seen in patients with PPMS despite post-mortem evidence of meningeal inflammation and a gradient of demyelination (Choi *et al.*, 2012). Whether this reflects a true absence of cortical gradients in PPMS – perhaps explained by the absence of meningeal lymphoid follicles found at post-mortem in PPMS (Magliozzi *et al.*, 2007) - or simply the methodology (for example smaller numbers of PPMS (19) versus SPMS (25) or RRMS (44) were examined), remains unclear. A true absence of these surface-based pathologies might suggest a key pathogenic difference between relapse-onset MS and PPMS.

Normal-appearing white matter (NAWM)

NAWM - regions free of lesions seen using conventional (PD/T2-weighted and FLAIR) MRI - are abnormal when assessed by a variety of techniques including MTR (Filippi and Rocca, 2005). However, like in GM, NAWM abnormalities are not uniform. Perilesional tissue is abnormal, for up to 4mm from the T2-defined lesion edge (Vrenken et al., 2006). Moreover, if meningeal inflammation drives superficial cortical pathology via a soluble factor released into the CSF

(Magliozzi *et al.*, 2010), then one might also expect to see gradients at other tissue-CSF boundaries, such as the periventricular white matter. Indeed, my colleagues at UCL's NMR Research Unit had identified a periventricular gradient of MTR abnormality just prior to my arrival. In healthy controls, the MTR was highest adjacent to the lateral ventricles and decreased with increasing distance from them, while in patients with RRMS – and even more so in SPMS – the MTR was lowest adjacent to the lateral ventricles and increased with increasing distance from them (Liu *et al.*, 2015). WM lesions are frequently seen in the periventricular region (Brownell and Hughes, 1962), so perilesional MTR reductions (Vrenken *et al.*, 2006) or MRI-invisible lesions might confound a NAWM periventricular gradient. To circumvent perilesional MTR reductions, a 2mm cuff around each lesion was also removed when generating the NAWM masks, and a sensitivity analysis excluding a 3mm cuff found virtually identical results (Liu *et al.*, 2015). Indeed, the periventricular gradient was visible in both NAWM and lesional tissue. However, by definition MRI-invisible lesions could not be circumvented, and, because lesions accrue with time, the relatively long disease duration, even in the RRMS group (mean >11 years) may have meant a number of invisible lesions and thereby spuriously lower periventricular MTR. The Liu paper did not explore periventricular gradients in early relapse-onset MS or PPMS, nor did it examine the clinical correlations of periventricular gradients, their change over time or thir response to DMTs.

Aims and objectives

The overall aims of my PhD were twofold. First, to examine the timing, evolution and clinical correlations of surface-based gradients in multiple sclerosis, and whether or not the periventricular gradient is influenced by peripheral immunodepletion; and second to explore the associations between DMT use in RRMS with subsequent conversion to SPMS.

Project 1

By looking for an abnormal periventricular MTR gradient in people who have recently had a CIS, we would be able to establish if it is seen from the earliest clinical stages of MS, whether it predicts subsequent disease activity, and - given that people usually have very few WM lesions immediately after a CIS - determine if it is closely associated with WM lesions. The identification of an early abnormal periventricular MTR gradient that is not directly related to lesion formation, but linked with clinical outcomes might suggest that there is a pathological process distinct to that underlying lesion formation that should be targeted from the earliest clinical stages of relapse-onset MS. Using previously acquired MTR data from a longitudinal study of people with a recent CIS, we aimed to (1) look for gradients in NAWM abnormalities around the lateral ventricles and, if present, to determine (2) whether or not they were associated with WM lesions, or (3) were associated with the subsequent risk of developing CDMS and disability.

Project 2

There is ongoing debate as to whether or not PPMS and SPMS are essentially the same disease, barring the preceding relapsing-remitting phase: the age at onset and rate of progression are similar (Kremenchutzky *et al.*, 2006) and lesion morphology in relapse-onset and PPMS are

identical (Kuchling *et al.*, 2014) but differences have been observed in both MRI and histopathological studies (Revesz *et al.*, 1994; Correale *et al.*, 2017). Post-mortem studies have revealed meningeal inflammation in both types of MS (Magliozzi *et al.*, 2007; Choi *et al.*, 2012) although the most structured form - lymphoid follicle-like aggregates - have only been observed in SPMS, not in PPMS (Magliozzi *et al.*, 2007). The processes underlying abnormal cortical and periventricular MTR gradients remain unknown, but one possibility is that they are both linked with meningeal inflammation, perhaps through a CSF-mediated factor (Magliozzi *et al.*, 2010). This raises seemingly conflicting possibilities that either lymphoid follicles are themselves not relevant to progression, or that the mechanisms leading to progression differ significantly between PPMS and SPMS. Using an early processing pipeline and smaller cohort, our group previously reported the absence of a statistically significant cortical MTR gradient in PPMS (Samson *et al.*, 2014) supporting the latter hypothesis (but did not investigate periventricular gradients). If a common factor links cortical and periventricular MTR gradients, we would expect the latter to also be absent in PPMS.

Using our recently optimised pipeline for WM and cortical GM segmentation (Pardini *et al.*, 2016), plus a larger cohort, we re-analysed healthy controls and patients with progressive MS to explore (i) whether periventricular and cortical gradients are seen in patients with PPMS compared to healthy controls; and if so, (ii) to explore whether either gradient correlates with disability; (iii) to compare the gradients and their evolution between patients with PPMS and SPMS; and (iv) to examine the relationship between periventricular and cortical gradient severity in both PPMS and SPMS.

Project 3

Alemtuzumab is a potent immunomodulator licensed for RRMS, which stabilises MTR in the normal-appearing white matter (Button *et al.*, 2013). It depletes peripheral mature lymphocytes (Coles *et al.*, 2006) and substantially reduces the long-term risk of relapses (Tuohy *et al.*, 2015). Alemtuzumab does not cross the blood-CSF barrier (Moreau *et al.*, 1994) and should have no direct effect on isolated intrathecal pathological processes. If alemtuzumab were to affect the periventricular MTR gradient this would suggest the processes underlying it are influenced by the peripheral immune system.

We therefore aimed to (i) examine the untreated evolution of the MTR gradient in RRMS; (ii) explore if alemtuzumab alters this; and (iii) determine if the pre-treatment MTR gradient predicts on-treatment relapses or change in disability.

Project 4

Using a recently-published validated definition of SPMS (Lorscheider *et al.*, 2016) we aimed to compare the rate of SPMS conversion between different DMTs and an untreated cohort to determine whether individual DMTs are associated with a reduced rate of conversion from RRMS to SPMS. We then explored whether any additional advantage was conferred by initial treatment with fingolimod, natalizumab or alemtuzumab compared to glatiramer acetate or interferon beta, or treatment commencement or escalation within versus after 5 years of disease onset, in the rate of conversion to SPMS.

Chapter 2: Methods: Outside-in gradients of tissue abnormality

Project 1: Periventricular gradients after a clinically isolated syndrome

Performed in collaboration with Matteo Pardini (joint first author); plus Wallace Brownlee, Kryshani Fernando, Rebecca Samson, Ferran Prados Carrasco, Sebastien Ourselin, Claudia Gandini Wheeler-Kingshott, David Miller and Declan Chard.

My role: conception and design of study; gathered existing scans and clinical information; planned and performed image processing pipeline (with Matteo Pardini); quality-assurance steps; analysed data (with assistance from Matteo Pardini); wrote manuscript and amended following co-author and journal reviews.

Participants

From a prospectively recruited CIS cohort (Fernando *et al.*, 2005) we included data from 81 people who had presented with a clinically isolated optic neuritis (ON), who had no previous history of neurological symptoms, were aged between 16 and 50 years at symptom onset, had 3D fast spoiled gradient echo (FSPGR) as part of their baseline MRI assessments and MTR three months later. Participants were recruited from Moorfields Eye Hospital (London) by a single experienced neuro-ophthalmologist. They were evaluated clinically and with MRI a median of 1.4 (range 0.1-3.5) months after ON onset ('baseline') and underwent a further scan (including magnetization transfer imaging) on the same scanner three months later (median 4.6; mean 4.8;

range 2.0-7.5 months after ON onset); patients were followed up clinically two and five years later (Brownlee *et al.*, 2015) and had EDSS and paced serial addition test (PASAT, 3 second intervals (Cutter *et al.*, 1999)) scores assessed at five years. This work therefore describes cross-sectional MTR data (collected 4.6 months after symptom onset) with clinical data at 4.6 months plus two and five years after symptom onset. We also studied a group of 39 healthy controls with no known neurological disorder or clinical follow up. Demographic and clinical data are reported in Table 3.

All participants gave written informed consent and the study was approved by the Joint Medical Ethics Committee of the Institute of Neurology and National Hospital for Neurology and Neurosurgery, and the Moorfields Eye Hospitals Ethics Committee.

Clinical assessments

MS was diagnosed on the basis of further relapses (clinically definite multiple sclerosis (CDMS, (Poser *et al.*, 1983) and using the 2010 McDonald criteria (Polman *et al.*, 2011).

Magnetic resonance imaging

All magnetic resonance studies were performed on a 1.5 Tesla (T) GE Signa Echospeed scanner (General Electric Medical Systems, Milwaukee, WI). The following sequences were acquired: (i) an FSPGR scan of the whole brain (124x1.5mm slices; matrix, 256x160, interpolated to a final in-plane resolution of 1.1mm, TR= 10.9 ms, TE= 4.2 ms, TI= 450 ms) for volumetric measures; (ii) dual echo proton-density (PD)/T2 scans of the whole brain (46x3 mm contiguous axial-oblique slices parallel to the anterior/posterior commissural line, matrix 256x256, field of view (FOV) 24x18 cm, repetition time (TR) =3200 ms, echo time (TE) =15/90 ms), for the evaluation of WM

lesions; (iii) T1-weighted pre- and post-gadolinium (0.1 mmol/kg body weight) spin echo sequences of the brain (46x3 mm contiguous axial-oblique slices parallel to the anterior/posterior commissural line, matrix 256x256, FOV 24x18 cm, TR=600 ms, TE=17 ms) to evaluate the presence of pathologically enhancing lesions; and (iv) MTR data using a dual-echo, spin-echo sequence of the whole brain (28x5mm contiguous, axial-oblique slices parallel to the anterior/posterior commissural line with an interleaved sequence described by Barker (TR=1720 ms, TE=30/80ms, number of excitations 0.75, matrix 256x128, FOV 24x24cm, MT-weighted by the application of a pre-saturation pulse (Hamming apodized 3 lobe sinc pulse, duration 64ms, flip angle 1430°, and a peak amplitude of 14.6 μT giving a normal bandwidth of 62.5 Hz, applied 1kHz from the water resonance (Barker *et al.*, 1996))). MTR maps were calculated on a voxel-by-voxel basis using the short echo data because of its higher signal to noise compared to the longer echo data. Proton density (PD) and T2-weighted images are included in this sequence, intrinsically registered to the MT data, and were used to facilitate registrations to native MT space as described below. The FSPGR scan was acquired at baseline (when magnetisation transfer imaging was not performed); all other scans and lesion counts used for this analysis were acquired three months later (when the FSPGR was not repeated (Fernando *et al.*, 2005)).

Image analysis

MTR map calculation

For each participant, MTR maps were calculated using the following equation: MTR (in percentage units (pu)) = ((MTR_{off} – MTR_{on}) / MT_{off}.) x 100). The interleaved nature of the MTR sequence used meant that co-registration of MT_{on} and MT_{off} data was not required. MTR values were extracted from each NAWM and lesion band using FSLstats (http://www.fmrib.ox.ac.uk/fsl/).

Tissue segmentation

T1-hypointensities were outlined by WJB using a semi-automated edge-finding tool (JIM v6.0, Xinapse systems, Aldwincle, United Kingdom) on the 3D FSPGR images and these masks were used to perform lesion filling on the 3D FSPGR scans (Chard *et al.*, 2010; Prados *et al.*, 2016). After lesion filling the FSPGR scans were segmented into GM, WM and CSF probability maps using the new segmentation pipeline in Statistical Parametric Mapping 12 (SPM12; Wellcome Trust Centre for Neuroimaging, London, UK; www.fil.ion.ucl.ac.uk/). Brain parenchymal fraction (BPF) was calculated using SPM12-derived tissue segmentations for use as a covariate in the statistical models (Chard *et al.*, 2010).

Generation of NAWM masks

WM lesions were identified on the dual echo PD/T2-weighted scans, and outlined by WJB using JIM v6.0 (Xinapse systems, Aldwincle, United Kingdom). This had been performed for a previous project (thus explaining why lesions were not marked on the PD/T2 scan interleaved with the MT sequence). Using NiftyReg (Modat *et al.*, 2010; Modat *et al.*, 2014) the T2-weighted image was linearly co-registered with the T2-weighted image embedded in the MT sequence, thus aligning the WM lesion masks with the MTR maps. NiftyReg implements a symmetric and inverse-consistent registration ensuring that the results are unbiased towards the directionality of the registration process because the forward and backward transformations are optimised concurrently in an inverse-consistent manner. The symmetric full affine approach (Modat *et al.*, 2014) with 12 degrees of freedom is based on the asymmetric block-matching approach (Ourselin *et al.*, 2001).

The PD and T2 images embedded in the MT sequence were used to generate a pseudo-T1 image, by subtracting the PD scans from the T2 images (Hickman *et al.*, 2002). For each participant, the 3D FSPGR scan was then linearly co-registered to the pseudo-T1 using NiftyReg (Modat *et al.*, 2014) and the transformation applied to the GM, WM and CSF tissue segmentation maps. In MTR space the GM, WM and CSF maps were binarised using a probabilistic threshold of > 90% (Samson *et al.*, 2014). In MTR space, WM lesion masks were dilated by two voxels (to account for perilesional MTR abnormalities (Vrenken *et al.*, 2006)), and the dilated lesion masks were subtracted from the thresholded WM tissue probability maps to produce NAWM masks.

Segmentation of NAWM into concentric periventricular bands

Given the voxel size of MT images (1x1x5 mm), to reduce the potential for partial volume effects between CSF and WM, all analyses were limited to two axial slices orthogonal to the wall of the lateral ventricles, i.e. a slice immediately above the insula, and the slice immediately below this. We used an automated method to reproducibly identify these slices in all participants: a position marker was placed in the lateral ventricles just superior to the insula on a MNI152 brain template (Grabner *et al.*, 2006). The MNI152 brain template was registered to each participant's native MTR space with a non-linear transformation as previously described (Muhlert *et al.*, 2013) using NiftyReg (Modat *et al.*, 2010). The position of the marker was checked and corrected as needed by one investigator and then the two axial slices were selected relative to this template marker.

To identify the lateral ventricles we used a previously described approach (Liu *et al.*, 2015). Briefly, a mask of the lateral ventricles was created in MNI152 space using the Wake Forest University School of Medicine PickAtlas toolbox (Maldjian *et al.*, 2003) and then registered to each participant's MTR native space using the previously computed transformation. The lateral

ventricle mask was then intersected with each participant's CSF mask on the two previously selected axial slices. These masks were checked and manually edited by one investigator to ensure anatomical accuracy, and then sequentially dilated in the axial plane by 1 voxel (1mm) using DilM (part of FSL software package (http://www.fmrib.ox.ac.uk/fsl/) producing concentric bands around the lateral ventricles (Figure 3). For this project, a periventricular band is therefore defined as a 1mm ring in the axial plane surrounding the lateral ventricles. These were intersected with the NAWM mask to generate bands of NAWM. We intersected the CSF masks with the rings and found that the first two bands contained CSF in over half of participants (first band 117/120 participants; second band 63/120), so these bands were discarded to limit partial volume effects from CSF in all patients. Residual CSF was identified in the first of these ten bands in ten people with ON and two controls and so these participants were excluded, leaving 71 people with ON and 37 healthy controls. Bands of WM lesional tissue were derived by intersecting the bands with the lesion masks. As per previous work (Liu *et al.*, 2015), the percentage of lesioned WM in each band were also computed (number of lesional voxels per band / total number of WM voxels per band).

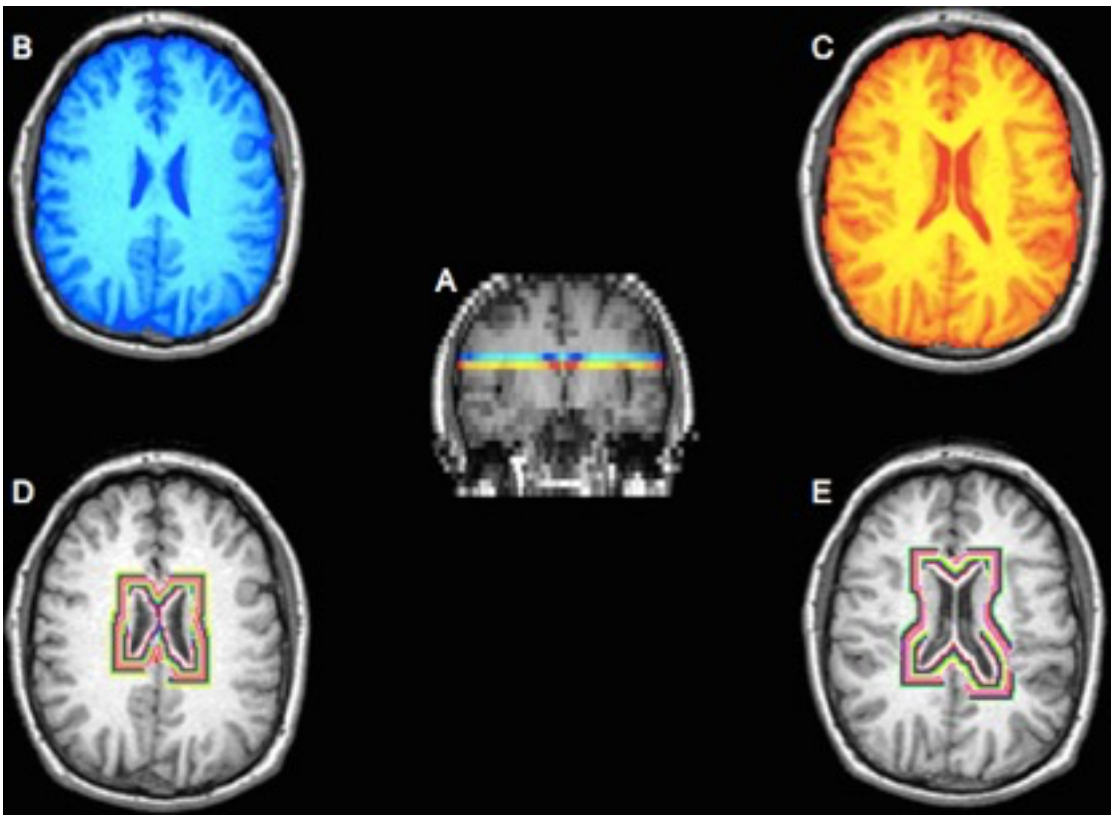

Figure 3: A: Normal appearing white matter (NAWM) from two 5mm axial slices were extracted at (B) and immediately below (C) the level of the insula. Bands of concentric MTR values from the normal-appearing white matter around the ventricles were then extracted (D and E). The first two bands were excluded to minimise partial volume effects.

We also recalculated the mean NAWM and GM MTR (as previously reported (Fernando *et al.*, 2005)) for use as covariates in the statistical models.

Statistical analyses

Statistical analyses were performed using SPSS (IBM SPSS version 22 for Windows (SPSS, Inc., Chicago, IL, USA)). Demographic data are presented as mean (standard deviation) and MTR data as mean (standard error), while EDSS values are presented as median (range). In each participant, mean MTR values were calculated in the 1 mm bands in both axial slices, and then averaged across both slices, weighted by the number of voxels in each band. After discarding the first two bands (see above), we calculated periventricular MTR gradients over the next 5mm closest to the ventricles (i.e. NAWM MTR in band five – NAWM MTR in band one) and deep MTR gradients over

the subsequent 5mm (i.e. NAWM MTR in band ten – NAWM MTR in band six), dividing both by the number of intervals to give the MTR change in percentage units (pu) per mm. This division was consistent with previous work (Liu *et al.*, 2015), and coincided with the point at which the MTR gradients in the ON and control groups converged.

In the ON cohort, 58/71 patients were followed-up two and five years after their baseline MRI scan. These patients were subdivided into those who developed CDMS or McDonald MS within two years of their ON. We also examined those developing CDMS and McDonald MS within five years of their ON. To assess associations with gadolinium-enhancing lesions, the ON cohort was subdivided into those with or without enhancing lesions. To explore associations with WM lesions, the ON cohort was also subdivided into those who did or did not have T2 brain WM lesions and, in those with lesions, those who did or did not have periventricular lesions. Independent sample t-tests and analysis of variance (ANOVA) tests were used to compare clinical and MRI measures between groups. For the MTR gradient measures, the same comparisons were also performed using general linear models firstly correcting for BPF (to control for the possible effects of atrophy on periventricular MTR gradients), then correcting for mean NAWM and GM MTR (to ensure diffuse MTR changes were not driving MTR gradients). Spearman correlation was used to explore the relationship between MTR gradients and both EDSS and PASAT scores. Factors predicting conversion to CDMS status were examined with multivariate binary logistic regression. Results were considered statistically significant at the $p<0.05$ level.

Project 2: Periventricular and cortical gradients in progressive multiple sclerosis

Performed in collaboration with Azmain Chowdhury (joint first author), plus Baris Kanber, Ferran Prados Carrasco, Arman Eshaghi, Carole Sudre, Matteo Pardini, Rebecca Samson, Steven van de Pavert, Claudia Gandini Wheeler-Kingshott and Declan Chard.

My role: conception and design of study; gathered existing scans and clinical information; planned and performed image processing pipeline (with Ferran Prados Carrasco); quality-assurance steps; analysed data (with assistance from Arman Eshaghi); wrote manuscript and amended following co-author and journal reviews.

Subjects

From an observational cohort (Samson *et al.*, 2014) we analysed data from healthy controls and people with PPMS, SPMS or RRMS (as defined by the Lublin-Reingold criteria (Lublin and Reingold, 1996)) that had undergone MRI scanning with a protocol including the acquisition of volumetric T1-weighted images and MTR data. Some had repeat imaging performed 1-4 years later. All people in the MS groups additionally required an EDSS (Kurtzke, 1983) score at baseline. The study was approved by our local institutional ethics committee and written informed consent was provided by each participant.

MRI

Imaging was performed on a 3T Philips Achieva system (Philips Healthcare, Best, The Netherlands), and included: (i) Dual-echo PD / T2 weighted scans (1x1x3 mm^3, TR = 3500 ms, TE = 19/85 ms) for lesion identification; (ii) T1-weighted scans (3D inversion-prepared (1x1x1 mm^3,

T1=824 ms) fast field echo sequence (TR/TE = 6.9/3.1 ms, flip angle = 8°)) for volumetric measures and segmentation; and (iii) interleaved MTR data using a 3D-slab-selective fast field echo sequence with two echoes (1x1x1 mm^3, TR = 6.4 ms, TE1/TE2 = 2.7/4.3 ms, flip angle = 9° with and without sinc-Gaussian shaped MT pulses of nominal flip angle 360°, offset frequency 1 kHz, duration 16 ms). All images were acquired sagittally with a field-of-view of 256x256x180mm^3 across the whole brain.

Image analysis

WM lesions were outlined on PD/T2-weighted images by SvdP using the semi-automated tool 3D-slicer (Fedorov *et al.*, 2012) and checked by DC. The resultant lesion masks were affine co-registered to the T1-weighted images via pseudo-T1 images (as previously described (Hickman *et al.*, 2002)) and transformed to T1-space using nearest-neighbour interpolation to enable lesion-filling of the T1-weighted images (Prados *et al.*, 2016). The MTon and MToff images were then registered to the T1-weighted volume using NiftyReg (Modat *et al.*, 2014), and MTR maps (in pu), were calculated as follows: (((MToff – MTon) / MToff) x100). T1-weighted volumes were segmented into WM, GM and CSF using the geodesic information flows (GIF) algorithm (Cardoso *et al.*, 2015). Lesions (plus a 2mm perilesional rim (Vrenken *et al.*, 2006)) were subtracted from each participant's WM mask, generating a NAWM mask. The NAWM and cortical GM (CGM) volumes were used as covariates in the periventricular and cortical models respectively. BPF was used as an alternative covariate in both periventricular and cortical gradient models in a sensitivity analysis to mirror a previous paper (Pardini *et al.*, 2016). It was calculated as follows: (GM volume + WM volume) / (GM volume + WM volume + CSF volume).

The NAWM mask was intersected with the MTR map, and segmented into 10 concentric bands using the normalised distance map derived from the normal to the Laplace equation isolines

(Pardini *et al.*, 2016). Unlike in project 1 (performed before the updated method was optimised), this approach generates bands of varying thickness, which accounts for the differences in brain thickness within different brain regions plus the effects of atrophy: the relative position of a given band to the surface of the brain should therefore be maintained. Consistent with previous work using 3D MTR data, the innermost (periventricular) and outermost (pericortical) bands were excluded to mitigate partial volume effects (Liu *et al.*, 2015). From the remaining 8 bands the periventricular NAWM gradient was calculated as follows: ((mean NAWM MTR band 3 – mean NAWM MTR band 1) / 2). Consistent with previous work, the CGM was also segmented into two bands using the Laplace method (Samson *et al.*, 2014) but rather than using the absolute outer-band MTR value (Samson *et al.*, 2014) (which will be subject to inter-individual variations in whole brain MTR (Barker *et al.*, 2005)), the cortical gradient was instead calculated as: (mean cortical GM MTR band 2 (outer) – mean cortical GM MTR band 1 (inner)). An alternative method for calculating the cortical gradient – applying the CGM mask to a 12-band segmentation, removing the outermost band, then calculating the cortical gradient over the 3 outermost bands – requires a lower probabilistic segmentation threshold (Pardini *et al.*, 2016) to achieve similarly-sized bands, so increasing the chances of partial volume with adjacent WM and CSF, affecting results, and it also does not account for cortical folding as well as the present method. The mean NAWM and cortical GM MTR were also calculated in each participant for use as covariates in sensitivity analyses. Finally, to explore whether differences between current and previous (Samson *et al.*, 2014) results reflected the greater number of people studied, we restricted the groups to the 19 people with PPMS and 35 healthy controls previously examined (Samson *et al.*, 2014) and repeated the analyses.

Statistics

MTR gradient values are presented as mean ± standard error, and all longitudinal differences were annualised to circumvent variable interscan intervals. We used general linear models to compare baseline gradients between groups and mixed-effects linear models to compare the rate of gradient change between disease subtypes. Consistent with previous work these models were adjusted for age and sex. Additionally, these models were also adjusted for either NAWM volume (periventricular gradient models) or cortical volume (cortical gradient models); and then repeated adjusting for BPF for comparison to previous work (Pardini *et al.*, 2016). To examine whether differences in gradients might be driven by more diffuse MTR changes we performed sensitivity analyses, additionally adjusting all periventricular gradient models for mean NAWM MTR, and all cortical gradient models for mean CGM MTR.

Finally, we ran univariate general linear models comparing (i) baseline periventricular gradients with baseline cortical gradients; and (iii) baseline gradients with baseline disease duration, EDSS score and time from the last relapse. All analyses were performed in R (v3.3.1). Results were considered statistically significant at the $p < 0.05$ level.

Project 3: Periventricular gradient evolution following peripheral immunotherapy

Performed in collaboration with Ferran Prados Carrasco (joint first author); plus Arman Eshaghi, Carole Sudre, Tom Button, Matteo Pardini, Rebecca Samson, Sebastien Ourselin, Claudia Gandini Wheeler-Kingshott, Joanne Jones, Alasdair Coles, and Declan Chard.

My role: conception and design of study; gathered existing scans and clinical information (including updating 13-year alemtuzumab data from research clinic); planned and performed image processing pipeline (with Ferran Prados Carrasco); quality-assurance steps; analysed data (with assistance from Arman Eshaghi); wrote manuscript and amended following co-author and journal reviews.

Participants

This study utilised the same early relapsing-remitting multiple sclerosis cohorts as Button *et al*., 2013. Twenty alemtuzumab-treated patients from the CAMMS223 trial (ClinicalTrials.gov identifier: NCT0050778) were scanned immediately before treatment then annually for 3 years (scans performed between 2003-2007). Twenty-two people from a natural history cohort with annual imaging were scanned three times between 1998-2003 (Davies *et al.*, 2005). In the alemtuzumab cohort, clinical follow-up (including Expanded Disability Status Scale (EDSS) scores (Kurtzke, 1983)) was undertaken every 3 months for 3 years then annually thereafter.

Ethical approval was granted by the joint ethics committee for the Institute of Neurology and the National Hospital for Neurology and Neurosurgery, Queen Square, London (for the natural

history cohort) and by local review boards and ethics committees (for the CAMMS223 cohort). Written informed consent was obtained from all participants.

Magnetic resonance imaging

All images were acquired using the same 1.5 T Signa scanner (General Electric, Milwaukee, USA) at the Institute of Neurology, University College London using the same protocol (Davies *et al.*, 2005). The acquisition included (i) dual echo T2-weighted/PD images of the whole brain (50x3mm contiguous axial-oblique slices parallel to the anterior/posterior commissural line, matrix 256x256, FOV 220x220mm, TR=3200ms) for lesion-identification and segmentation; (ii) T1-weighted spin-echo whole-brain images (50x3mm contiguous axial-oblique slices parallel to the anterior/posterior commissural line, matrix 256x256, FOV 220x220mm, TR=600ms, echo time=17ms) for segmentation; and (iii) 2D interleaved dual-echo, spin echo magnetisation transfer imaging of the whole brain (28x5mm contiguous axial-oblique slices parallel to the anterior/posterior commissural line with an interleaved sequence (TR=1720ms, echo time=30/80ms, number of excitations 0.75, matrix 256x256, FOV 240x240mm, magnetisation transfer-weighted by the application of pre-saturation pulse (Hamming apodized 3 lobe sinc pulse, duration 64ms, flip angle 1430°, peak amplitude of 14.6mT giving a normal bandwidth of 62.5Hz, applied 1 kHz from the water resonance)).

The scanner was upgraded in April 2004; statistical analyses were adjusted to account for the small resultant MTR step-increase.

Image analysis

WM lesions were outlined on PD/T2-weighted images by TB using JIM v5.0 (Xinapse systems, Aldwincle, UK). The WM lesion mask was then resampled from PD/T2 to T1-weighted image

space using a transformation obtained by registering the pseudo-T1 image (generated from the PD/T2-weighted image (Hickman *et al.*, 2002)) to the T1-weighted image. Lesion filled T1-weighted images (Popescu *et al.*, 2014; Prados *et al.*, 2016) were segmented into WM, cortical grey matter (GM), deep GM and CSF using the GIF algorithm (Cardoso *et al.*, 2015) and tissue masks were binarised with a 90% probabilistic threshold (Brown *et al.*, 2017). These segmentations were also used to calculate brain parenchymal fraction, calculated as follows: (GM volume + WM volume) / (GM volume + WM volume + CSF volume).

Lesions were dilated by 2 voxel layers to remove perilesional MTR abnormalities (Vrenken *et al.*, 2006), then subtracted from the WM segmentations to produce NAWM masks. MTR maps were calculated in T1-weighted image space on a voxel-by-voxel basis as follows: MTR (in pu) = (((MT$_{off}$ - MT$_{on}$) / MT$_{off}$) x100) using the short-echo data because of its higher signal-to-noise ratio.

The whole brain was segmented into 12 concentric bands between the ventricular walls and pial surfaces using the normalised distance map derived from the Laplace equation isolines between the two surfaces (Yezzi and Prince, 2003; Pardini *et al.*, 2016). The NAWM mask was superimposed over these bands (removing the deep GM (DGM) and cortical GM) then applied to the MTR maps, generating 12 bands of NAWM. Consistent with previous work using 2D MTR data (Brown *et al.*, 2017), the first two (periventricular) bands were excluded to mitigate partial-volume effects with CSF (Figure 4).

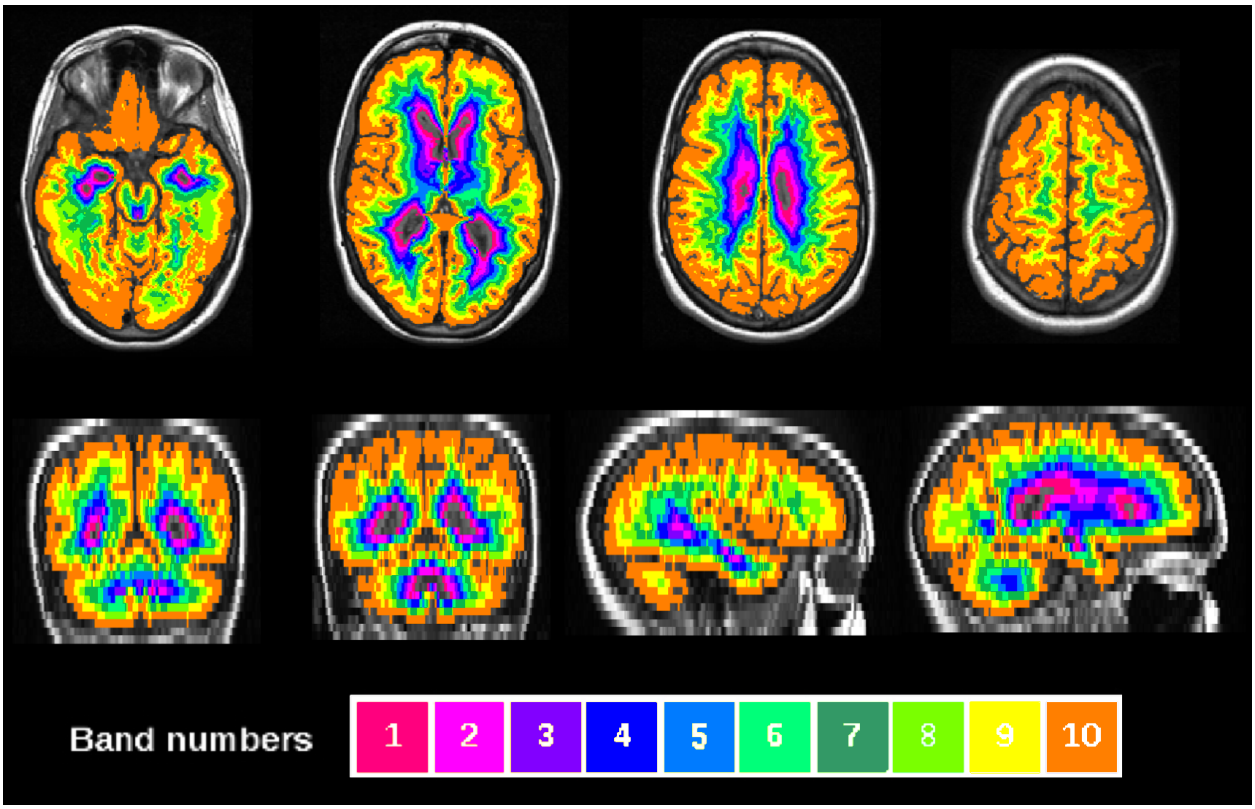

Figure 4: Brain segmentation into 12 concentric bands using the iterative application of the normalised central curve of the Laplace equation. The first 2 periventricular bands were excluded to mitigate partial volume effects, leaving 10 bands. Each band is represented by a different colour.

Statistics

Mean and standard error MTR (in pu) were calculated in each band, the periventricular NAWM (over the first 3 bands), the whole brain NAWM, the DGM and the cortical GM. Mean and standard error periventricular MTR gradients were calculated over the first three bands adjacent to the ventricles ((MTR in NAWM band 3 – MTR in NAWM band 1)/2) as previously described (Pardini *et al.*, 2016). Higher periventricular gradients are more abnormal; while higher mean MTR values are less abnormal.

Nested mixed-effects models adjusted for age, gender, prior relapse rate, BPF, scanner upgrade status and multiple comparisons compared the change in (i) periventricular NAWM MTR

gradients; and for comparison (ii) mean whole brain NAWM MTR and (iii) mean DGM MTR between the alemtuzumab and untreated groups. Further mixed-effects models adjusted for the same covariates compared the baseline (i) periventricular MTR gradient, (ii) mean whole brain NAWM MTR and (iii) mean DGM MTR between those who did or did not relapse following treatment with alemtuzumab. We used a 4-year cut-off (reflecting the time when half of those that relapsed had done so); and performed sensitivity analyses using different cut-offs. We previously reported the predictive value of the periventricular MTR gradient in untreated patients following a clinically-isolated ON (Brown *et al.*, 2017), in which 3D MTR was used in more patients (n=71) compared to the present study. The present study necessarily excluded patients in the untreated cohort that began disease-modifying treatment before their finals scan. However, for completeness, we repeated our analyses in this smaller untreated cohort and report them seperately (p.**Error! Bookmark not defined.**).

To determine whether or not changes in the periventricular MTR gradient were independent of lesional changes, we repeated each statistical model additionally adjusting for change in WM lesion number (first adjusting for change in whole brain lesion number; then adjusting for change in periventricular lesion number (calculated over the first 3 bands)). To explore whether changes in periventricular MTR gradient were distinct from more diffuse MTR changes, we additionally adjusted each MTR gradient model for change in periventricular NAWM MTR and whole brain NAWM MTR; and each mean whole brain NAWM MTR model for change in periventricular MTR gradient.

Spearman rank statistics explored the correlations between (i) changes in whole brain NAWM MTR and periventricular MTR gradient (to further examine the relationship between the two metrics); and (ii) periventricular gradient and EDSS score. Statistics were performed in R (v3.3.1). Results were considered statistically significant at the $p<0.05$ level.

Chapter 3: Methods – The effect of disease-modifying therapies on conversion to secondary progressive multiple sclerosis

Project 4

Performed in collaboration with Alasdair Coles (joint first author); plus Dana Horakova, Eva Havrdova, Guillermo Izquierdo, Alexandre Prat, Marc Girard, Pierre Duquette, Maria Trojano, Alessandra Lugaresi, Roberto Bergamaschi, Pierre Grammond, Raed Alroughani, Raymond Hupperts, Pamela McCombe, Vincent Van Pesch, Patrizia Sola, Diana Ferraro, Francois Grand'Maison, Murat Terzi, Jeannette Lechner-Scott, Schlomo Flechter, Mark Slee, Vahid Shaygannejad, Eugenio Pucci, Franco Granella, Vilija Jokubaitis, Mark Willis, Claire Rice, Neil Scolding, Alastair Wilkins, Owen R Pearson, Tjalf Ziemssen, Michael Hutchinson, Katharine Harding, Joanne Jones, Christopher McGuigan, Helmut Butzkueven, Tomas Kalincik and Neil Robertson.

My role: conception and design of study; analysis of data with assistance from Tomas Kalincik; wrote manuscript and amended following co-author and journal reviews. Contributed to data collection.

Ethical approval was granted by the Melbourne Health Human Research Ethics Committee and by each site's institutional review board. All enrolled patients provided written or verbal consent, as per local regulations.

Patients and inclusion criteria

This international observational cohort study utilised prospectively-collected clinical data from three sources (all accessed in February 2017). Untreated patients were selected from the neuroinflammatory service database at the University Hospital of Wales, a tertiary referral centre in South-East Wales. Clinical data was initially collected as part of a cross-sectional study (Swingler and Compston, 1988) then through annual or semi-annual appointments. Treated patients were identified from MSBase, an observational cohort study collecting real-world data from patients with MS across 105 centers in 29 countries (Ingram *et al.*, 2010). Additional alemtuzumab-treated patients were identified from five European non-MSBase centers using alemtuzumab before it was licensed (Bristol, Cardiff, Swansea, Dublin and Dresden (Kalincik *et al.*, 2017a)). Within MSBase, glatiramer acetate or interferon beta, fingolimod and natalizumab had sufficient patient numbers with more than 4-years on-treatment follow-up (while teriflunomide and dimethyl-fumarate did not, so they were not included). The 4-year minimum follow-up period represented the longest follow-up period without excluding the majority of patients in MSBase treated with natalizumab or fingolimod. Data were subject to rigorous data-quality procedures (see p.139).

For inclusion, patients needed to be classified as RRMS (clinically definite MS (Poser *et al.*, 1983)) at baseline, required the complete MSBase minimum dataset (sex, date of birth, date of clinical onset and dates of relapses (Butzkueven *et al.*, 2006)), at least one EDSS score (Kurtzke, 1983) no more than 6 months before baseline and at least two EDSS scores after baseline (one to detect

disability progression and another to confirm the increase later (see definition below)). Patients stopping their initial therapy within 6 months were excluded (as some drugs require 6 months to exert their effect (Freedman *et al.*, 2013)). The untreated cohort received no DMTs, even briefly. DMT dose, frequency and timing followed published protocols (He *et al.*, 2015; Kalincik *et al.*, 2017a): alemtuzumab (12–24 mg intravenous once per day for 5 days [cycle 1] or for 3 days [cycle 2 or more]); interferon-β-1a (30-250 μg subcutaneous or intramuscular injections administered between every other day to every other week); glatiramer acetate (20 mg subcutaneous injection once per day); fingolimod (0·5 mg oral once per day), and natalizumab (300 mg intravenously every 4 weeks). Given its administration schedule, quantifying the duration of alemtuzumab treatment effectiveness is challenging: first, the published period of reduced CD4 lymphocyte count (35 months/cycle (Hill-Cawthorne *et al.*, 2012)) was used, and then a sensitivity analysis using the median period to re-treatment (7 years (Willis *et al.*, 2016)) was performed. If patients received multiple DMTs, the first was used as the DMT under study (except when comparing early versus late escalation from interferon-β-1a or glatiramer acetate to fingolimod, alemtuzumab or natalizumab). Patients subsequently receiving different DMTs were excluded from analyses of single drugs versus untreated patients but were included in all other analyses. Patients receiving therapies at any time during the study period that were unlicensed were excluded (mitoxantrone, cladribine, rituximab, ocrelizumab, siponimod or autologous stem-cell transplantation). Although ocrelizumab and cladribine have subsequently been licensed, there were insufficient numbers meeting the minimum 4 years' clinical follow-up criterion within MSBase to examine individually.

No licensed therapies have shown greater reduction in relapse rates than natalizumab or alemtuzumab (Kalincik *et al.*, 2017a). Patients receiving natalizumab or alemtuzumab who experienced relapses or disability-progression in this study were therefore already at the

therapeutic ceiling of treatment. This was replicated for patients receiving glatiramer acetate or interferon beta (in all analyses) by restricting inclusion to patients treated and followed-up before fingolimod, alemtuzumab or natalizumab became available, preventing the exclusion of patients who might have been prescribed these more potent therapies as first-line or escalation therapy during follow-up, and thereby preventing selection bias towards milder disease among the glatiramer acetate / interferon beta group. (During this period, mitoxantrone was occasionally employed as escalation therapy for particularly aggressive disease: to ensure the glatiramer acetate / interferon beta cohorts were not biased towards milder disease, sensitivity analyses including these patients were performed). Consistent with previous work, patients participating in clinical trials were excluded as their trial treatment assignation was not documented within MSBase, and trial EDSS frequencies often differ to clinical practice (Kalincik *et al.*, 2017a). Patients with previous stem cell transplantation were also excluded.

Study design

To examine whether individual DMTs were associated with delayed or reduced conversion to SPMS, matching and analyses were repeated four times comparing untreated patients to those receiving initial treatment with (a) glatiramer acetate or interferon beta, (b) fingolimod, (c) natalizumab, or (d) alemtuzumab. In these analyses, the date of DMT commencement acted as the baseline date for treated patients. For untreated patients, the baseline date was the visit date when clinical and demographic parameters (calculated at each visit and quantified using the propensity score) most closely matched the corresponding baseline values of individual treated patients.

Fingolimod (Cohen *et al.*, 2010), alemtuzumab (Coles *et al.*, 2008) and natalizumab (Spelman *et al.*, 2016) confer greater reductions in relapse rate than glatiramer acetate or interferon beta. To

examine whether they are associated with different effects on conversion to SPMS, patients receiving fingolimod, alemtuzumab or natalizumab as their initial DMT were matched and compared to patients initially treated with glatiramer acetate or interferon beta.

To examine the association between timing of DMT commencement and conversion to SPMS, patients initially treated with glatiramer acetate or interferon beta within 5 years of disease onset were matched and compared with those initially treated after 5 years. For patients treated within 5 years, the baseline was set at DMT commencement. For all patients treated after 5 years, the baseline was set at a visit within 5 years of symptom-onset, before therapy began, incorporating the period from baseline to treatment initiation into the follow-up. The date of this visit was identified by extracting the matching variables at each eligible visit within 5 years of symptom-onset, then using a matching process to identify when these variables most closely matched those of a patient treated within 5 years. By handling treatment exposure as a time-dependent variable, the analyses accounted for immortal time bias, including the untreated time from baseline to treatment initiation in the group treated after 5 years. This technique was repeated when comparing escalation from glatiramer acetate or interferon beta to fingolimod, alemtuzumab or natalizumab within or after 5 years of disease onset.

Outcome

The outcome in all analyses was conversion to SPMS based on an objective definition without functional scores (Lorscheider *et al.*, 2016): patients required an EDSS increase (if the EDSS score was 5.5 or less, an increase of 1 point was required; if the EDSS score was over 5.5 an increase of 0.5 points was required). This EDSS increase had to (i) occur in the absence of a relapse, (ii) be confirmed at subsequent appointments over at least 3 months; and (iii) reach an EDSS score of 4 or more.

Matching

Using the MatchIt package (v2.4-22) the propensity of treatment was estimated using a multivariable logistic regression model using baseline age, sex, annualised-relapse rate in the year prior to baseline, EDSS score and disease duration. To minimise the difference in proportions of time on therapy during follow-up in the glatiramer acetate / interferon beta versus fingolimod / alemtuzumab / natalizumab analysis, patients were additionally matched on the proportion of time on therapy during the median follow-up period (first 5.8 years). Patients in the early versus late escalation from glatiramer acetate / interferon beta to fingolimod / alemtuzumab / natalizumab analysis were also matched on disease duration at the time of starting glatiramer acetate or interferon beta plus the individual therapy they were escalated to. To increase matching precision (Rassen *et al.*, 2012; Kalincik *et al.*, 2017a), patients were matched in a variable matching ratio (10:1 to 1:1) by nearest neighbour matching using the optimal caliper (0.1 standard deviations (SD) of the propensity score (Austin, 2011; Lunt, 2014)). Where treatment initiation was not used as the baseline (the late group in the early versus late glatiramer acetate or interferon beta and escalation analyses; and the untreated group in all untreated analyses), any visit could serve as baseline (to optimise matching). Consequently, multiple treatment periods from the same patient could be matched to different patients in the respective early or treated groups in these analyses. To prevent these patients contributing disproportionately, the matching regression models for these analyses allowed replacement of these early or treated patients such that they too could also contribute multiple times to these analyses. Additionally, all subsequent models were weighted to account for the variable matching ratio (see below). Each patient's follow-up was censored to the shortest of the two follow-up times from each set, resulting in identical follow-up durations between groups. Sets where either patient subsequently had less than two EDSS scores following baseline were excluded.

Statistics

All analyses were performed using the survival package (v3.3.1) in R. Setwise weighted conditional proportional hazards models (Cox) clustered for matched patient sets examined the proportions of patients free from conversion to SPMS. All models were adjusted for EDSS frequency plus any variables showing residual imbalance following matching (as denoted by a standardised difference (quantified by Cohen's d value) ≥ 0.2 (Cohen, 1988) (which indicates less than 92% overlap between the groups)). The weights were calculated as the inverse of the number of times a patient was included in an analysis to account for the variable matching ratio. The models comparing (i) glatiramer acetate or interferon beta with fingolimod, alemtuzumab or natalizumab, (ii) early versus late glatiramer acetate or interferon beta and (iii) early versus late escalation from glatiramer acetate or interferon beta to fingolimod, alemtuzumab or natalizumab were also adjusted for the proportion of time on therapy during the entire post-baseline setwise-censored follow-up. The Schoenfeld's global test was used to detect violation of the proportional hazards assumption (Schoenfeld, 1980); when violated, Weibull accelerated failure time regression models were used. To estimate the conditional hazard ratio, robust estimation of variance based on the Huber sandwich estimator was used. The Efron approximation was used to resolve tied survival times. Graphs were censored at the latest point that each group contained at least 10 patients or less than 10% of the original group, whichever came first. The percentage of patients that had converted to SPMS are presented at 5 years and the last year before censor in the text. Two-sided significance testing was used. Results were considered significant at the $p<0.05$ level. Because there was no adjustment for multiple comparisons, secondary analyses should be interpreted as exploratory.

Chapter 4: Results – Outside-In Gradients

This chapter details results from the imaging studies (Projects 1-3),

Project 1: Periventricular gradients after a clinically isolated syndrome

This work was published in Brain, 2017:

Brown JW, Pardini M*, Brownlee WJ, Fernando K, Samson RS, Prados Carrasco F, et al. An abnormal periventricular magnetization transfer ratio gradient occurs early in multiple sclerosis. Brain : a journal of neurology 2017; 140(Pt 2): 387-98. *Joint First Author*

There were no significant demographic differences between the clinically isolated ON group and controls (Table 3). At the three-month scan, 55/71 (77.5%) of the ON group had WM lesions, 46/71 (64.8%) had periventricular lesions and 22/71 (31.0%) had gadolinium-enhancing lesions. Thirteen patients were lost to follow-up. After two years, 18/58 (31%) had experienced a further clinical relapse and so developed CDMS while 40/58 (69%) had McDonald MS. Five years after ON, these figures had risen to 31/58 (53.5%) and 45/58 (77.6%) respectively.

	Healthy Controls	**People with optic neuritis**
N	N = 37	N = 71
Mean age, years ± SD (range)	34.4 ± 4.8 (27-47)	33.5 ± 6.7 (20-48)
Female : male	25 : 12	49 : 22
Median baseline EDSS (range)	-	1 (0-3)

Number with abnormal T2 scan (excluding symptomatic lesion)	-	55
Number with periventricular lesions	-	46
Number with Gd-enhancing lesions	-	22
Mean T2 lesion volume (ml) ± SD	-	1.47 ± 3.32
Mean brain parenchymal fraction ± SD	0.84 ± 0.04	0.85 ± 0.03
Number attaining CDMS at time of MTR scan	-	8
Number attaining McDonald MS at time of MTR scan	-	33
Number with clinical follow-up at two and five years	-	58
Number converting to CDMS within two years of ON (of 58 with clinical follow up)	-	18
Number converting to McDonald MS within two years of ON (of 58 with clinical follow up)	-	40
Number converting to CDMS within five years of ON (of 58 with clinical follow up)	-	31
Number converting to McDonald MS within five years of ON (of 58 with clinical follow up)	-	45
Median (range) EDSS score at five year follow-up (assessed in 50/58)	-	1 (0-8.5)
Median (range) PASAT score at five years follow-up (assessed in 31/58)	-	46.5 (17-59)

Table 3: Baseline demographics. In the optic neuritis group, MTR scans were undertaken three months after first enrolment in the study, and so lesion measures from scans obtained at three months are shown. Volumetric brain scans were acquired at baseline but not three months. CDMS = clinically definite multiple sclerosis. EDSS = Expanded Disability Status Scale. ON = optic neuritis. PASAT = paced serial addition test, 3 second intervals. SD = standard deviation.

Band	*Mean ± SE MTR in pu*		*Mean ± SE MTR in pu*		
	Healthy controls **(n=37)**	All Optic Neuritis **(n=71)**	**Optic Neuritis subgroups**		
			Converted to CDMS <2y ***(n=18)***	Converted to CDMS 2-5y ***(n=13)***	Did not convert to CDMS ***(n=27)***
1	38.364 ± 0.138	**37.670 ± 0.102 p = 0.000**	**37.371 ± 0.183 p = 0.000**	37.831 ± 0.180 p = 0.062	**37.805 ± 0.203 p = 0.013**
2	38.334 ± 0.113	**37.836 ± 0.085 p = 0.001**	**37.639 ± 0.166 p = 0.001**	**37.773 ± 0.205 p = 0.020**	**37.951 ± 0.156 p = 0.043**
3	38.254 ± 0.095	**37.912 ± 0.080 p = 0.007**	37.862 ± 0.176 p = ns	37.946 ± 0.209 p = ns	37.903 ± 0.133 p = ns
4	38.293 ± 0.080	**37.959 ± 0.075 p = 0.003**	37.944 ± 0.158 p = ns	37.942 ± 0.190 p = ns	37.918 ± 0.132 p = ns
5	38.232 ± 0.080	**37.936 ± 0.076 p = 0.009**	37.901 ± 0.163 p = ns	37.916 ± 0.204 p = ns	37.859 ± 0.126 p = ns
6	38.109 ± 0.087	**37.827± 0.077 p = 0.017**	37.822 ± 0.162 p = ns	37.807 ± 0.209 p = ns	37.765 ± 0.129 p = ns
7	38.006 ± 0.083	**37.751 ± 0.074 p = 0.025**	37.751 ± 0.166 p = ns	37.772 ± 0.194 p = ns	37.706 ± 0.124 p = ns
8	38.024 ± 0.084	**37.774 ± 0.073 p = 0.027**	37.754 ± 0.174 p = ns	37.805 ± 0.192 p = ns	37.740 ± 0.115 p = ns
9	38.113 ± 0.084	**37.864 ± 0.075 p = 0.030**	37.805 ± 0.187 p = ns	37.942 ± 0.192 p = ns	37.822 ± 0.117 p = ns
10	38.187 ± 0.085	**37.952 ± 0.078 p = 0.044**	37.850 ± 0.191 p = ns	38.048 ± 0.198 p = ns	37.945 ± 0.123 p = ns

Table 4: Mean band MTR in healthy controls and patients with optic neuritis. Independent sample t-tests were used to compare the healthy control and whole optic neuritis groups; one-way ANOVA to compare the optic neuritis subgroups. pu = percentage units; ns = not significant. Bold P-values < 0.05.

Periventricular MTR gradients in ON compared with controls

Table 4 and Figure 5 show the mean and standard error (SE) NAWM MTR per band in the ON and control groups. The mean MTR of each NAWM band was lower in the ON group than in healthy controls. In controls, mean MTR was highest in the bands nearest the ventricles and declined with distance from them. In contrast, in the ON group, mean MTR was lowest in the band nearest the ventricles, increased over the first 5mm and then paralleled control values.

Over the first 5mm from the ventricles, we found significantly different MTR gradients between the ON and control groups (ON: mean +0.059 pu/mm ± 0.028; controls mean -0.033 pu/mm ± 0.028, t=-2.62, p=0.010). This difference remained significant after adjustment for BPF (p=0.009). Conversely, the MTR gradient over the next five bands showed no significant difference between the groups (ON: +0.003 pu/mm ± 0.008, controls -0.009 pu/mm ± 0.012, p=0.541).

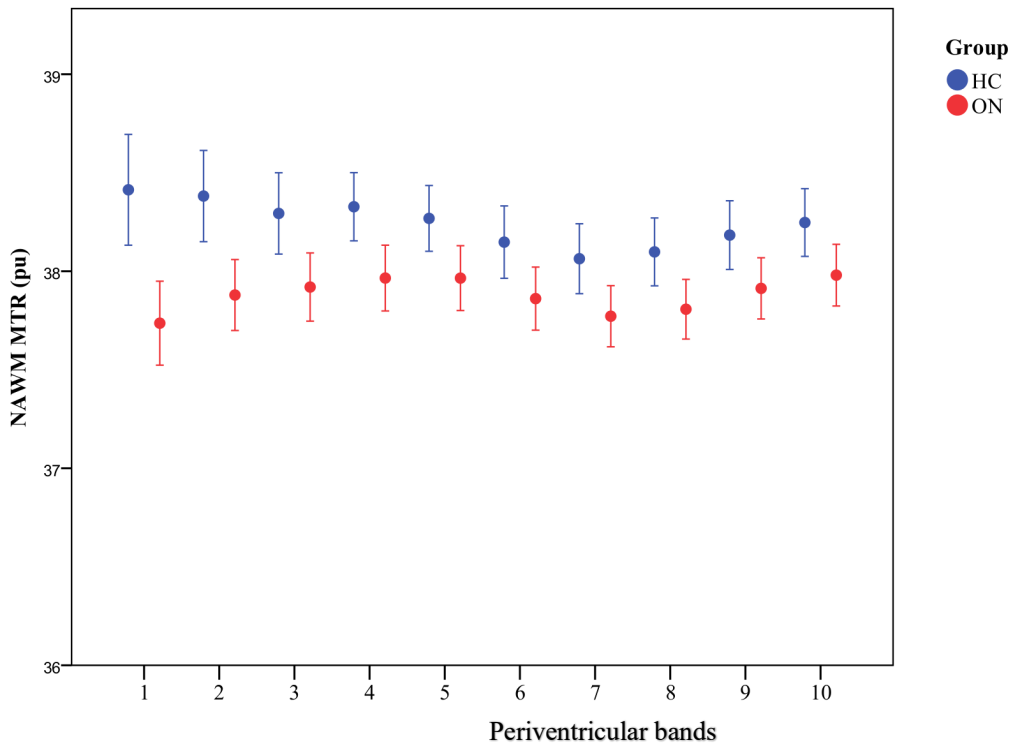

Figure 5: Normal-appearing white matter (NAWM) MTR of bands in healthy controls (HC - blue) and people with optic neuritis 4.6 months after symptom onset (ON - red). Mean ± 2 standard error (SE). MTR is expressed as percentage units (pu). Band 1 is closest to the ventricular surface.

Associations of periventricular MTR gradients with lesions

In the ON group, over the first 5mm periventricular MTR gradients did not differ significantly between those with or without brain WM lesions seen on a T2-weighted scan from the same scanning session (+0.058 pu/mm ± 0.024 vs +0.063 pu/mm ± 0.043 respectively, p=0.918), Figure 6. The periventricular MTR gradient in the ON group who did not have brain lesions showed a non-significant trend to be higher than healthy controls (+0.063 pu/mm ± 0.043 vs -0.033 pu/mm ± 0.028 respectively, p=0.064).

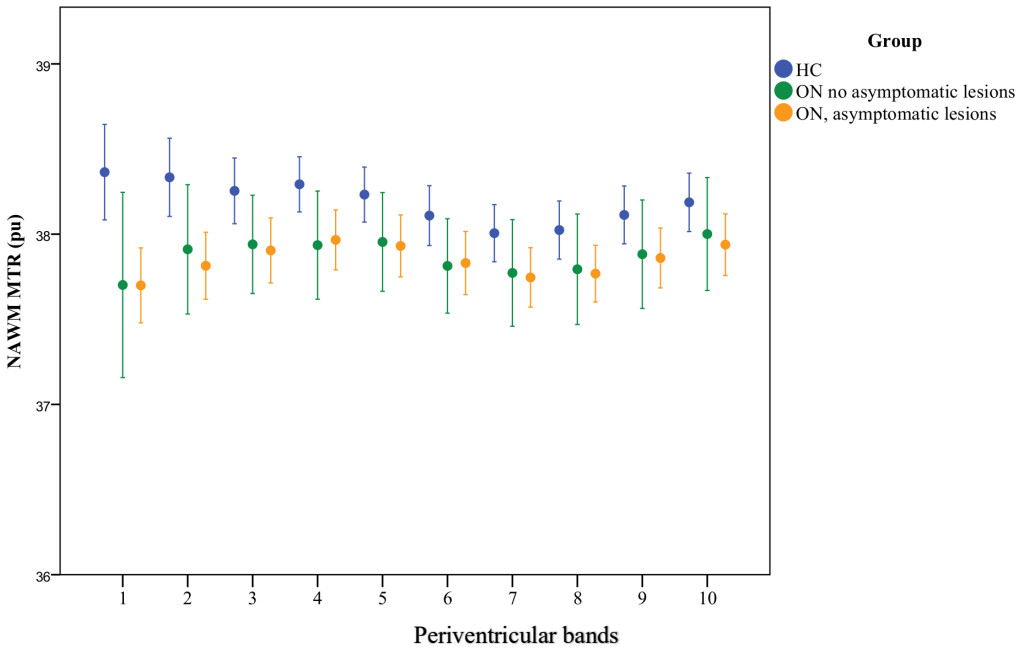

Figure 6: Normal appearing white matter (NAWM) MTR in healthy controls (HC - blue) and people with optic neuritis 4.6 months after symptom onset (ON), divided into those with (green) and without (yellow) lesions on their baseline scan. Mean ± 2 standard errors (SE) is shown. MTR is expressed as percentage units (pu). Band 1 is closest to the ventricular surface.

The presence of periventricular lesions seen on a T2-weighted scan had no significant effect on the periventricular gradient (0.068 pu/mm ± 0.028 (with periventricular lesions) vs 0.043 pu/mm ± 0.030 (without periventricular lesions), p=0.580, Figure 7). The mean gradient in those with and without gadolinium-enhancing lesions similarly did not differ significantly (0.067 pu/mm ± 0.040 vs 0.055 pu/mm ± 0.025 respectively, p=0.794).

Associations of periventricular MTR gradients with conversion to MS and disability

Table 5 and Figure 8 show the gradients over the first and second 5mm of NAWM extending from the ventricles in the ON groups who did or did not develop CDMS within two years.

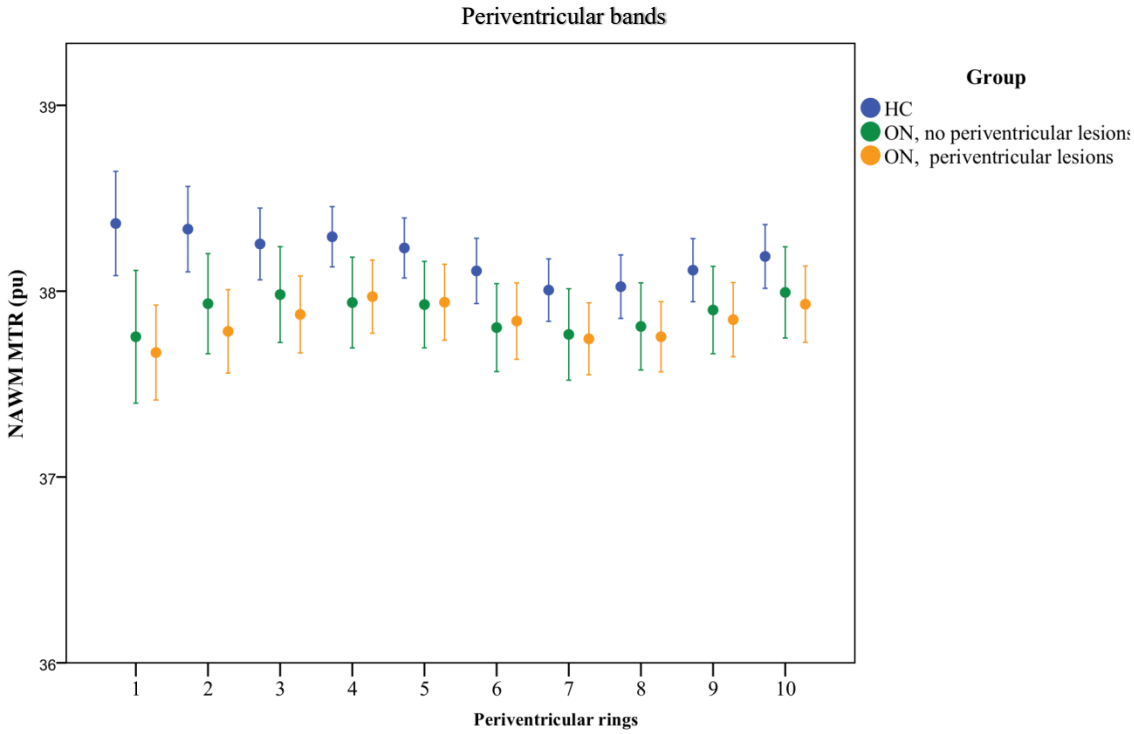

Figure 7: Normal appearing white matter (NAWM) MTR in people with optic neuritis 4.6 months after symptom onset (ON) plus lesions, divided into those with (n=46, green circles) and without (n=9, yellow circles) periventricular lesions. Mean ± 2 standard error (SE). MTR is expressed as percentage units (pu). Band 1 is closest to the ventricular surface.

	Clinical classification at 2 years	**N**	**MTR gradient mean ± SE (pu/mm)**	
			Periventricular (1 to 5 mm)	*Deep (6 to 10 mm)*
Healthy controls		37	-0.033 ± 0.028	-0.009 ± 0.012
Optic Neuritis	Did not convert to CDMS	40	0.016 ± 0.029	0.020 ± 0.010
	Converted to CDMS	18	0.132 ± 0.041*	-0.010 ± 0.019
	Did not convert to McDonald MS	18	0.015 ± 0.048	0.021 ± 0.015
	Converted to McDonald MS	40	0.069 ± 0.028**	0.006 ± 0.011

*Table 5: Periventricular (1-5mm) and deep (6-10mm) MTR gradients in normal appearing white matter (NAWM) of people with optic neuritis (ON) and healthy controls (HC). Optic neuritis group divided according to conversion to clinically definite multiple sclerosis (CDMS) status within two years. *Converters vs. healthy controls p=0.001, converters vs. non-converters: p=0.020, non-converters vs. healthy controls p=0.221). Optic neuritis group also divided according to conversion to McDonald MS within two years. **converters vs healthy controls p=0.014; otherwise, no significant differences in gradients detected.*

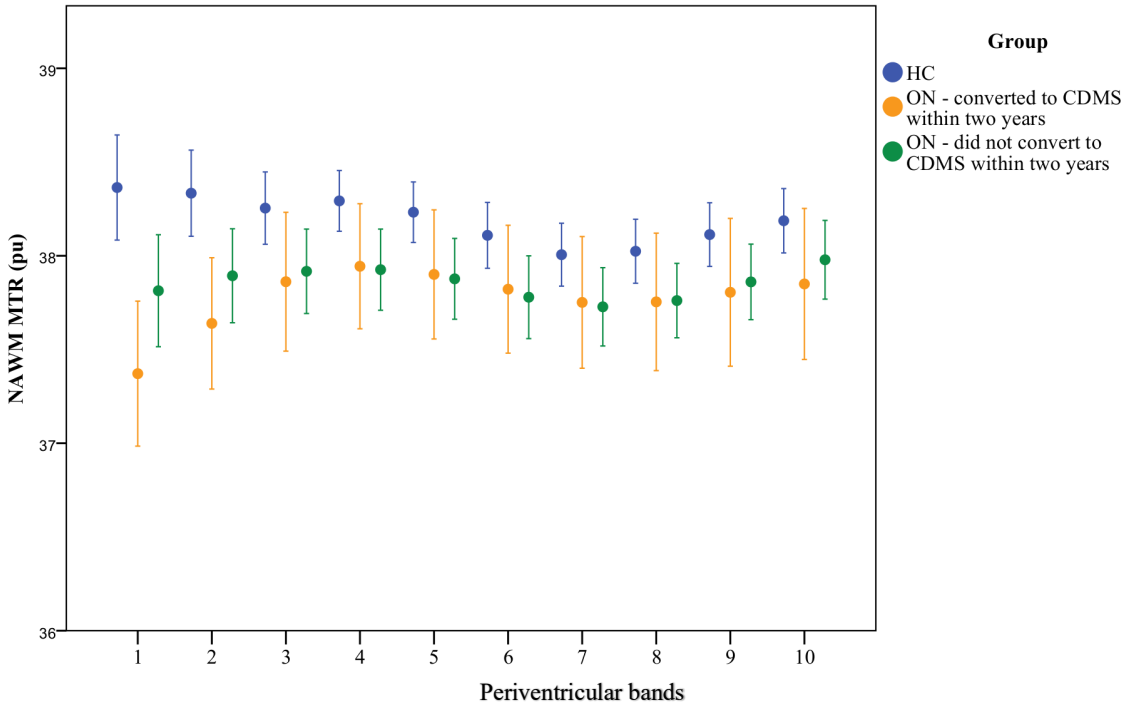

Figure 8: Normal appearing white matter (NAWM) MTR in healthy controls (HC - blue) and people with optic neuritis 4.6 months after symptom onset (ON), divided into those who did convert to clinically definite multiple sclerosis (CDMS) within two years (gold) and those that did not (green). Mean ± 2 standard errors (SE) is shown. MTR is expressed as percentage units (pu). Band 1 is closest to the ventricular surface.

The periventricular MTR gradient in the group who developed CDMS within two years differed from healthy controls and the ON group who did not convert to CDMS within two years (Table 5; overall effect p=0.006; converters vs. healthy controls p=0.001, converters vs. non-converters p=0.020, non-converters vs. healthy controls p=0.221). The periventricular MTR gradient also differed between those who converted to CDMS within five years and healthy controls, while the difference between converters and non-converters did not reach significance; overall effect p=0.026; converters vs. healthy controls p=0.007, converters vs. non-converters p=0.123, non-converters vs. healthy controls p=0.304). The differences between those who developed MS and HC remained significant when McDonald MRI criteria were used instead of CDMS (Table 5). The group effect on the periventricular MTR gradient did not materially change after including BPF in

the statistical models. The group effect on the periventricular MTR gradient also remained significant after adjustment for mean NAWM MTR (p=0.014) and mean GM MTR (p=0.022). When both NAWM MTR and GM MTR were added, the model remained significant (p=0.021) as did differences in MTR gradients between converters and non-converters (p=0.037) and between converters and healthy controls (p=0.006).

We also examined whether or not periventricular MTR gradients over 1-5mm had an effect on conversion to CDMS independent of the presence of lesions. A multivariate binary logistic regression showed that the MTR gradient over 1-5mm was independently associated with conversion to CDMS at two years (MTR gradient: odds ratio (OR) 61.708 p=0.023; presence of T2 lesions OR 8.500 p=0.071). A similar pattern was seen when the MTR gradient was compared to periventricular T2 lesions (MTR gradient: OR 44.100 p=0.029; presence of periventricular T2 lesions OR 5.84 p=0.040). However, the MTR gradient did not predict conversion to CDMS over five years.

There was no significant difference in 6-10 mm MTR gradients between ON groups who did or did not develop CDMS at two or five years (p=0.124 and *p*=0.231 respectively).

Unlike the periventricular MTR gradient, the mean MTR of band 1 or 5 in the ON group converting to CDMS within 2 years was not significantly higher than in those not converting to CDMS (see p.97).

Associations of MTR gradient, mean NAWM MTR and mean GM MTR with disability.

A weak correlation was found between the MTR gradient over the first 5mm and EDSS status five years later (Spearman r=0.313, p=0.027; EDSS measured in 50/58 patients at this time point). No significant correlation was found between inner MTR gradient and PASAT score at five years (*p*=0.815), although this was only undertaken in 31/58 patients at this time point.

No significant correlations were found between EDSS five years later and mean MTR in band 1 (p=0.165) or band 5 (p=0.540), NAWM MTR (p=0.506) or GM MTR (p=0.109).

Lesion measures

The mean MTR of lesional voxels, like the NAWM MTR, was lowest at the ventricular margin and increased with distance from it (see Figure 9). The percentage of lesional WM per band is shown in Figure 10.

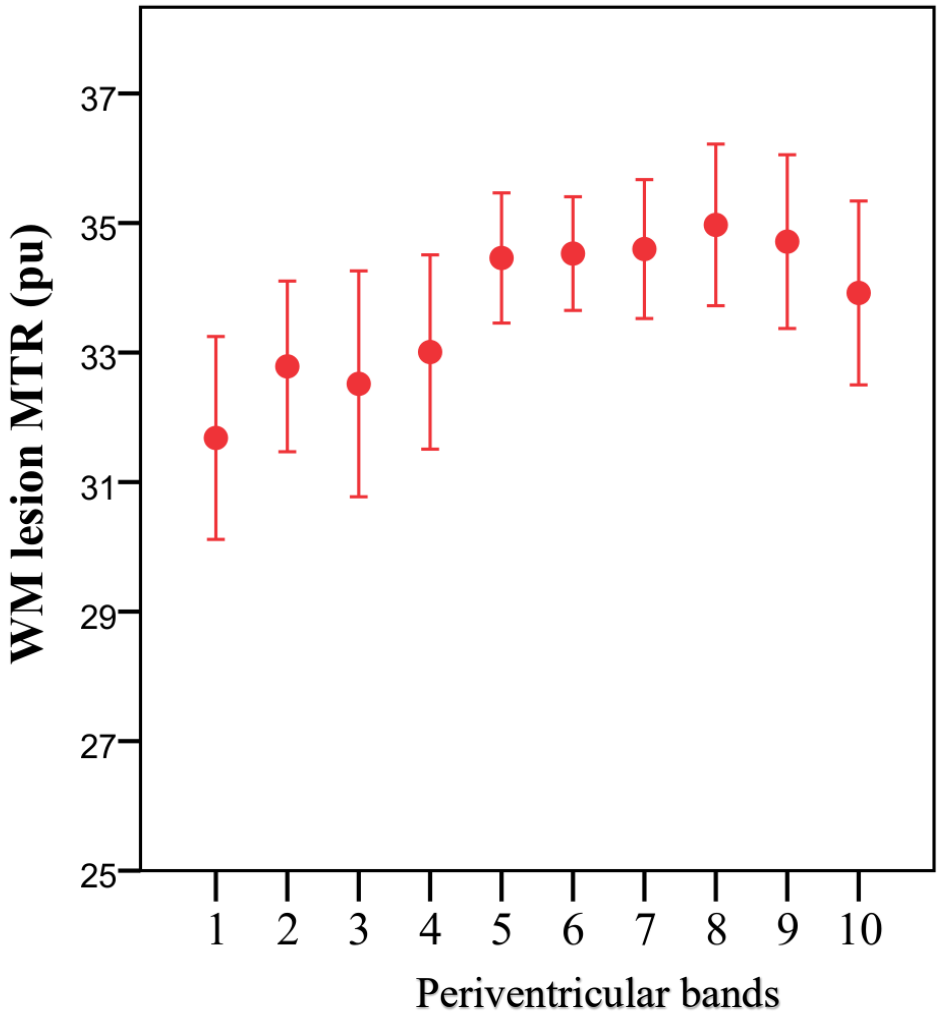

Figure 9: Mean MTR of white matter (WM) lesional voxels in patients with optic neuritis 4.6 months after symptom onset (ON). Mean ± 2 standard error (SE). MTR is expressed as percentage units (pu). Band 1 is closest to the ventricular surface.

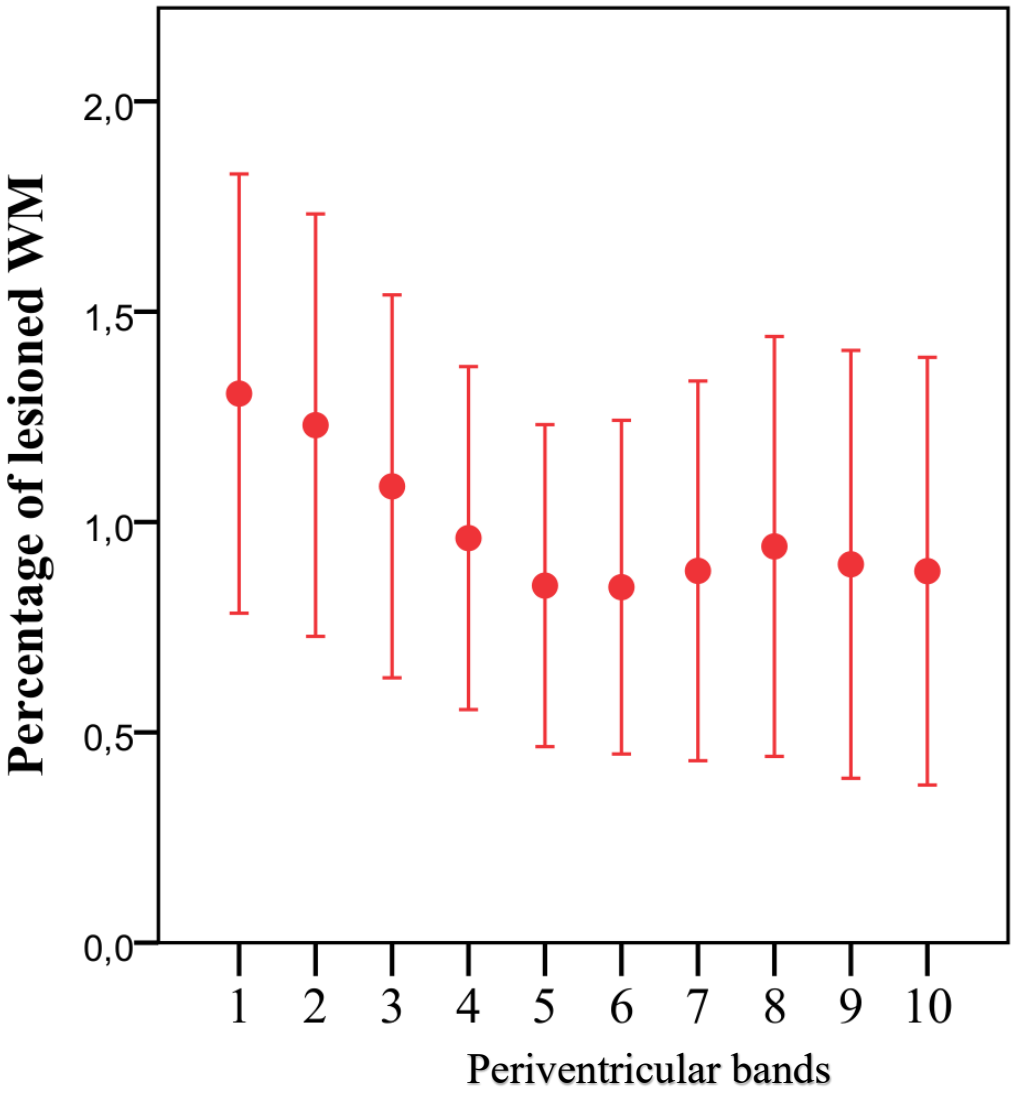

Figure 10: Percentage of lesional white matter (WM) per band in patients with optic neuritis 4.6 months after symptom onset (ON). Mean ± 2 standard error (SE). Band 1 is closest to the ventricular surface.

	People with optic neuritis		Significance
	People with clinical follow-up	**People without clinical follow-up**	
N	N = 58	N = 13	
Mean age, years ± SD (range)	33.5 ± 6.4 (27-48)	33.6 ± 8.1 (21-46)	*p* = 0.966
female : male	40 : 18	9 : 4	*p* = 1.000
Median baseline EDSS (range)	1 (0-3)	1 (0-2)	*p* = 0.585
Number with abnormal T2 scan (excluding symptomatic lesion)	46	9	*p* = 0.471
Number with periventricular lesions	40	6	*p* = 0.197
Number with Gd-enhancing lesions	19	3	*p* = 0.741
Mean brain parenchymal fraction ± SD	0.85 ± 0.04	0.85 ± 0.03	*p* = 0.388
Mean inner MTR gradient ± SE	0.05 ± 0.02	0.09 ± 0.04	*p* = 0.378

Table 6: Comparison of baseline clinical and radiological demographics in those with and without follow up at two and five years.

Comparative results: capability of mean MTR in band 1 and band 5 for predicting conversion to CDMS and EDSS at 5 years

Conversion to CDMS – band 1.

In one-way ANOVA, the mean MTR of band 1 in the ON group who developed CDMS within two years was significantly smaller than in healthy controls, but was not significantly different when compared to the ON group who did not develop CDMS within two years (converters vs healthy controls p=0.000; converters vs non-converters p=0.077; non-converters vs healthy controls

p=0.007). The results for conversion at five years were broadly similar (converters vs healthy controls p=0.000; converters vs non-converters p=0.301; non-converters vs healthy controls p=0.014).

Conversion to CDMS – band 5.

In one-way ANOVA, the mean MTR of band 5 in the ON group who developed CDMS within two years was not significantly smaller than in healthy controls or the ON group who did not develop CDMS within two years (converters vs healthy controls p=0.062; converters vs non-converters p=0.893; non-converters vs healthy controls p=0.012). The results at five years were broadly similar (converters vs healthy controls p=0.031; converters vs non-converters p=0.764; non-converters vs healthy controls p=0.017).

Disability

We found no correlation between the mean MTR values in bands 1 and 5 with EDSS score at five years (p=0.165 and p=0.540 respectively).

Effect of conversion to CDMS before MTR scan.

As a confirmatory analysis we excluded those 8 ON subjects who converted to MS in the 3 month interval between the baseline clinical MRI and the MTR acquisition. Despite the reduced power, the pattern in group differences in periventricular MTR gradients was maintained: ON vs healthy controls (0.050 pu/mm ± 0.022 vs. -0.033 pu/mm ± 0.028, p=0.022); ON converting to CDMS within two years vs HC (0.114 pu/mm ±0.051 vs. -0.033 pu/mm ± 0.028, p=0.016); ON converting to CDMS within two years vs non-converters (0.114 pu/mm ± 0.051 vs. 0.016 pu/mm ± 0.028, p=0.102).

MTR gradient threshold calculations

The range of periventricular MTR gradients found in those who developed CDMS within 2 years (-0.20 to 0.40 pu/mm) compared to those who did not (-0.41 to 0.62 pu/mm) - and in those who developed McDonald MS within two years (-0.41 to 0.40 pu/mm) compared to those who did not (-0.35 to 0.62 pu/mm) - overlapped substantially, and there was no clear cut off beyond which conversion from a CIS to MS was inevitable. The same pattern was seen when examining conversion versus no conversion at 5 years (CDMS: -0.41 to 0.40 pu/mm; -0.35 to 0.62 pu/mm) (McDonald MS: -0.41 to 0.40 pu/mm; -0.35 to 0.62 pu/mm).

When we used the mean MTR gradient of the group who did not develop CDMS within 2 years as a cut-off (n=40), 13/18 (72%) of those converting to CDMS within 2 years had a greater MTR gradient; if a mean + 1 SD threshold is used, 7/18 (39%, expected by chance 16%); and greater than the mean + 2 SD 1/18 (6%, expected by chance 2%). In comparison, the proportion of controls exceeding these thresholds were: mean 14/37 (38%); mean + 1 SD 3/37 (8%); mean + 2 SD 1/37 (3%). When we repeated this using the mean MTR gradient of controls as the threshold (n=37), 15/18 (83%) of those converting to CDMS within 2 years had a greater MTR gradient compared to 26/40 (65%) of those not converting within 2 years; if a mean + 1 SD threshold was used, respectively 9/18 (50%) and 9/40 (23%) exceeded the threshold, and greater than the mean + 2 SD 4/18 (22%) and 1/40 (3%).

Project 2: Periventricular and cortical gradients in progressive multiple sclerosis

This work was published in Multiple Sclerosis Journal, 2019:

Brown JW, Chowdhury A*, Kanber B, Prados F, Eshaghi A, Sudre C, et al. Magnetisation transfer ratio abnormalities in primary and secondary progressive multiple sclerosis. Multiple Sclerosis Journal. [Accepted; In Press] *Joint First Author*

Imaging was performed in 51 healthy controls (12 with follow-up imaging after median 2.1 (range 1.5 – 2.7) years), 28 people with PPMS (14 with follow-up imaging after median 2.3 (range 1.2 – 3.5) years) and 35 people with SPMS (15 with follow-up imaging after median 1.6 (range 1.1 – 2.4) years). The control group were younger than either progressive group (Table 7), and the SPMS group had a greater proportion of females than the PPMS and control groups (all models were adjusted for age, gender and either NAWM volume or CGM volume).

The MTR in each band was greater in healthy controls compared to those with PPMS and SPMS (Figure 11, Figure 12). The NAWM periventricular gradient was significantly shallower in healthy controls (0.122 ± 0.038 pu/band) compared to those with both PPMS (0.952 ± 0.185 pu/band, $p < 0.0001$) and SPMS (1.360 ± 0.143 pu/band, $p < 0.0001$), Table 8, Figure 13.

	Healthy controls	**People with progressive multiple sclerosis**	
	N = 51	PPMS N = 28	SPMS N = 35
Mean age, years ± SD	41.7 ± 12.6	52.5 ± 9.3	53.9 ± 7.2
Female : male	27 : 24	18 : 10	26 : 9
Mean disease duration, y ± SD	N/A	13.61 ± 7.39	22.6 ± 10.33
Median (range) baseline EDSS	N/A	6 (3 – 8)	6 (4 – 8.5)
Number (%) with radiological follow-up	12 (24%)	14 (50%)	15 (43%)
Median (range) interval between MRI scans, years	2.1 (1.5 – 2.7)	2.3 (1.2 – 3.5)	1.6 (1.1 – 2.4)
Median (range) EDSS at follow-up	N/A	6 (2.5 – 8)	6.5 (5 – 8.5)

Table 7: Participant baseline demographics. SD=standard deviation. EDSS=Expanded Disability Status Scale; NA=not available.

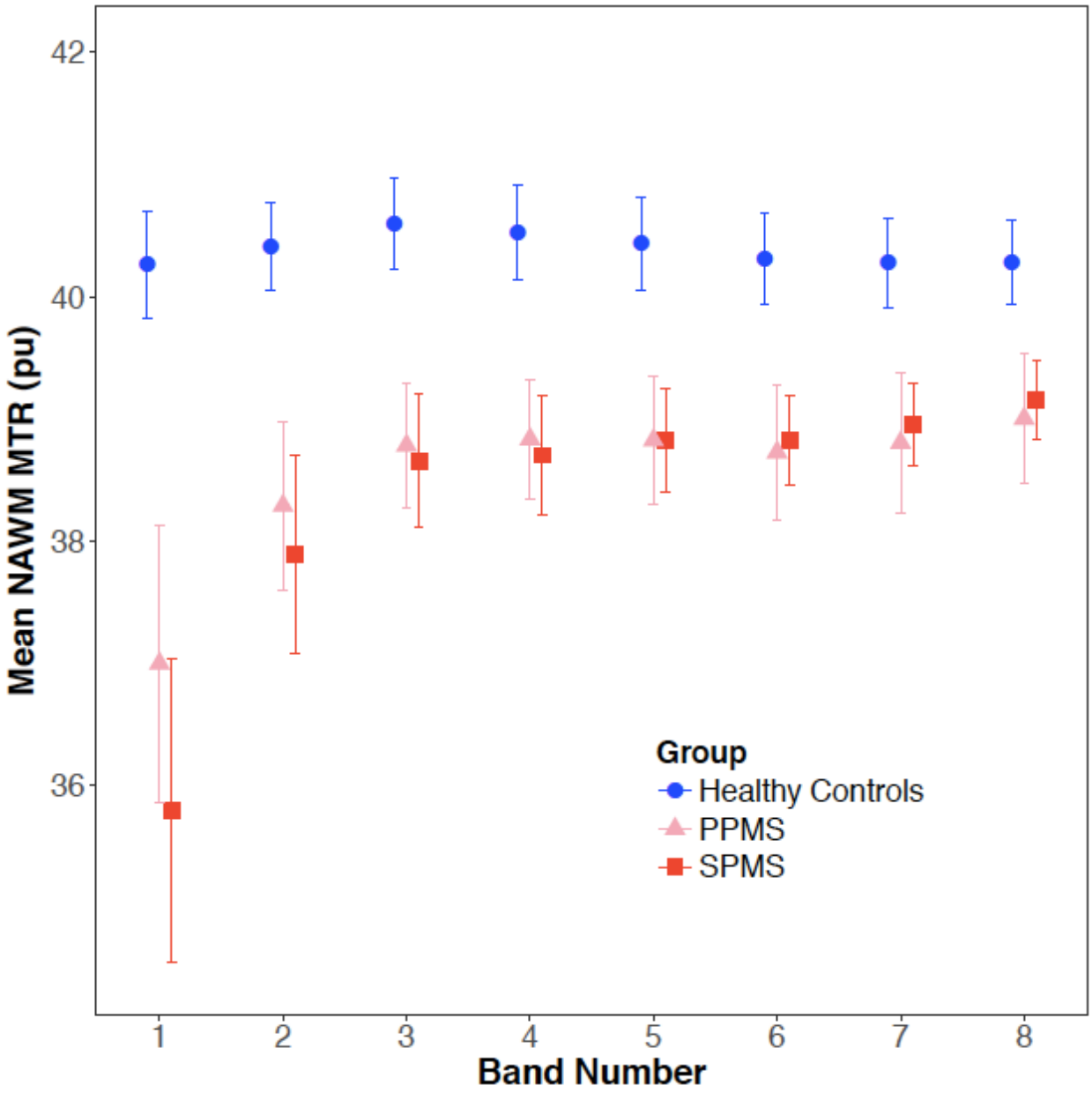

Figure 11: Mean MTR per band for healthy controls (circles), people with primary progressive multiple sclerosis (PPMS – triangles) and people with secondary progressive multiple sclerosis (SPMS – squares) in normal-appearing white matter (NAWM). Error bars = 2 standard errors. MTR expressed in percentage units (pu). Band 1 is closest to the ventricular surface. Band 10 is closest to the cortical surface. Periventricular gradients measured in NAWM over bands 1-3, and cortical gradients measured in cortical GM over bands 8-10.

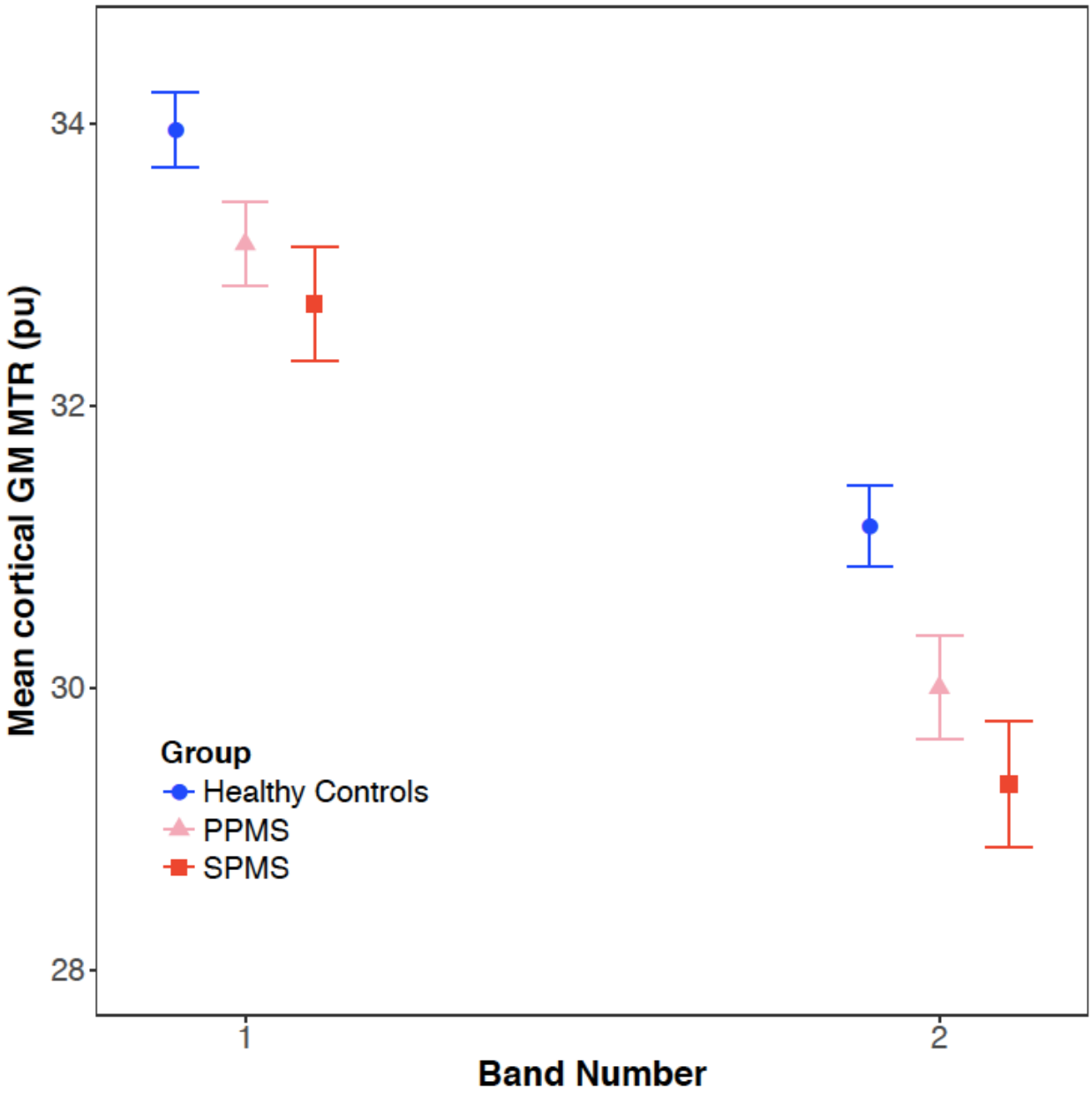

Figure 12: Mean MTR per band for healthy controls (circles), people with primary progressive multiple sclerosis (PPMS – triangles) and people with secondary progressive multiple sclerosis (SPMS – squares) in cortical grey matter (GM). Error bars = 2 standard errors. MTR expressed in percentage units (pu). Band 2 is closest to the cortical surface. Cortical gradients measured in cortical GM over bands 1-2.

	Healthy Controls	Progressive Multiple Sclerosis	
	All, N = 51	PPMS, N = 28	SPMS, N = 35
Mean periventricular NAWM MTR gradient ± SE -baseline (pu/band) -annual change (pu/band/year)	 0.122 ± 0.038 -0.011 ± 0.051	 0.952 ± 0.185 0.090 ± 0.040	 1.360 ± 0.143 0.021 ± 0.030
Mean NAWM MTR ± SE -baseline (pu) -annual change (pu/year)	 39.779 ± 0.111 -0.289 ± 0.150	 38.254 ± 0.281 -0.231 ± 0.107	 38.282 ± 0.143 -0.446 ± 0.099
Mean NAWM volume ± SE -baseline (cm^3) -annual change (cm^3/year)	 460.091 ± 6.665 -4.671 ± 3.973	 415.386 ± 10.490 -1.248 ± 0.442	 383.094 ± 7.337 -1.314 ± 0.541
Mean cortical GM MTR gradient ± SE -baseline (pu) -annual change (pu/band/year)	 -2.860 ± 0.051 0.090 ± 0.146	 -3.214 ± 0.103 -0.018 ± 0.039	 -3.328 ± 0.101 0.037 ± 0.009
Mean cortical GM MTR ± SE -baseline (pu) -annual change (pu/year)	 32.183 ± 0.093 -0.071 ± 0.239	 30.998 ± 0.206 -0.238 ± 0.090	 30.556 ± 0.154 -0.346 ± 0.097
Mean CGM volume ± SE -baseline (cm^3) -annual change (cm^3/year)	 612.545 ± 7.463 -5.490 ± 5.393	 570.030 ± 12.886 -3.427 ± 1.071	 534.389 ± 8.917 -1.363 ± 0.888
Mean brain parenchymal fraction ± SE -baseline -annual change	 0.761 ± 0.001 0.001 ± 0.001	 0.738 ± 0.004 -0.001 ± 0.001	 0.726 ± 0.003 -0.001 ± 0.001
Mean T2 lesion number ± SE -baseline -annual change	 N/A N/A	 41.1 ± 5.8 -3.3 ± 1.3	 43.2 ± 4.1 -2 ± 1.5

Table 8: Imaging outcomes at baseline and annualised changes during follow-up in healthy controls, people with primary progressive multiple sclerosis (PPMS) and people with secondary progressive multiple sclerosis (SPMS). BPF=brain parenchymal fraction. GM=grey matter. NAWM=normal appearing white matter. SE=standard error. MTR is expressed as percentage units (pu).

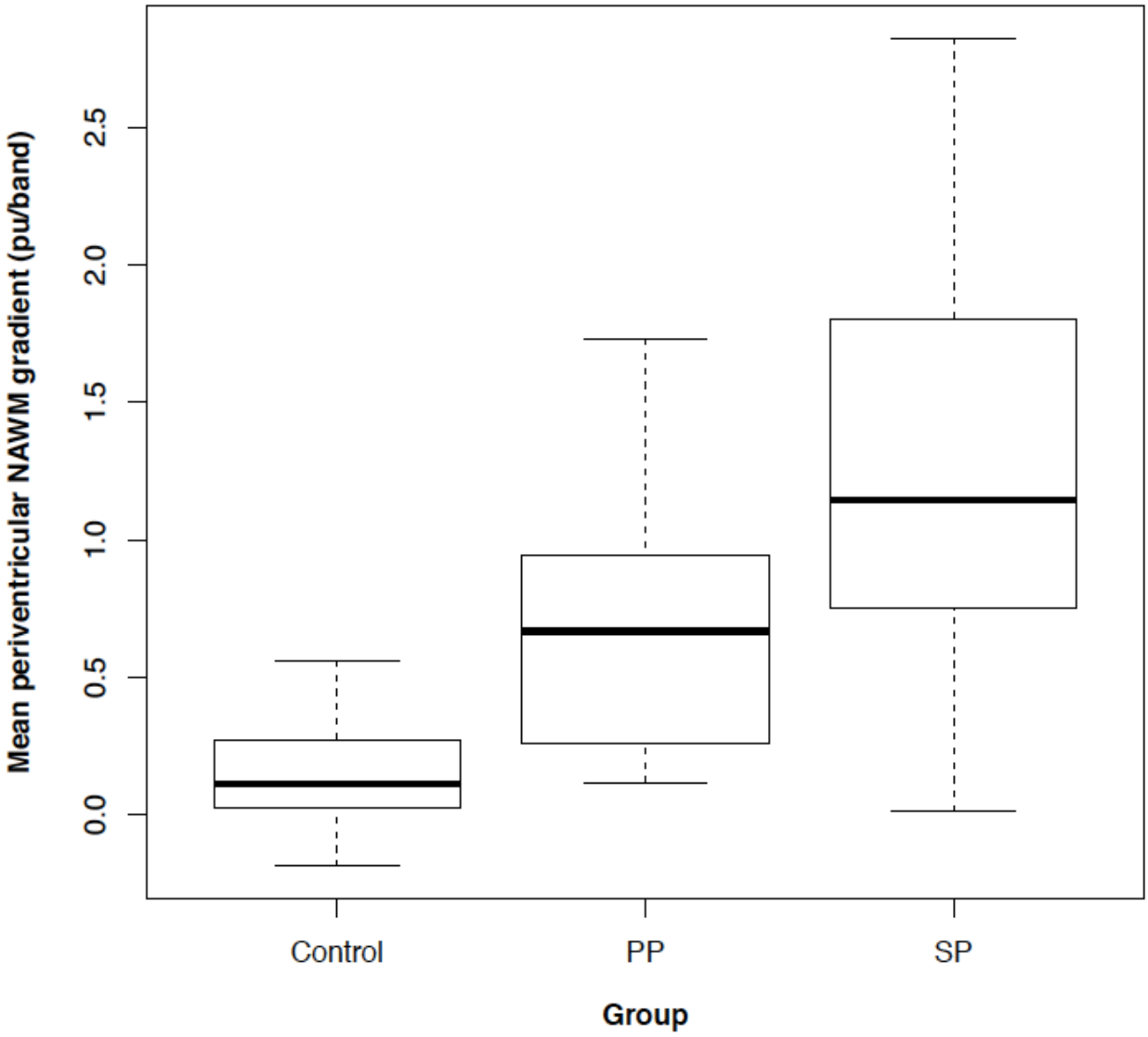

Figure 13: Mean periventricular gradient in normal-appearing white matter (NAWM) in healthy controls, people with primary progressive multiple sclerosis (PPMS) and secondary progressive multiple sclerosis (SPMS). Error bars = 2 standard errors. MTR gradients expressed in percentage units per band (pu/band).

These differences persisted when the models were additionally adjusted for mean NAWM MTR ($p = 0.015$ and $p < 0.0001$ respectively) and when the models were adjusted for BPF instead of NAWM volume ($p < 0.001$ and $p = 0.003$ respectively). No significant differences in periventricular gradient were found between people with PPMS and SPMS ($p = 0.444$), including after adjustment for mean NAWM MTR ($p = 0.191$) or when covarying for BPF instead of NAWM volume ($p = 0.604$). The cortical gradient was significantly shallower in healthy controls (-2.860 ± 0.051 pu/band) compared with both PPMS (-3.214 ± 0.103 pu/band, $p = 0.038$) and SPMS (-3.328 ± 0.101 pu/band, $p = 0.016$), Figure 14. These differences lost significance when the models were additionally adjusted for mean cortical GM MTR ($p = 0.570$ and $p = 0.589$ respectively), and when the models covaried for BPF instead of cortical volume ($p = 0.575$ and $p = 0.530$ respectively). When the MS and healthy control groups were limited to those analysed previously (Samson *et al.*, 2014) the results were consistent with those previously seen: a significant difference was seen between healthy controls and SPMS ($p=0.030$) but not PPMS ($p = 0.150$). No significant differences in cortical gradient were found between people with PPMS and SPMS ($p = 0.372$), including after adjustment for mean cortical MTR ($p = 0.915$).

The baseline demographics and imaging outcomes (including model results) for people with RRMS are presented in Table 10 and Table 11.

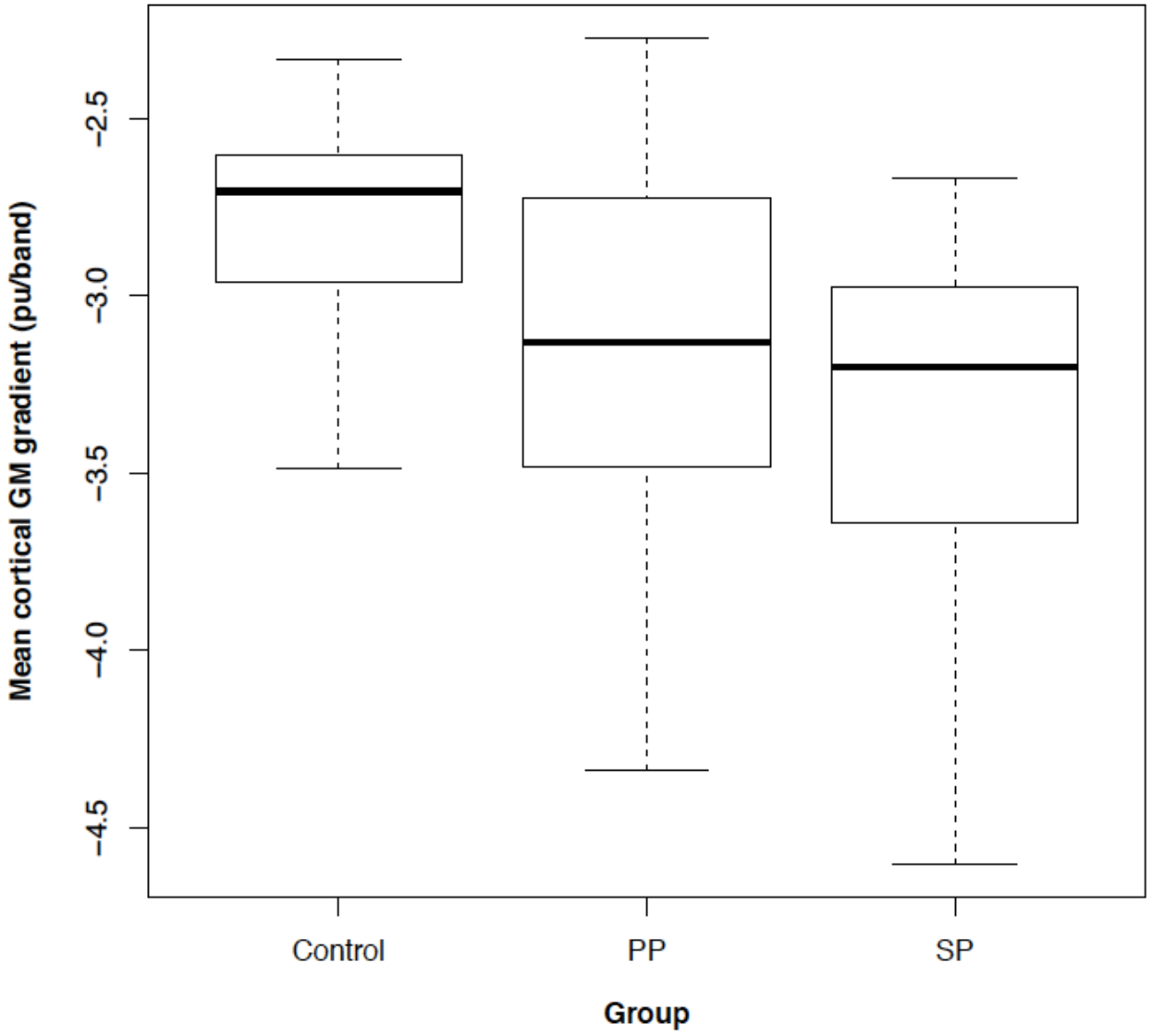

Figure 14: Mean cortical gradient in cortical grey matter (GM) in healthy controls, people with primary progressive multiple sclerosis (PPMS) and secondary progressive multiple sclerosis (SPMS). Error bars = 2 standard errors. MTR gradients expressed in percentage units per band (pu/band).

When all people with MS were grouped (RRMS, SPMS, PPMS), both the periventricular and cortical gradients showed very weak correlations with EDSS score (β 0.100, p=0.011; and β -0.082, p=0.001 respectively) and disease duration (β 0.023, p=0.005; and β -0.015, p=0.004 respectively) but not time from last relapse (β 0.021, p=0.357; and β -0.011, p=0.554). These associations did not materially change when additionally adjusted for clinical classification (Table 9). Results for each disease subgroup are shown in Table 9. A significant association was found between the periventricular gradient and cortical gradient (β -0.609, p<0.0001) which remained unchanged after additionally adjusting for disease group (Table 9).

In those with radiological follow-up (Table 8), the annualised change in periventricular gradient was not significantly different between healthy controls -0.011 ± 0.051 pu/band/year) and people with either PPMS (0.090 ± 0.040 pu/band/year, p = 0.951) or SPMS (0.021 ± 0.030 pu/band/year, p = 0.473). Including change in mean NAWM MTR in the model did not materially alter the results (p = 0.882 and p = 0.343, respectively). Similarly, no change in the annualised rate of change in cortical gradient was seen between healthy controls (0.090 ± 0.146 pu/band/year) and people with either PPMS (-0.018 ± 0.039 pu/band/year, p = 0.553) or SPMS (0.037 ± 0.009 pu/band/year, p = 0.913). Including change in mean cortical GM MTR in the model did not materially alter the results (p = 0.964 and p = 0.350, respectively).

		Coefficient (p-value)				
		PPMS N = 28	SPMS N = 35	RRMS N = 56	All MS patients	
					No adjustment for clinical classification	*Adjusted for clinical classification*
Periventricular NAWM MTR gradient	Cortical GM MTR gradient	-0.497 P = 0.139	-0.411 P = 0.089	**-0.738** **P = 0.0001**	**-0.609** **P < 0.0001**	**-0.585** **P < 0.0001**
Periventricular NAWM MTR gradient	Disease duration, years	-0.024 P = 0.325	0.016 P = 0.244	**0.039** **P = 0.005**	**0.023** **P = 0.005**	**0.019** **P = 0.036**
	EDSS score	0.126 P = 0.344	-0.103 P = 0.473	**0.127** **P = 0.039**	**0.100** **P = 0.011**	0.096 P = 0.065
	Time from last relapse, years	N/A	0.027 P = 0.417	4.902 P = 0.729	0.021 P = 0.357	0.019 P = 0.502
Cortical GM MTR gradient	Disease duration, years	-0.0002 P = 0.99	**-0.022** **P = 0.024**	-0.008 P = 0.392	**-0.015** **P = 0.004**	**-0.012** **P = 0.041**
	EDSS score	-0.098 P = 0.199	-0.076 P = 0.470	-0.067 P = 0.112	**-0.082** **P = 0.001**	**-0.073** **P = 0.033**
	Time from last relapse, years	N/A	-0.002 P = 0.943	-0.389 P = 0.975	-0.011 P = 0.554	-0.191 P = 0.422

Table 9: Model results comparing gradients with (i) other gradients; and (ii) clinical associations

Baseline demographics of patients including those with RRMS

	Healthy controls	**People with multiple sclerosis**		
	N = 51	PPMS N = 28	SPMS N = 35	RRMS N = 56
Mean age, years ± SD	41.7 ± 12.6	52.5 ± 9.3	53.9 ± 7.2	42 ± 9.7
Female : male	27 : 24	18 : 10	26 : 9	39 : 17
Mean disease duration, years ± SD	N/A	13.61 ± 7.39	22.6 ± 10.33	11.5 ± 8.1
Median (range) EDSS at baseline	N/A	6 (3 – 8)	6 (4 – 8.5)	2 (1 – 7)
Number (%) with radiological follow-up	12 (24%)	14 (50%)	15 (43%)	29 (52%)
Median (range) interval between MRI scans, years	2.1 (1.5 – 2.7)	2.3 (1.2 – 3.5)	1.6 (1.1 – 2.4)	1.8 (0.9 – 2.8)
Median (range) EDSS at follow-up	N/A	6 (2.5 – 8)	6.5 (5 – 8.5)	1.5 (1 – 6)

Table 10: Participant baseline demographics. SD=standard deviation. EDSS=Expanded Disability Status Scale; N/A=not available.

	Healthy Controls	**Multiple Sclerosis**		
	All (N = 51)	PPMS (N = 28)	SPMS (N = 35)	RRMS (N = 56)
Mean periventricular NAWM MTR gradient ± SE -baseline (pu/band) -annual change (pu/band/year)	 0.122 ± 0.038 -0.011 ± 0.051	 0.952 ± 0.185 0.090 ± 0.040	 1.360 ± 0.143 0.021 ± 0.030	 1.031 ± 0.117 0.046 ± 0.069
Mean NAWM MTR ± SE -baseline (pu) -annual change (pu/year)	 39.779 ± 0.111 -0.289 ± 0.150	 38.254 ± 0.281 -0.231 ± 0.107	 38.282 ± 0.143 -0.446 ± 0.099	 38.780 ± 0.142 0.032 ± 0.139
Mean NAWM volume ± SE -baseline (cm^3) -annual change (cm^3/year)	 460.091 ± 6.665 -4.671 ± 3.973	 415.386 ± 10.490 -1.248 ± 0.442	 383.094 ± 7.337 -1.314 ± 0.541	 413. 295 ± 7.477 -0.611 ± 0.515
Mean cortical GM MTR gradient ± SE -baseline (pu) -annual change (pu/band/year)	 -2.860 ± 0.051 0.090 ± 0.146	 -3.214 ± 0.103 -0.018 ± 0.039	 -3.328 ± 0.101 0.037 ± 0.009	 -3.072 ± 0.058 0.047 ± 0.070
Mean cortical GM MTR ± SE -baseline (pu) -annual change (pu/year)	 32.183 ± 0.093 -0.071 ± 0.239	 30.998 ± 0.206 -0.238 ± 0.090	 30.556 ± 0.154 -0.346 ± 0.097	 31.509 ± 0.140 -0.145 ± 0.148
Mean CGM volume ± SE -baseline (cm^3) -annual change (cm^3/year)	 612.545 ± 7.463 -5.490 ± 5.393	 570.030 ± 12.886 -3.427 ± 1.071	 534.389 ± 8.917 -1.363 ± 0.888	 570.364 ± 8.241 -2.668 ± 0.741
Mean brain parenchymal fraction ± SE -baseline -annual change	 0.761 ± 0.001 0.001 ± 0.001	 0.738 ± 0.004 -0.001 ± 0.001	 0.726 ± 0.003 -0.001 ± 0.001	 0.743 ± 0.002 -0.001 ± 0.000

Mean T2 lesion number ± SE -baseline -annual change	 N/A N/A	 41.1 ± 5.8 -3.3 ± 1.3	 43.2 ± 4.1 -2 ± 1.5	 42.6 ± 4.1 0.3 ± 0.8

Table 11: Imaging outcomes at baseline and annualised changes during follow-up in healthy controls, people with primary progressive multiple sclerosis (PPMS), people with secondary progressive multiple sclerosis (SPMS) and people with relapsing-remitting multiple sclerosis (RRMS). BPF=brain parenchymal fraction. GM=grey matter. NAWM=normal appearing white matter. SE=standard error. MTR is expressed as percentage units (pu).

The NAWM periventricular gradient was significantly shallower in healthy controls (0.122 ± 0.038 pu/band) compared to those with RRMS (1.031 ± 0.117 pu/band, $p < 0.0001$). This persisted when the model was additionally adjusted for mean NAWM MTR ($p = 0.002$) or when adjusted for BPF instead of NAWM volume ($p = 0.034$). The cortical gradient was significantly shallower in healthy controls (-2.860 ± 0.051 pu/band) compared to RRMS (-3.072 ± 0.058 pu/band, $p = 0.030$). These differences lost significance when the model was additionally adjusted for mean cortical GM MTR ($p = 0.668$) or when the model covaried for BPF instead of cortical volume ($p = 0.975$).

Project 3: Periventricular gradient evolution following peripheral immunotherapy

This work was published in Multiple Sclerosis Journal, 2019:

Brown JW, Prados F*, Eshaghi A, Sudre C, Button T, Pardini M, et al. Periventricular magnetisation transfer ratio abnormalities in multiple sclerosis improve after alemtuzumab. Multiple Sclerosis Journal. [Accepted; In Press] *Joint First Author*

Seven patients in the natural history cohort received beta-interferon before the last scan so were excluded. One patient in the alemtuzumab cohort did not complete the imaging protocol so was excluded, leaving 34 for analysis (19 treated and 15 untreated patients). Baseline demographics were comparable between the groups (Table 12) except age (alemtuzumab group 32.8 years, untreated group 37.5 years) and prior annualised relapse rate (alemtuzumab group 2.73 relapses/year, untreated group 1.72 relapses/year): all models were adjusted for these variables.

	Untreated	Alemtuzumab-treated		
	N=15	All N=19	With further relapse within 4 years N=4	Without further relapse within 4 years N=15
Mean age, years ± SD	37.5 ± 7	32.8 ± 9.5	29.9 ± 2.3	33.6 ± 7.7
Female : male	10 : 5	13 : 6	3 : 1	10 : 5
Mean disease duration, years ± SD	1.69 ± 0.72	1.59 ± 0.77	2.03 ± 1.19	1.48 ± 0.62
Mean annualised relapse rate ± SD	1.72 ± 1.03	2.73 ± 1.28	2.92 ± 1.01	2.68 ± 1.38
Median EDSS (range)	1 (0-4)	1.5 (0-3)	2.25 (0-2.5)	1.5 (0-3)

Table 12: Participant baseline demographics. SD=standard deviation. EDSS=Expanded Disability Status Scale

Evolution over time: alemtuzumab versus untreated groups

The mean MTR in each band decreased (became more abnormal) in the untreated group with time but increased (became less abnormal) in the alemtuzumab group (Figure 15).

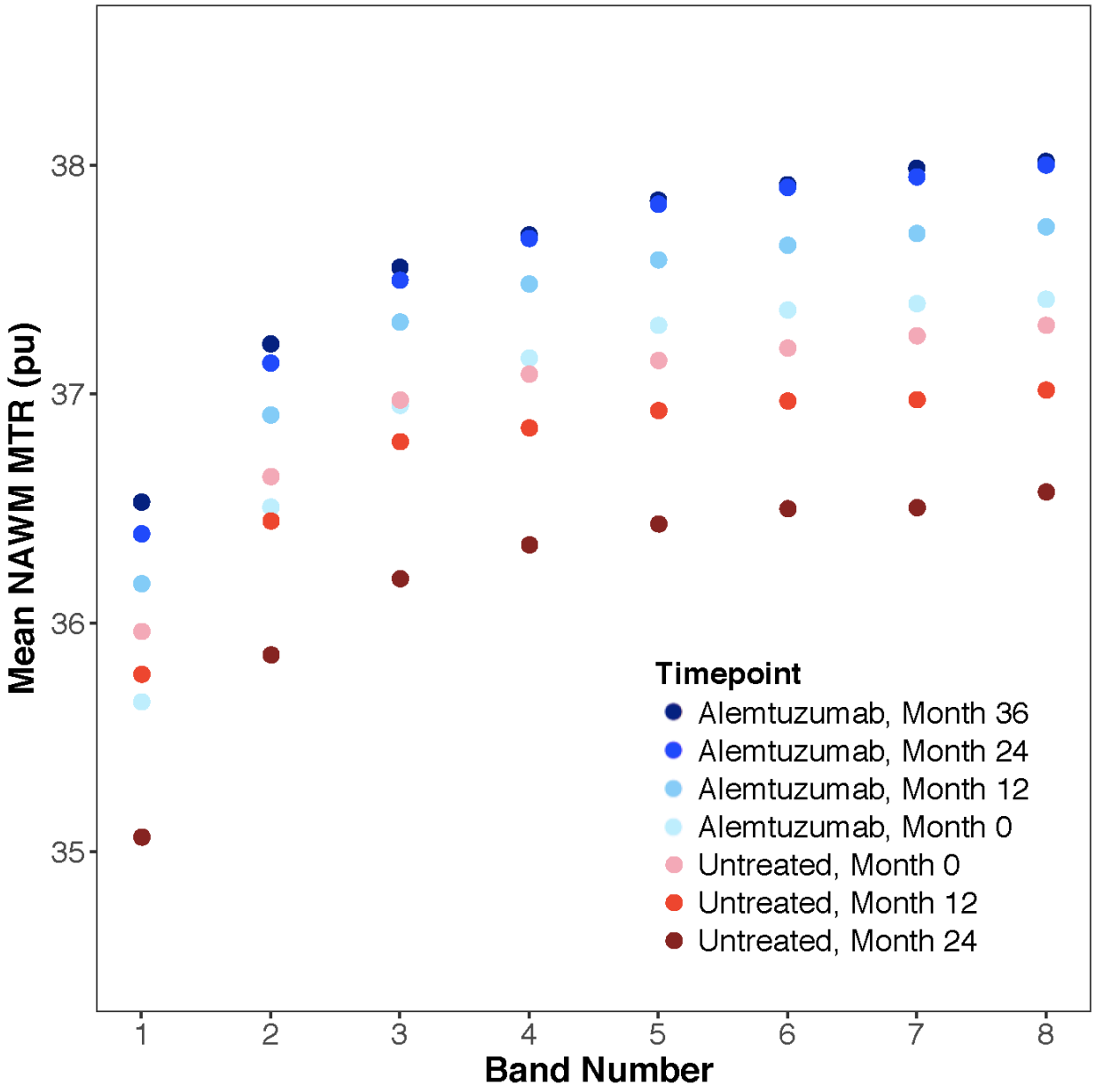

Figure 15: Normal appearing white matter (NAWM) MTR in untreated patients and patients treated with alemtuzumab. MTR is expressed as percentage units (pu). Band 1 is closest to the ventricles.

The mean periventricular MTR gradient worsened (increased) in the untreated group by 0.030 ± 0.025pu/band/year but improved (decreased) in the alemtuzumab group by -0.045 ± 0.016pu/band/year (Table 8, Figure 16). The rate of change was significantly different between the groups (p=0.028) and did not materially change after adjustment for change in whole-brain lesion number (p=0.037) or periventricular lesion number (p=0.050) but lost significance when

adjusted for change in periventricular NAWM MTR (p=0.124) or whole brain NAWM MTR (p=0.195). While the mean NAWM MTR, mean DGM MTR and mean cortical GM MTR decreased (becoming more abnormal) in the untreated group (-0.183 ± 0.030 pu/year; -0.394 ± 0.122 pu/year and -0.261 ± 0.032 pu/year respectively), all stabilised or improved following alemtuzumab treatment with significant differences compared to untreated patients (0.279 ± 0.062 pu/year, p=0.001; -0.011 ± 0.023 pu/year, p=0.001; and 0.052 ± 0.019, p = 0.0001 respectively). These differences persisted after adjustment for change in whole-brain lesion number (p=0.006, p=0.003 and p=0.0002 respectively) and periventricular gradient (p=0.019, p=0.002 and p<0.0001 respectively).

At baseline the periventricular MTR gradient correlated with mean whole brain NAWM MTR in both the alemtuzumab (r=-0.570, p=0.012) and untreated (r=-0.595, p=0.019) groups, but no correlation was found between the annualized change in these metrics in either the alemtuzumab (r=0.138, p=0.570) nor untreated (r=0.130, p=0.643) groups.

Baseline predictive capabilities: those who relapsed versus those who did not (alemtuzumab only group)

During clinical follow-up (median 13.5 (range 4.6-14.5) years), 8/19 patients treated with alemtuzumab relapsed (half within the first 4 years). The baseline MTR gradient was significantly more abnormal in those who relapsed within 4 years compared to those who did not (0.871 ± 0.197pu/band versus 0.588 ± 0.054pu/band respectively, p=0.020), and remained significantly

	Untreated	**Alemtuzumab-treated**	p-value	**Alemtuzumab-treated**		p-value
	All N=15	All N=19		Relapse within 4y N=4	No relapse within 4y N=15	
Mean periventricular MTR gradient ± SE -baseline (pu/band) -annual change (pu/band/year)	 0.504 ± 0.068 0.030 ± 0.025	 0.647 ± 0.062 -0.045 ± 0.016	 **0.044** **0.028**	 0.871 ± 0.197 -0.116 ± 0.060	 0.588 ± 0.054 -0.026 ± 0.010	 **0.020** **0.042**
Mean periventricular NAWM MTR ± SE -baseline (pu) -annual change (pu/year)	 33.518 ± 0.329 -0.306 ± 0.119	 33.112 ± 0.339 0.279 ± 0.062	 0.211 **0.008**	 32.590 ± 0.994 0.412 ± 0.227	 33.251 ± 0.353 0.244 ± 0.053	 0.275 0.559
Mean whole brain NAWM MTR ± SE -baseline (pu) -annual change (pu/year)	 37.134 ± 0.166 -0.183 ± 0.030	 37.076 ± 0.176 0.208 ± 0.038	 0.831 **0.001**	 36.951 ± 0.635 0.275 ± 0.166	 37.109 ± 0.163 0.190 ± 0.026	 0.931 0.559
Mean DGM MTR ± SE -baseline (pu) -annual change (pu/year)	 33.795 ± 0.137 -0.394 ± 0.122	 33.770 ± 0.133 -0.011 ± 0.023	 0.930 **0.001**	 33.580 ± 0.202 -0.028 ± 0.055	 33.909 ± 0.171 -0.007 ± 0.027	 0.822 0.872
Mean CGM MTR ± SE -baseline (pu) -annual change (pu/year)	 31.802 ± 0.193 -0.261 ± 0.032	 31.740 ± 0.137 0.052 ± 0.019	 0.339 **0.0001**	 31.495 ± 0.188 0.038 ± 0.047	 31.917 ± 0.176 0.056 ± 0.022	 0.410 0.501
Mean whole-brain T2 lesion number ± SE -baseline -annual change (lesions/year)	 16.400 ± 2.891 0.867 ± 0.503	 25.579 ± 3.465 -0.632 ± 0.480	 0.056 **0.010**	 23.000 ± 6.621 0.167 ± 0.319	 26.267 ± 4.110 -0.844 ± 0.594	 0.568 0.280
Mean periventricular T2 lesion number ± SE -baseline -annual change (lesions/year)	 11.200 ± 2.154 1.633 ± 0.557	 21.158 ± 3.209 -0.736 ± 0.499	 **0.011** **0.001**	 17.250 ± 6.183 -0.750 ± 1.250	 22.200 ± 3.771 -0.733 ± 0.562	 0.799 0.724

Mean brain parenchymal fraction ± SE -baseline -annual change	 0.713 ± 0.006 -0.003 ± 0.000	 0.712 ± 0.003 -0.003 ± 0.000	 0.453 0.450	 0.715 ± 0.001 -0.002 ± 0.000	 0.710 ± 0.003 -0.003 ± 0.000	 0.187 0.737

Table 13: Imaging outcomes at baseline and annualised change during follow-up. SE = standard error.

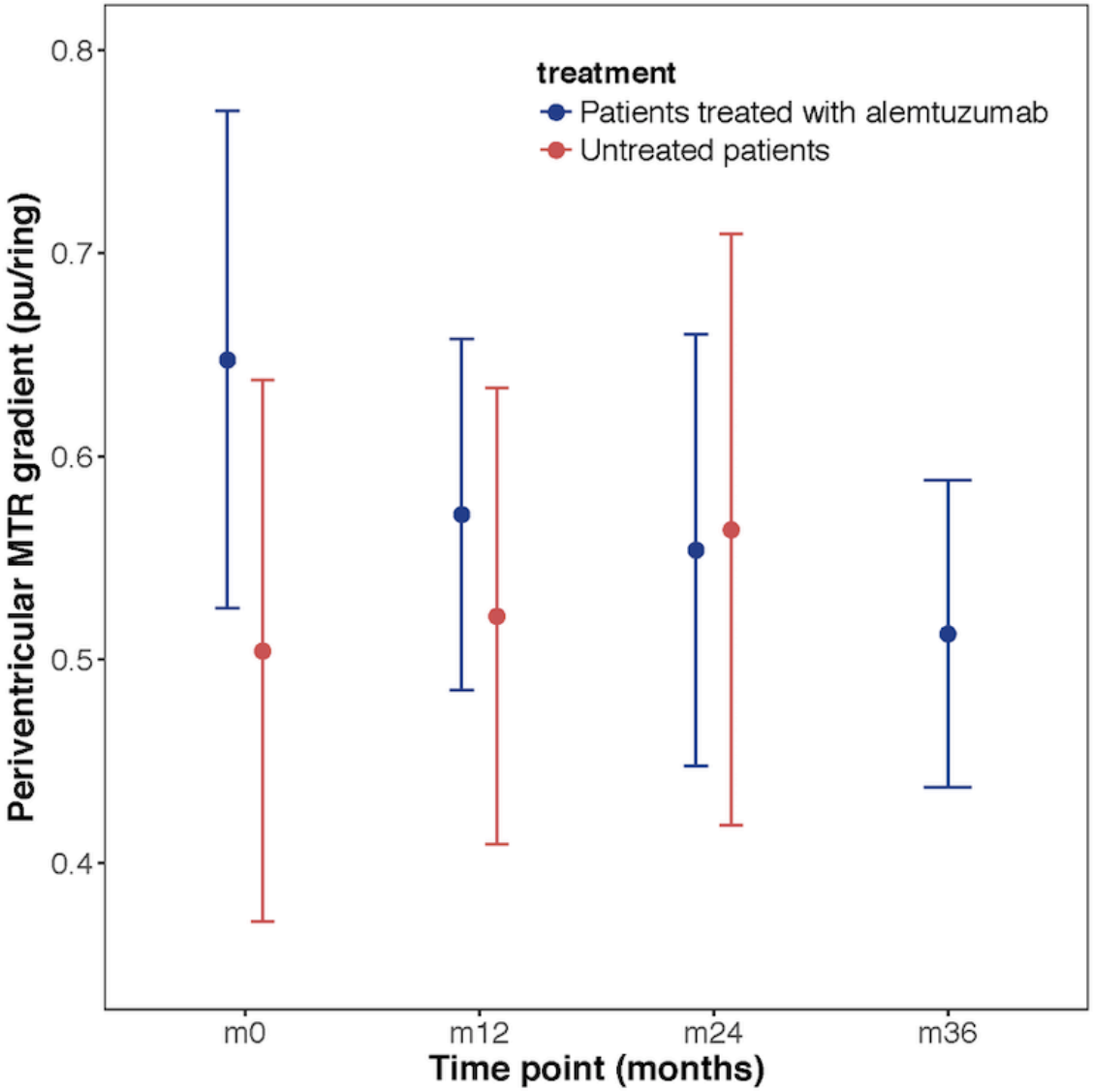

Figure 16: Normal appearing white matter (NAWM) MTR periventricular gradient in the untreated group and those treated with alemtuzumab (Mean ± 2 x standard error). MTR gradient is expressed as percentage units per band (pu/band).

more abnormal after adjustment for baseline whole-brain lesion number (p=0.022), baseline periventricular lesion number (p=0.035), baseline periventricular NAWM MTR (p=0.034) or baseline mean whole brain NAWM MTR (p=0.003). These adjusted differences persisted when non-relapsers were compared to those relapsing within 2 or 3 years (n=3 for both, p=0.041) or 5 years (n=5, p=0.014), but lost significance when comparing those who relapsed throughout follow-up (13.5 years, n=8, p=0.075). In contrast, no significant differences were found in baseline whole-brain lesion number (23.0 ± 6.6 versus 26.3 ± 4.1 respectively, p=0.568), baseline periventricular lesion number (17.3 ± 6.2 versus 22.2 ± 3.8 respectively, p=0.799), baseline brain parenchymal fraction (0.715 ± 0.001 versus 0.710 ± 0.003 respectively, p=0.187) or baseline mean whole brain NAWM MTR (36.951 ± 0.635pu versus 37.109 ± 0.163pu respectively, p=0.931) between those that relapsed within 4 years versus those that did not.

Evolution over time: those who relapsed versus those who did not (alemtuzumab only group)

The rate of change in MTR gradient was significantly different between those who relapsed within 4 years and those who did not (-0.116 ± 0.060pu/band/year versus -0.026 ± 0.010pu/band/year respectively, p=0.042), and remained significant when change in whole brain lesion number (p=0.023), change in periventricular lesion number (p=0.035) or change in whole brain NAWM MTR (p=0.039) were added to the model. The rate of change in mean whole brain NAWM MTR was not significantly different between those who relapsed within 4 years and those who did not (0.275 ± 0.166pu/year versus 0.190 ± 0.026pu/year respectively, p=0.559), nor were the rates of change in whole-brain lesion number (0.17 ± 0.32/year versus -0.84 ± 0.59/year respectively, p=0.280), periventricular lesion number (-0.75 ± 1.25 /year versus -0.73 ± 0.56/year respectively, p=0.724) nor brain parenchymal fraction (-0.002 ± 0.000/year versus -0.003 ± 0.000/year respectively, p=0.737).

The baseline median EDSS score (1.5, range 0-3) remained unchanged 13.5 years later (1.5, range 0-6) in the alemtuzumab group. EDSS scores increased in the same 8/19 patients who relapsed during follow-up (occurring at the same time as the relapses). As no patients converted to SPMS during follow-up, the disability increases were therefore all attributed to the relapses, so further modelling was not performed. Neither the baseline MTR gradient nor mean whole brain NAWM MTR correlated with EDSS score at baseline (r=-0.002, *p*=0.994 and r=0.034, *p*=0.890 respectively) or at follow-up (r=0.163, *p*=0.504 and r=-0.271, *p*=0.261 respectively).

The predictive capability of the baseline periventricular gradient and its evolution with time in the untreated group is detailed below.

Baseline predictive capabilities: those who relapsed versus those who did not (untreated group)

During clinical follow-up (5 years), 10/15 untreated patients relapsed (all within the first 3 years). No difference was found in the baseline periventricular MTR gradient between those who relapsed compared to those who did not (0.462 ± 0.084pu/band versus 0.590 ± 0.120pu/band respectively, *p*=0.551), including after adjustment for baseline whole-brain lesion number (*p*=0.847), baseline periventricular lesion number (*p*=0.607) or baseline mean whole brain NAWM MTR (*p*=0.438). While a significant difference was found in baseline whole-brain lesion number (14.6 ± 2.8 versus 20 ± 6.9 respectively, *p*=0.043), and a trend was seen in baseline periventricular lesion number (10.2 ± 2.4 versus 13.2 ± 4.7 respectively, *p*=0.052), no differences were found in baseline brain parenchymal fraction (0.713 ± 0.008 versus 0.712 ± 0.007 respectively, *p*=0.978) or baseline mean whole brain NAWM MTR (37.183 ± 0.216pu versus 37.036 ± 0.275pu respectively, *p*=0.898) between those that relapsed versus those who did not.

Evolution over time: those who relapsed versus those who did not (untreated group)

The rate of change in MTR gradient was significantly different between those who relapsed and those who did not (0.071 ± 0.026pu/band/year versus -0.052 ± 0.036pu/band/year respectively, *p*=0.001), and remained significant when change in whole brain lesion number (*p*=0.006), change in periventricular lesion number (p=0.005) or change in whole brain NAWM MTR (*p*=0.003) were added to the model. The rate of change in mean whole brain NAWM MTR was not significantly different between those who relapsed and those who did not (-0.185 ± 0.038pu/year versus -0.181 ± 0.053pu/year respectively, *p*=0.850), nor were the rates of change in whole-brain lesion number (1 ± 0.7/year versus 0.7 ± 0.6/year respectively, *p*=0.415), periventricular lesion number (1.8 ± 0.8/year versus 1.4 ± 0.8/year respectively, *p*=0.561) nor brain parenchymal fraction (-0.002 ± 0.001/year versus -0.005 ± 0.001/year respectively, *p*=0.273).

Conclusions: outside-in gradients

Outside-in MTR gradients of tissue damage were seen in periventricular and cortical regions at all stages of relapse-onset MS and primary-progressive MS. The periventricular MTR gradient was reversed by peripheral immunomodulation and independently predicted subsequent relapse activity on and off DMTs. The underlying process(es) appear at least partially distinct from those underlying lesion formation.

Chapter 5: Results – The effect of disease-modifying therapies on conversion to secondary progressive multiple sclerosis

Project 4.

This chapter details the results from the observational study (Project 4).

This work was published in JAMA, 2019:

Brown JW, Coles AJ*, Horakova D, Havrdova E, Izquierdo G, Prat A, et al. Association of initial disease-modifying therapy with later conversion to secondary progressive multiple sclerosis. JAMA 2019; 321(2): 175-87.*

44,217 patients with multiple sclerosis (1,091 from the Welsh untreated cohort; 43,048 from MSBase; and 78 alemtuzumab-treated patients from non-MSBase centers) were assessed for eligibility (Figure 17). To avoid informed censoring bias, the glatiramer acetate / interferon beta groups were limited to those treated and followed-up before fingolimod, alemtuzumab or natalizumab became available for escalation (baseline year 1996-1998 (Table 14)). Following exclusion of ineligible patients (Figure 17), the matching process then matched 1,555 patients from 68 centers in 21 countries: 230 from the Welsh untreated cohort; 1,272 from MSBase and 53 alemtuzumab-treated patients from non-MSBase centers (Table 14, Table 17, Table 18, Table

19, Table 20, Table 21, Table 22, Table 23 and Table 24). Propensity scores before and after matching are shown in Table 25. The assumption of proportionality was not met in 6/9 analyses (requiring Weibull accelerated failure time regression models). Differing follow-up duration with different drugs in the untreated comparisons (Figure 18) largely reflects the variable time from drug licensing.

Compared with no treatment, treatment with each included therapy was associated with a significantly lower probability of converting to SPMS. For patients initially treated with glatiramer acetate or interferon beta (n=407), the hazard ratio (HR) was 0.71 (95% confidence interval (CI) 0.61−0.81), p<0.001 in comparison to untreated patients (n=213); median censored follow-up 7.6 (IQR 5.8-9.6) years); at 5 years 12% vs 27% respectively had converted, while at 11 years 47% vs 57% had converted (Figure 18). Fewer patients initially treated with fingolimod (n=85) converted compared to untreated patients (n=174) (HR 0.37 (95% CI 0.22−0.62), p<0.001; median censored follow-up 4.5 (IQR 4.3-5.1) years): at 5 years 7% vs 32% respectively had converted, while at 6 years 7% vs 39% had converted (Figure 18). Conversion to SPMS was also significantly lower for patients initially treated with natalizumab (n=82) compared to untreated

	Initial Treatment			Initial Treatment			Initial Treatment			Initial Treatment		
	Glatiramer Acetate or Interferon Beta (n = 407)	Untreated (n = 213)	Cohen d[a]	Fingolimod Treatment (n = 85)	Untreated (n = 174)	Cohen d[a]	Natalizumab Treatment (n = 82)	Untreated (n = 164)	Cohen d[a]	Alemtuzumab Treatment (n = 44)	Untreated (n = 92)	Cohen d[a]
Age, mean (SD), y	35 (8)	35 (8)	0	39 (12)	39 (10)	0	39 (9)	38 (9)	0.03	35 (8)	35 (7)	0.08
Sex, No. (%)												
Male	115 (28)	58 (27)		26 (31)	47 (27)		28 (34)	56 (34)		14 (32)	27 (29)	
Female	292 (72)	155 (73)	0.05	59 (69)	127 (73)	0.04	54 (66)	108 (66)	0.06	30 (68)	65 (71)	0.04
Disease duration, median (IQR), y	5.7 (3.1-10.5)	5.1 (2-9.8)	0.05	4.9 (1.7-9.7)	5.1 (2.1-9)	0.03	6.2 (2-10.5)	5.2 (2.3-8.9)	0.15	3.2 (2-5.8)	3.8 (1.9-6.7)	0.17
No. of relapses in year before baseline, mean (SD)	1.1 (1)	1.1 (0.9)	0	0.9 (0.9)	0.9 (1)	0.02	1.1 (1)	1.1 (1)	0.01	1.3 (1)	1.3 (1)	0.03
Disability, EDSS step, median (IQR)	2.5 (1.5-3.5)	2 (1-3.5)	0.1	2 (1-3.5)	2 (1.5-3.5)	0	2.5 (2-4.5)	3 (2-4.5)	0.28	3.5 (2-4.5)	3.5 (2-5.5)	0
Baseline year of inclusion, median (IQR)	1996 (1996-1997)	2007 (2004-2009)		2011 (2011-2012)	2007 (2007-2009)		2010 (2009-2011)	2006 (2005-2008)		2006 (2003-2006)	2006 (2005-2008)	
Length of setwise-censored follow-up, median (IQR), y	7.6 (5.8-9.6)	7.6 (5.8-9.6)	0	4.5 (4.3-5.1)	4.5 (4.3-5.1)	0	4.9 (4.4-5.8)	4.9 (4.4-5.8)	0	7.4 (6.0-8.6)	7.4 (6.0-8.6)	0
EDSS frequency during follow-up per year, median (IQR)	2 (1-3.2)	1 (0.7-1.5)	0.75	1.6 (1.1-2.6)	1 (0.7-1.5)	0.58	1.9 (1.3-2.9)	1.2 (0.7-1.8)	0.55	1.1 (0.9-1.5	1.2 (0.9-1.9)	0.11
Proportion of time receiving therapy before censor or secondary progressive MS, median (IQR)	1 (0.9-1)			1 (1-1)			1 (1-1)			0.8 (0.6-1)		

Table 14: Baseline Characteristics of Matched Patient Groups. EDSS, Expanded Disability Status Scale, range 0 (no disability due to MS) to 10 (death due to MS), 2 indicates minimal disability in 1 of 8 functional systems (but no impairment to walking); 3.5, moderate disability in 1 or 2 functional systems plus minimal disability in several others (but no impairment to walking); IQR, interquartile range; MS, multiple sclerosis. [a]Standardized difference quantified by the Cohen d value. Reproduced with permission from The American Medical Association (License number 4720830643128; granted 2nd December 2019)

	Initial Glatiramer Acetate or Interferon Beta Treatment			Initial Treatment			Initial Treatment			Escalation to Fingolimod, Alemtuzumab, or Natalizumab			Initial Treatment		
	≤5 y (n = 120)	>5 y (n = 38)	Cohen *d*[a]	Glatiramer Acetate or Interferon Beta ≤5 y (n = 164)	Untreated (n = 104)	Cohen *d*[a]	Glatiramer Acetate or Interferon Beta at 5-10 y (n = 95)	Untreated (n = 158)	Cohen *d*[a]	≤5 y (n = 307)	>5 y (n = 331)	Cohen *d*[a]	Fingolimod, Alemtuzumab, or Natalizumab (n = 235)	Glatiramer Acetate or Interferon Beta (n = 380)	Cohen *d*[a]
Age, mean (SD), y	30 (7)	31 (7)	0.14	33 (8)	33 (7)	0.02	37 (7)	36 (8)	0.08	33 (9)	32 (8)	0.03	34 (11)	34 (9)	0.06
Sex, No. (%)															
Male	88 (73)	27 (70)		51 (31)	28 (27)		29 (31)	47 (30)		89 (29)	98 (30)		73 (31)	113 (30)	
Female			0.06	13 (69)	76 (73)	0.07	66 (69)	111 (70)	0.02	218 (71)	233 (70)	0.09	162 (69)	267 (70)	0.01
Disease duration, median (IQR), y	3.2 (2.1-4.1)	3.5 (2.7-4.2)[b]	0.26	3 (2.1-4)	2.1 (1-3.5)	0.5	6.8 (5.9-8.3)	5.3 (2.1-10)	0.31	3 (2.1-4)	3.5 (2.5-4.3)[c]	0.41	6.5 (2.1-12)	5.1 (2.7-9.6)	0.2
No. of relapses in year before baseline, mean (SD)	1.0 (1.1)	1.0 (0.9)	0	1.3 (1)	1.2 (1)	0.06	1.1 (1)	0.9 (0.9)	0.18	1 (1.1)	1 (1)	0	1.2 (1.1)	1.3 (1.1)	0.1
Disability, EDSS step, median (IQR)	2 (1.5-3)	2 (1-2.5)	0	2 (1-3)	2 (1-3)	0	2.5 (1.5-3.5)	2.5 (1.5-3.5)	0	2 (1.5-3.5)	2 (1.1-3.0)	0	2 (1.5-3)	2 (1.5-3.5)	0.02
Baseline year of inclusion, median (IQR)	1996 (1995-1997)	1992 (1988-1994)		1996 (1995-1997)	2006 (2005-2008)		1996 (1995-1997)	2006 (2004-2008)		2010 (2009-2011)	2005 (2003-2007)		2009 (2008-2011)	1996 (1996-1997)	
Length of setwise-censored follow-up median (IQR), y	13.4 (11-18.1)	13.4 (11-18.1)	0	7.5 (5.7-9.8)	7.5 (5.7-9.8)	0	7.7 (5.8-9.7)	7.7 (5.8-9.7)	0	5.3 (4.6-6.4)	5.3 (4.6-6.4)	0	5.8 (4.7-8.0)	5.8 (4.7-8.0)	0
EDSS frequency during follow-up per year, median (IQR)	1.8 (1.1-2.6)	1.4 (0.9-2.1)	0.41	2.4 (1.3-3.3)	1 (0.8-1.4)	1.37	1.7 (0.8-2.9)	1 (0.7-1.4)	0.61	2.3 (1.5-3.4)	2 (1.3-3.3)	0.17	1.8 (1.2-2.8)	2.2 (1.1-3.5)	0.3
Proportion of time receiving therapy before censor or secondary progressive MS, median (IQR)	1 (0.8-1)	0.6 (0.4-0.7)	1.64	1 (0.6-1)			1 (0.9-1)			1 (0.9-1)	0.9 (0.7-1)	0.54	1 (1-1)	1 (0.9-1)	0

Table 15: Baseline Characteristics of Matched Patient Groups. EDSS, Expanded Disability Status Scale, range 0 (no disability due to MS) to 10 (death due to MS), 2 indicates minimal disability in 1 of 8 functional systems (but no impairment to walking); 3.5, moderate disability in 1 or 2 functional systems plus

minimal disability in several others (but no impairment to walking); IQR, interquartile range; MS, multiple sclerosis. [a]Standardized difference quantified by the Cohen d value. [b]Median disease duration at the time of commencing interferon beta or glatiramer acetate in the late group was 6.8 years (IQR, 5.7-10.8). [c]Median disease duration at the time of commencing fingolimod or alemtuzumab or natalizumab in the late group was 7.3 years (IQR, 6.1-10.4). Reproduced with permission from The American Medical Association (License number 4720830643128; granted 2nd December 2019)

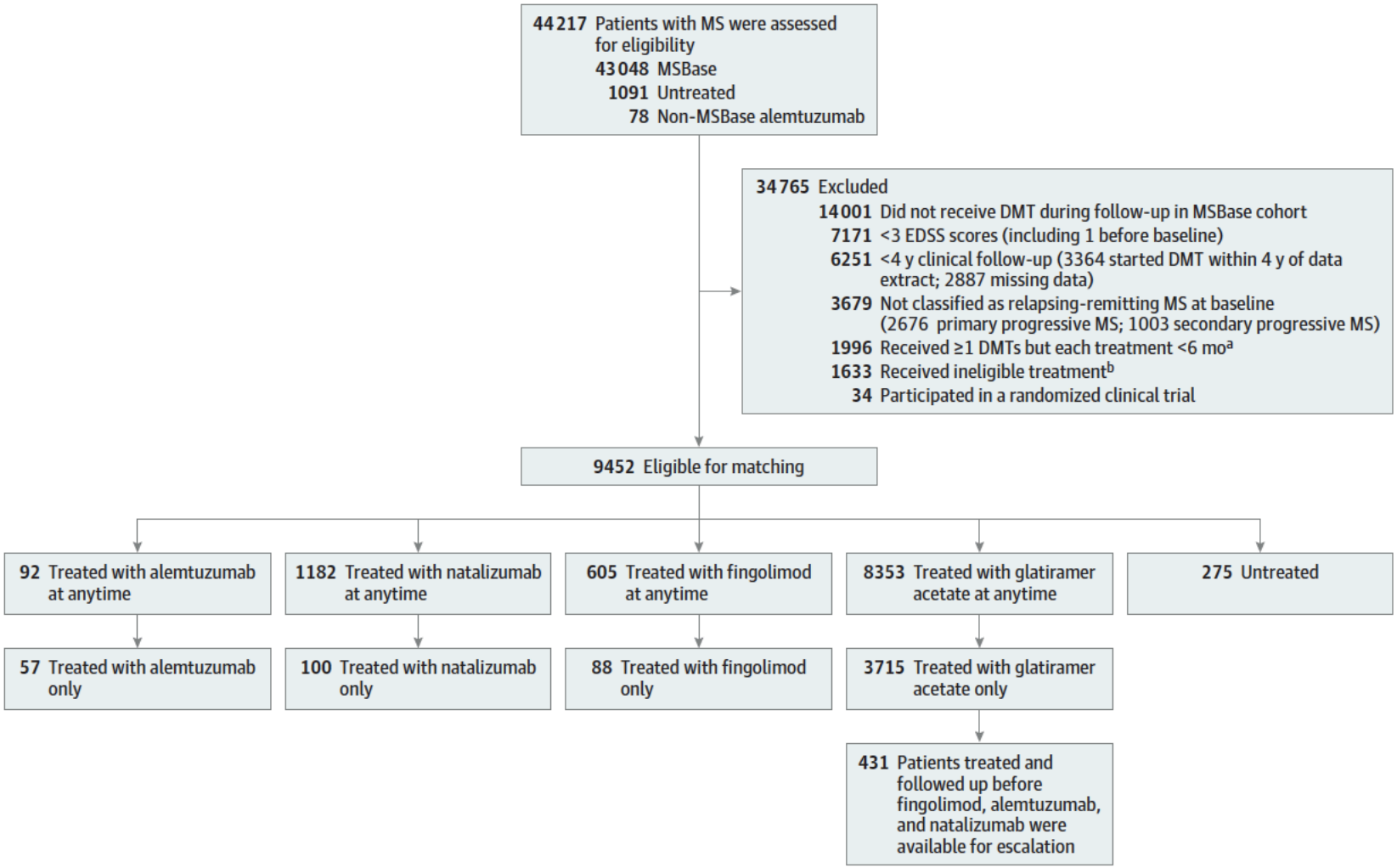

Figure 17: MSBase Study Design of Patients with Multiple Sclerosis (MS). [a] When recorded, reasons for stopping included: 341 due to intolerance; 65, inconvenience; 42, pregnancy (or planned pregnancy); 65, inefficacy (relapses, EDSS progression, magnetic resonance imaging activity, or patient perception of lack of improvement); and 15, nonadherence. [b] Ineligible treatments were defined as treatments not licensed for relapsing remitting MS at the time of the study period (mitoxantrone, cladribine, rituximab, ocrelizumab, siponimod, or autologous stem-cell transplant). DMT indicates disease-modifying therapy; EDSS, Expanded Disability Status Scale. Reproduced with permission from The American Medical Association (License number 4720830643128; granted 2nd December 2019)

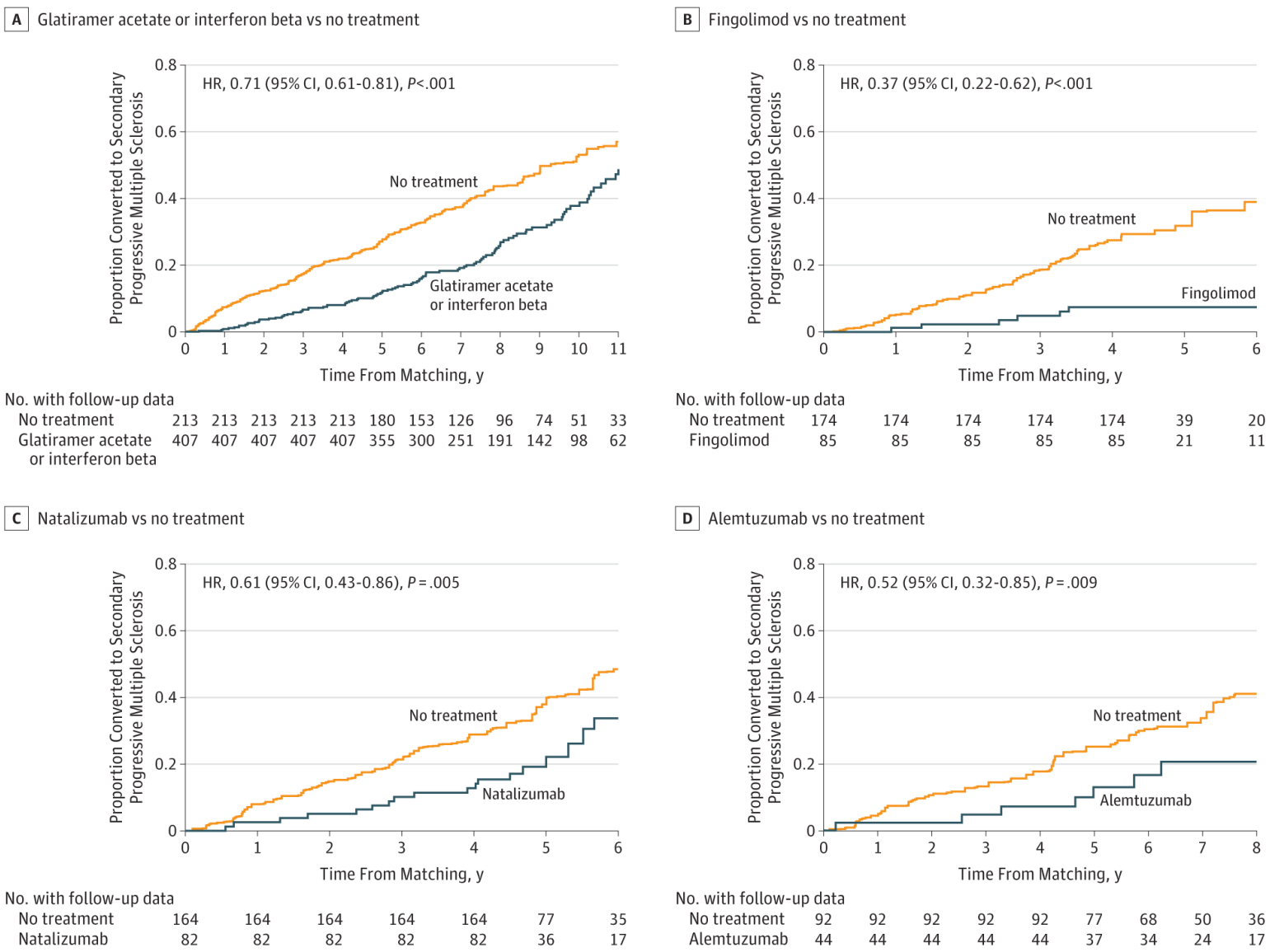

Figure 18: Comparison of the Cumulative Hazard of Conversion to Secondary Progressive Multiple Sclerosis in Untreated Patients vs Matched Treated Patients Compared by Initial Treatment. HR indicates hazard ratio. Reproduced with permission from The American Medical Association (License number 4720830643128; granted 2nd December 2019)

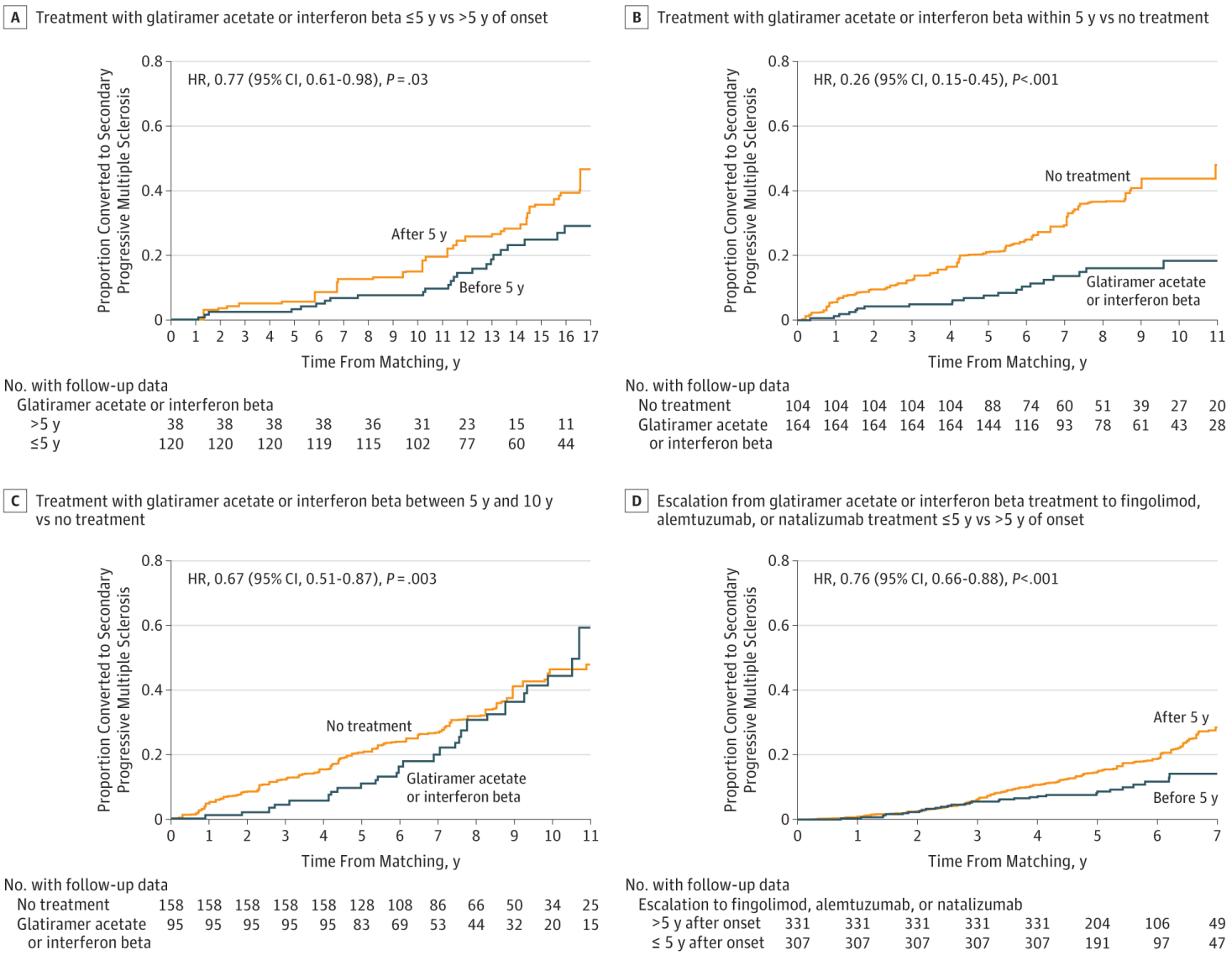

Figure 19: Comparison of the Cumulative Hazard of Conversion to Secondary Progressive Multiple Sclerosis by Timing of Treatment. HR indicates hazard ratio. Reproduced with permission from The American Medical Association (License number 4720830643128; granted 2nd December 2019)

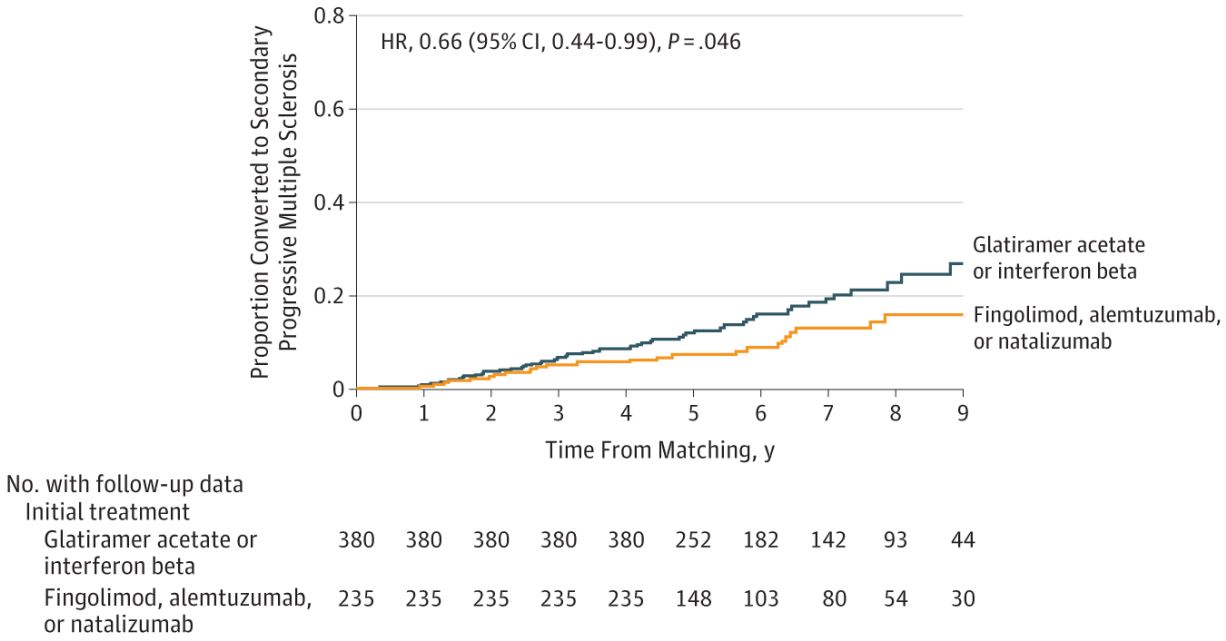

Figure 20: Comparison of Cumulative Hazard of Conversion to Secondary Progressive Multiple Sclerosis for Initial Treatment with Glatiramer Acetate or Interferon Beta vs Fingolimod, Alemtuzumab, or Natalizumab. HR indicates hazard ratio. Reproduced with permission from The American Medical Association (License number 4720830643128; granted 2nd December 2019).

patients (n=164) (HR 0.61 (95% CI 0.43−0.86), p=0.005; median censored follow-up 4.9 (IQR 4.4-5.8) years): at 5 years 19% vs 38% respectively had converted, while at 6 years 34% vs 48% had converted (Figure 18). The hazard ratio for converting to SPMS was significantly lower for patients initially treated with alemtuzumab (n=44) compared to untreated patients (n=92) (0.52 (95%CI 0.32−0.85), p=0.009; median censored follow-up 7.4 (IQR 6.0-8.6) years): at 5 years 10% vs 25% respectively had converted, while at 8 years 21% vs 41% had converted (Figure 18).

The probability of converting to SPMS was significantly lower for patients initially receiving glatiramer acetate or interferon beta within 5 years of disease onset (n=120) compared to matched patients treated with glatiramer acetate or interferon beta later (n=38) (HR 0.77 (95%CI 0.61-0.98), p=0.03), median censored follow-up 13.4 (IQR 11-18.1) years. Five years after baseline 3% vs 6%, respectively, had converted to SPMS, while at 17 years 29% vs 47% had converted (Figure 19). Including patients escalated to mitoxantrone did not materially alter the

results (HR 0.82 (95%CI 0.67-1.00), p=0.05). The probability of converting to SPMS was significantly lower when initial treatment with glatiramer acetate or interferon beta was commenced within 5 years of disease onset (n=164) compared to untreated patients (n=104) (HR 0.26 (95%CI 0.15-0.45), p<0.001) with the difference increasing proportionally throughout the 11 years of follow-up (corresponding to 14 years disease duration (Figure 19)). In contrast, the significantly lower probability of conversion following initial treatment with glatiramer acetate or interferon beta commencing 5-10 years after disease onset (n=95) compared to untreated patients (n=158, HR 0.67 (95%CI 0.51-0.87), p=0.003) waned after 5 years of treatment (disease duration 11.8 years) and disappeared at 7.8 years (disease duration 14.6 years, Figure 19)). The probability of converting to SPMS was significantly lower for patients escalated from glatiramer acetate or interferon beta to fingolimod, alemtuzumab or natalizumab within 5 years of disease onset (n=307) compared to matched patients escalated later (n=331, HR 0.76 (95%CI 0.66-0.88), p<0.001; median censored follow-up 5.3 (IQR 4.6-6.1) years): at 5 years, 8% vs 14% respectively had converted while at 7 years, 14% vs 28% had converted (Figure 19). This difference persisted when the alternative (7-year) definition of alemtuzumab treatment duration was employed in a sensitivity analysis (HR 0.78 (95%CI 0.67-0.91), p=0.001).

Patients initially receiving fingolimod, alemtuzumab or natalizumab (n=235) had a significantly lower risk of conversion to SPMS than matched patients initially receiving glatiramer acetate or interferon beta (n=380) (HR 0.66 (95% CI 0.44-0.99), p=0.046; median censored follow-up 5.8 (IQR 4.7-8.0) years). At 5 years, 7% vs 12% respectively had converted, while at 9 years, 16% vs 27% respectively had converted (Figure 20). This persisted in sensitivity analyses when the alternative (7-year) definition of alemtuzumab treatment duration was used (HR 0.60 (95%CI 0.39-0.90), p=0.01); and when patients in the glatiramer acetate or interferon beta group escalated to mitoxantrone were included (HR 0.88 (95%CI 0.84-0.91), p<0.001).

Data quality procedure

•Duplicate patient records were removed.

•Centres with <10 patient records were excluded.

•Patients with missing date of birth were excluded.

•MS onset dates after the MSBase / University Hospital Wales / European Alemtuzumab centres data extract dates were removed.

•Patients with missing date of the first clinical presentation of MS were excluded.

•Patients with primary progressive or relapsing-progressive MS were excluded

•The dates of MS onset and the first recorded MS course were aligned.

•Patients with the age at onset outside the 0-100 range were excluded.

•A logical sequence of the MS courses (i.e. clinically isolated syndrome, then relapsing-remitting MS, then secondary progressive MS) was assured.

•Patients where conversion to secondary progressive MS occurred prior to commencing therapy (or being randomised for untreated patients) were excluded.

•Visits with missing visit date or the recorded date before the clinical MS onset or after the date of MSBase data extract were removed.

•EDSS scores outside the range of possible EDSS values were removed.

•Duplicate visits were merged.

•MS relapses with missing onset date or the recorded date after the date of MSBase data extractwere removed.

•Duplicate MS relapses were merged.

•Relapses occurring within 30 days of each other were merged.

•Visits preceded by relapses were identified and time from the last relapse was calculated for each visit.

•Therapies were labelled as discontinued or continuing.

•Therapies with erroneous date entries were removed (e.g. commencement date > termination date, commencement after the MSBase data extract date, commencement of disease modifying therapy before the year 1980).

•MS disease modifying therapies were identified and labelled.

•Duplicate treatment entries were removed.

•Where multiple disease modifying therapies were recorded simultaneously, treatment end date of the previous therapy was imputed as the commencement date of the following therapy.

Baseline demographics for prematching cohorts, unmatched cohorts and matched cohorts

Initial ß-IFN / GA versus untreated

	Prematching ß-IFN|GA, n=431	Prematching Untreated, n=275	Standardized Difference	Unmatched ß-IFN|GA, n=24 (6%)	Unmatched Untreated, n=62 (23%)	Standardized Difference	Matched ß-IFN|GA, n=407 (94%)	Matched Untreated, n=213 (77%)	Standardized Difference
Age, years Mean (SD)	34 (8)	NA	NA	31 (9)	NA	NA	35 (8)	35 (8)	0.01
Sex, female Number (%)	303 (70%)	NA	NA	11 (46%)	NA	NA	292 (72%)	155 (73%)	0.05
Disease duration, years Median (IQR)	5 (3-10)	NA	NA	5 (2-10.2)	NA	NA	5.7 (3.1 - 10.5)	5.1 (2 - 9.8)	0.05
Relapses in year before baseline Mean (SD)	1.2 (1.1)	NA	NA	1.8 (1.6)	NA	NA	1.1 (1)	1.1 (0.9)	0.06
Disability, EDSS step Median (IQR)	2 (1.5-3.5)	NA	NA	2 (1.4-2.6)	NA	NA	2.5 (1.5 - 3.5)	2 (1 - 3.5)	0.1
Baseline year of inclusion Median (IQR)	1996 (1996-1997)	NA	NA	1996 (1995-1997)	NA	NA	1996 (1996-1997)	2007 (2004-2009)	NA

Table 16: The untreated groups and late groups do not have prematching or unmatched data presented in the tables. This is deliberate – to achieve the closest match, each untreated or late patient had baseline set at the visit when clinical and demographic parameters most closely matched those of individual treated patients or early patients respectively (as described in the Methods section). For untreated patients this is usually not the first visit; and for late-treated patients it is a visit before treatment started. The mean age and disease durations of the matched patients are therefore significantly different to the corresponding values in the pre-matching and unmatched data (for example, the mean age in the matched untreated cohorts is 35-39; but the mean age if all permutations of each patient are averaged is 51; alternatively, using the first visit for each untreated patient gives an unrepresentatively low age). ß-IFN|GA = beta-interferon or glatiramer acetate. EDSS: Expanded disability status scale. F|A|N = fingolimod, alemtuzumab or natalizumab. SPMS: secondary progressive multiple sclerosis. % in column headings: percentage of prematching patients.

Initial Fingolimod versus untreated

	Prematching Fingolimod, n=88	Prematching Untreated, n=275	Standardized Difference	Unmatched Fingolimod, n=3 (3%)	Unmatched Untreated, n=101 (37%)	Standardized Difference	Matched Fingolimod, n=85 (97%)	Matched Untreated, n=174 (63%)	Standardized Difference
Age, years Mean (SD)	37 (12)	NA	NA	30 (6)	NA	NA	39 (12)	39 (10)	0
Sex, female Number (%)	61 (69%)	NA	NA	2 (67%)	NA	NA	59 (69%)	127 (73%)	0.04
Disease duration, years Median (IQR)	4 (1-9)	NA	NA	2 (1-4.5)	NA	NA	4.9 (1.7 - 9.7)	5.1 (2.1 - 9)	0.03
Relapses in year before baseline Mean (SD)	1 (0.9)	NA	NA	1.7 (1.5)	NA	NA	0.9 (0.9)	0.9 (1)	0.02
Disability, EDSS step Median (IQR)	2 (1.5-3.1)	NA	NA	1.5 (1.5-1.8)	NA	NA	2 (1-3.5)	2 (1.5 - 3.5)	0
Baseline year of inclusion Median (IQR)	2011 (2011 - 2012)	NA	NA	2011 (2009 - 2011)	NA	NA	2011 (2011 - 2012)	2007 (2007 - 2009)	NA

Table 17: The untreated groups and late groups do not have prematching or unmatched data presented in the tables. This is deliberate – to achieve the closest match, each untreated or late patient had baseline set at the visit when clinical and demographic parameters most closely matched those of individual treated patients or early patients respectively (as described in the Methods section). For untreated patients this is usually not the first visit; and for late-treated patients it is a visit before treatment started. The mean age and disease durations of the matched patients are therefore significantly different to the corresponding values in the pre-matching and unmatched data (for example, the mean age in the matched untreated cohorts is 35-39; but the mean age if all permutations of each patient are averaged is 51; alternatively, using the first visit for each untreated patient gives an unrepresentatively low age). ß-IFN|GA = beta-interferon or glatiramer acetate. EDSS: Expanded disability status scale. F|A|N = fingolimod, alemtuzumab or natalizumab. SPMS: secondary progressive multiple sclerosis. % in column headings: percentage of prematching patients.

Initial Natalizumab versus untreated

	Prematching Natalizumab, n=100	Prematching Untreated, n=275	Standardized Difference	Unmatched Natalizumab n=18 (18%)	Unmatched Untreated, n=111 (40%)	Standardized Difference	Matched Natalizumab n=82 (82%)	Matched Untreated, n=164 (60%)	Standardized Difference
Age, years Mean (SD)	35 (10)	NA	NA	26 (8)	NA	NA	39 (9)	38 (9)	0.03
Sex, female Number (%)	61 (61%)	NA	NA	7 (39%)	NA	NA	54 (66%)	108 (66%)	0.06
Disease duration, years Median (IQR)	3.5 (1-9)	NA	NA	1 (1-1.8)	NA	NA	6.2 (2 - 10.5)	5.2 (2.3 - 8.9)	0.15
Relapses in year before baseline Mean (SD)	1.7 (1.4)	NA	NA	3.7 (1.2)	NA	NA	1.1 (1)	1.1 (1)	0.01
Disability, EDSS step Median (IQR)	3 (2-4)	NA	NA	3.5 (2-4)	NA	NA	2.5 (2 - 4.5)	3 (2 - 4.5)	0.28
Baseline year of inclusion Median (IQR)	2010 (2009-2011)	NA	NA	2011 (2010-2011)	NA	NA	2010 (2009 - 2011)	2006 (2005 - 2008)	NA

Table 18: The untreated groups and late groups do not have prematching or unmatched data presented in the tables. This is deliberate – to achieve the closest match, each untreated or late patient had baseline set at the visit when clinical and demographic parameters most closely matched those of individual treated patients or early patients respectively (as described in the Methods section). For untreated patients this is usually not the first visit; and for late-treated patients it is a visit before treatment started. The mean age and disease durations of the matched patients are therefore significantly different to the corresponding values in the pre-matching and unmatched data (for example, the mean age in the matched untreated cohorts is 35-39; but the mean age if all permutations of each patient are averaged is 51; alternatively, using the first visit for each untreated patient gives an unrepresentatively low age). ß-IFN|GA = beta-interferon or glatiramer acetate. EDSS: Expanded disability status scale. F|A|N = fingolimod, alemtuzumab or natalizumab. SPMS: secondary progressive multiple sclerosis. % in column headings: percentage of prematching patients.

Initial Alemtuzumab versus untreated

	Prematching Alemtuzumab, n=57	Prematching Untreated, n=275	Standardized Difference	Unmatched Alemtuzumab n=13 (23%)	Unmatched Untreated, n=183 (67%)	Standardized Difference	Matched Alemtuzumab n=44 (77%)	Matched Untreated, n=92 (33%)	Standardized Difference
Age, years Mean (SD)	32 (8)	NA	NA	26 (4)	NA	NA	35 (8)	35 (7)	0.08
Sex, female Number (%)	43 (75%)	NA	NA	10 (77%)	NA	NA	30 (68%)	65 (71%)	0.04
Disease duration, years Median (IQR)	3 (1-4)	NA	NA	2 (1-3)	NA	NA	3.2 (2 - 5.8)	3.8 (1.9 - 6.7)	0.17
Relapses in year before baseline Mean (SD)	2.1 (1.5)	NA	NA	3.6 (1.5)	NA	NA	1.3 (1)	1.3 (1)	0.03
Disability, EDSS step Median (IQR)	3.5 (1.5-5.5)	NA	NA	4 (1.5-6)	NA	NA	3.5 (2 - 4.5)	3.5 (2 - 5.5)	0
Baseline year of inclusion Median (IQR)	2005 (2003-2006)	NA	NA	2003 (2002-2005)	NA	NA	2006 (2003-6)	2006 (2005-8)	NA

Table 19: The untreated groups and late groups do not have prematching or unmatched data presented in the tables. This is deliberate – to achieve the closest match, each untreated or late patient had baseline set at the visit when clinical and demographic parameters most closely matched those of individual treated patients or early patients respectively (as described in the Methods section). For untreated patients this is usually not the first visit; and for late-treated patients it is a visit before treatment started. The mean age and disease durations of the matched patients are therefore significantly different to the corresponding values in the pre-matching and unmatched data (for example, the mean age in the matched untreated cohorts is 35-39; but the mean age if all permutations of each patient are averaged is 51; alternatively, using the first visit for each untreated patient gives an unrepresentatively low age). ß-IFN|GA = beta-interferon or glatiramer acetate. EDSS: Expanded disability status scale. F|A|N = fingolimod, alemtuzumab or natalizumab. SPMS: secondary progressive multiple sclerosis. % in column headings: percentage of prematching patients.

Initial ß-IFN / GA within 5 years versus initial ß-IFN / GA after 5 years

	Prematching ß-IFN|GA within 5y, n=175	Prematching ß-IFN|GA after 5y, n=53	Standardized Difference	Unmatched ß-IFN|GA within 5y, n=55 (31%)	Unmatched ß-IFN|GA after 5y, n=15 (28%)	Standardized Difference	Matched ß-IFN|GA within 5y, n=120 (69%)	Matched ß-IFN|GA after 5y, n=38 (72%)	Standardized Difference
Age, years Mean (SD)	31 (8)	NA	NA	33 (10)	NA	NA	30 (7)	31 (7)	0.14
Sex, female Number (%)	119 (68%)	NA	NA	31 (56%)	NA	NA	88 (73%)	27 (70%)	0.06
Disease duration, years Median (IQR)	3 (2-4)	NA	NA	2 (1-3)	NA	NA	3.2 (2.1 - 4.1)	3.5 (2.7 - 4.2)	0.26
Relapses in year before baseline Mean (SD)	1.4 (1.2)	NA	NA	1.6 (1.2)	NA	NA	1 (1.1)	1 (0.9)	0
Disability, EDSS step Median (IQR)	2 (1.5-3)	NA	NA	2 (1.2-3)	NA	NA	2 (1.5 - 3)	2 (1 - 2.5)	0
Baseline year of inclusion Median (IQR)	1996 (1996-1997)	NA	NA	1997 (1996-1997)	NA	NA	1996 (1995-1997)	1992 (1988-1994)	NA

Table 20: The untreated groups and late groups do not have prematching or unmatched data presented in the tables. This is deliberate – to achieve the closest match, each untreated or late patient had baseline set at the visit when clinical and demographic parameters most closely matched those of individual treated patients or early patients respectively (as described in the Methods section). For untreated patients this is usually not the first visit; and for late-treated patients it is a visit before treatment started. The mean age and disease durations of the matched patients are therefore significantly different to the corresponding values in the pre-matching and unmatched data (for example, the mean age in the matched untreated cohorts is 35-39; but the mean age if all permutations of each patient are averaged is 51; alternatively, using the first visit for each untreated patient gives an unrepresentatively low age). ß-IFN|GA = beta-interferon or glatiramer acetate. EDSS: Expanded disability status scale. F|A|N = fingolimod, alemtuzumab or natalizumab. SPMS: secondary progressive multiple sclerosis. % in column headings: percentage of prematching patients.

Initial ß-IFN / GA within 5 years versus untreated

	Prematching ß-IFN|GA within 5y, n=175	Prematching Untreated, n=275	Standardized Difference	Unmatched ß-IFN|GA within 5y, n=11 (6%)	Unmatched Untreated, n=171 (62%)	Standardized Difference	Matched ß-IFN|GA within 5y, n=164 (94%)	Matched Untreated, n=104 (38%)	Standardized Difference
Age, years Mean (SD)	31 (8)	NA	NA	27 (8)	NA	NA	33 (8)	33 (7)	0.02
Sex, female Number (%)	119 (68%)	NA	NA	6 (55%)	NA	NA	113 (69%)	76 (73%)	0.07
Disease duration, years Median (IQR)	3 (2-4)	NA	NA	1 (1-2)	NA	NA	3 (2.1 - 4)	2.1 (1 - 3.5)	0.5
Relapses in year before baseline Mean (SD)	1.4 (1.2)	NA	NA	2 (1.7)	NA	NA	1.3 (1)	1.2 (1)	0.06
Disability, EDSS step Median (IQR)	2 (1.5-3)	NA	NA	2 (1.9-2.2)	NA	NA	2 (1.5 - 3.5)	2 (1.5 - 3.5)	0
Baseline year of inclusion Median (IQR)	1996 (1996-1997)	NA	NA	1997 (1995-1997)	NA	NA	1996 (1995-1997)	2006 (2005-2008)	NA

Table 21: The untreated groups and late groups do not have prematching or unmatched data presented in the tables. This is deliberate – to achieve the closest match, each untreated or late patient had baseline set at the visit when clinical and demographic parameters most closely matched those of individual treated patients or early patients respectively (as described in the Methods section). For untreated patients this is usually not the first visit; and for late-treated patients it is a visit before treatment started. The mean age and disease durations of the matched patients are therefore significantly different to the corresponding values in the pre-matching and unmatched data (for example, the mean age in the matched untreated cohorts is 35-39; but the mean age if all permutations of each patient are averaged is 51; alternatively, using the first visit for each untreated patient gives an unrepresentatively low age). ß-IFN|GA = beta-interferon or glatiramer acetate. EDSS: Expanded disability status scale. F|A|N = fingolimod, alemtuzumab or natalizumab. SPMS: secondary progressive multiple sclerosis. % in column headings: percentage of prematching patients.

Initial ß-IFN / GA 5-10 years versus untreated

	Prematching ß-IFN|GA between 5-10y, n=102	Prematching Untreated, n=275	Standardized Difference	Unmatched ß-IFN|GA between 5-10y n=7 (7%)	Unmatched Untreated, n=117 (43%)	Standardized Difference	Matched ß-IFN|GA between 5-10y n=95 (93%)	Matched Untreated, n=158 (57%)	Standardized Difference
Age, years Mean (SD)	35 (8)	NA	NA	30 (9)	NA	NA	37 (7)	36 (8)	0.08
Sex, female Number (%)	71 (70%)	NA	NA	5 (71%)	NA	NA	66 (69%)	111 (70%)	0.02
Disease duration, years Median (IQR)	7 (6-8)	NA	NA	7 (6-7)	NA	NA	6.8 (5.9 - 8.3)	5.3 (2.1 - 10)	0.31
Relapses in year before baseline Mean (SD)	1 (1)	NA	NA	0.6 (0.8)	NA	NA	1.1 (1)	0.9 (0.9)	0.18
Disability, EDSS step Median (IQR)	2 (1.5-3)	NA	NA	2 (2-2.8)	NA	NA	2.5 (1.5 - 3.5)	2.5 (1.5 - 3.5)	0
Baseline year of inclusion Median (IQR)	1996 (1996-1997)	NA	NA	1997 (1997-1997)	NA	NA	1996 (1995 - 1997)	2006 (2004 - 2008)	NA

Table 22: The untreated groups and late groups do not have prematching or unmatched data presented in the tables. This is deliberate – to achieve the closest match, each untreated or late patient had baseline set at the visit when clinical and demographic parameters most closely matched those of individual treated patients or early patients respectively (as described in the Methods section). For untreated patients this is usually not the first visit; and for late-treated patients it is a visit before treatment started. The mean age and disease durations of the matched patients are therefore significantly different to the corresponding values in the pre-matching and unmatched data (for example, the mean age in the matched untreated cohorts is 35-39; but the mean age if all permutations of each patient are averaged is 51; alternatively, using the first visit for each untreated patient gives an unrepresentatively low age). ß-IFN|GA = beta-interferon or glatiramer acetate. EDSS: Expanded disability status scale. F|A|N = fingolimod, alemtuzumab or natalizumab. SPMS: secondary progressive multiple sclerosis. % in column headings: percentage of prematching patients.

Escalation from ß-IFN/GA to F/A/N within 5 years versus escalation from ß-IFN / GA to F/A/N after 5 years

	Prematching Escalation to F|A|N within 5y, n=376	Prematching Escalation to F|A|N after 5y, n=421	Standardized Difference	Unmatched Escalation to F|A|N within 5y n=69 (18%)	Unmatched Escalation to F|A|N after 5y, n=90 (21%)	Standardized Difference	Matched Escalation to F|A|N within 5y n=307	Matched Escalation to F|A|N after 5y, n=331	Standardized Difference
Age, years Mean (SD)	33 (10)	NA	NA	37 (11)	NA	NA	(82%) 33 (9)	(79%) 32 (8)	0.03
Sex, female Number (%)	266 (71%)	NA	NA	48 (70%)	NA	NA	218 (71%)	233 (70%)	0.09
Disease duration, years Median (IQR)	3 (2-4)	NA	NA	3 (2-4)	NA	NA	3 (2.1 - 4)	3.5 (2.5 - 4.3)	0.41
Relapses in year before baseline Mean (SD)	1.6 (1.2)	NA	NA	2.6 (1.5)	NA	NA	1 (1.1)	1 (1)	0
Disability, EDSS step Median (IQR)	2.5 (1.5-4)	NA	NA	4 (3-6)	NA	NA	2 (1.5 - 3.5)	2 (1.1 - 3.0)	0
Baseline year of inclusion Median (IQR)	2010 (2009-2011)	NA	NA	2009 (2007-2010)	NA	NA	2010 (2009 - 2011)	2005 (2003 - 2007)	NA

Table 23: The untreated groups and late groups do not have prematching or unmatched data presented in the tables. This is deliberate – to achieve the closest match, each untreated or late patient had baseline set at the visit when clinical and demographic parameters most closely matched those of individual treated patients or early patients respectively (as described in the Methods section). For untreated patients this is usually not the first visit; and for late-treated patients it is a visit before treatment started. The mean age and disease durations of the matched patients are therefore significantly different to the corresponding values in the pre-matching and unmatched data (for example, the mean age in the matched untreated cohorts is 35-39; but the mean age if all permutations of each patient are averaged is 51; alternatively, using the first visit for each untreated patient gives an unrepresentatively low age). ß-IFN|GA = beta-interferon or glatiramer acetate. EDSS: Expanded disability status scale. F|A|N = fingolimod, alemtuzumab or natalizumab. SPMS: secondary progressive multiple sclerosis. % in column headings: percentage of prematching patients.

Initial ß-IFN / GA versus initial F/A/N

	Prematching F|A|N, n=376	Prematching ß-IFN|GA, n=431	Standardized Difference	Unmatched F|A|N n=141 (37%)	Unmatched ß-IFN|GA, n=51 (12%)	Standardized Difference	Matched F|A|N, n=235 (63%)	Matched ß-IFN|GA, n=380 (88%)	Standardized Difference
Age, years Mean (SD)	35 (10)	34 (8)	0.11	36 (10)	37 (7)	-0.11	34 (11)	34 (9)	0.06
Sex, female Number (%)	267 (71%)	303 (70%)	0.02	105 (75%)	36 (70%)	0.06	162 (69%)	267 (70%)	0.01
Disease duration, years Median (IQR)	3 (1-8)	5 (3-10)	0.33	2 (1-6)	7 (4-12)	-0.85	6.5 (2.1 - 12)	5.1 (2.7 - 9.6)	0.2
Relapses in year before baseline Mean (SD)	1.5 (1.3)	1.2 (1.1)	0.25	1.8 (1.4)	0.5 (0.7)	1.19	1.2 (1.1)	1.3 (1.1)	0.1
Disability, EDSS step Median (IQR)	2.5 (1.5-4)	2 (1.5-3.5)	0.32	4 (2-5.5)	2.5 (2-3.5)	0.86	2 (1.5 - 3)	2 (1.5 - 3.5)	0.02
Baseline year of inclusion Median (IQR)	2010 (2007-2011)	1996 (1996-1997)	NA	2010 (2007-2011)	1996 (1995-1997)	NA	2009 (2008 - 2011)	1996 (1996 - 1997)	NA

Table 24: ß-IFN|GA = beta-interferon or glatiramer acetate. EDSS: Expanded disability status scale. F|A|N = fingolimod, alemtuzumab or natalizumab. SPMS: secondary progressive multiple sclerosis. % in column headings: percentage of prematching patients.

Propensity scores before and after matching

	ß-IFN|GA	Untreated	Difference	Fingolimod	Untreated	Difference	Natalizumab	Untreated	Difference	Alemtuzumab	Untreated	Difference
Before matching, mean	0.34	0.123	0.217	0.183	0.058	0.125	0.297	0.057	0.24	0.363	0.029	0.334
After matching, mean	0.328	0.327	0.001	0.175	0.175	0	0.205	0.204	0.001	0.245	0.244	0 .001
Mean % improvement, unmatched to matched	NA	NA	99.54%	NA	NA	100%	NA	NA	99.58%	NA	NA	100%

	ß-IFN|GA within 5y	ß-IFN|GA after 5y	Difference	ß-IFN|GA within 5y	Untreated	Difference	ß-IFN|GA between 5-10y	Untreated	Difference	Escalation to F|A|N within 5y	Escalation to F|A|N after 5y	Difference	ß-IFN|GA	F|A|N	Difference
Before matching, mean	0.483	0.017	0.466	0.467	0.075	0.392	0.245	0.062	0.183	0.162	0.023	0.139	0.559	0.385	0.174
After matching, mean	0.48	0.48	0	0.447	0.446	0.001	0.234	0.233	0.001	0.14	0.139	0 .001	0.474	0.462	0.012
Mean % improvement, unmatched to matched	NA	NA	99.79%	NA	NA	99.74%	NA	NA	99.45%	NA	NA	100%	NA	NA	92.53%

Table 25: Propensity scores before and after matching. ß-IFN|GA = beta-interferon or glatiramer acetate. F|A|N = fingolimod, alemtuzumab or natalizumab.

Clinical characteristics of patients excluded through missing data.

	Patients excluded due to data missingness*† n= 2,041	Patients presented for matching*† n=1,550
Age, years Mean (SD)	37 (11)	33 (9)
Sex, female Number (%)	1474 (72%)	1117 (72%)
Disease duration, years Mean (SD) Median (IQR)	7.4 (6.8) 3.2 (2 - 5)	4.5 (4.9) 3 (1 - 8.9)
Relapses in year before baseline Mean (SD) Median (IQR)	0.8 (1.0) 1 (0-1)	1.3 (1.1) 1 (0-2)
Disability, EDSS step Median (IQR)	2 (1.5-3.5)	1 (0-2)

*Table 26: Comparison of baseline demographics between patients excluded due to data missingness (<3 EDSS scores or <4 years of follow-up despite commencing the therapy more than 4 years data censor date) and those presented for matching.*minus untreated patients (as untreated patients have multiple potential baseline dates). †Baseline demographics presented at time of starting therapy.*

Chapter 6: Discussion

Project 1: Periventricular gradients after a clinically isolated syndrome

In a previous study in people with established RRMS and SPMS, MS effects on NAWM MTR were found to increase close to the lateral ventricles (Liu *et al.*, 2015). However, it could not be determined how early in the clinical course of MS this abnormal periventricular MTR gradient occurred, whether or not it was due to a mechanism independent of WM lesion formation, or if it was associated with subsequent disease activity. In the present study we found that an abnormal periventricular MTR gradient is present within five months of a clinically isolated ON, is not dependent on the presence of WM lesions and is associated with the subsequent risk of developing MS and disability. Both the periventricular NAWM MTR gradient and WM lesions independently predicted conversion to CDMS over two years. This raises the possibility that lesions and NAWM periventricular abnormalities in early MS may arise from different but nevertheless clinically relevant pathophysiological processes.

In the ON group we looked for significant differences in the periventricular MTR gradients between those with and without WM lesions, those with and without periventricular WM lesions, and those with and without gadolinium-enhancing lesions, and found none. Consistent with previous work (Liu *et al.*, 2015) MTR in lesions also showed periventricular gradients similar to those in NAWM. Collectively, this strongly suggests that abnormal gradients in NAWM MTR are not dependent on the presence of WM lesions. In keeping with

previous results (Barkhof *et al.*, 1997) periventricular lesions predicted conversion to CDMS over two years, and in a multivariate logistic regression the MTR gradient over 1-5mm also independently predicted conversion to CDMS over two years. The identification of an early abnormal periventricular MTR gradient that is not directly related to lesion formation, but linked with clinical outcomes suggests that there is a clinically relevant pathological process at least partially distinct to that underlying lesion formation.

The pathological basis of the abnormal periventricular MTR gradient is uncertain. MTR correlates with myelin and axonal density, which are themselves correlated (Schmierer *et al.*, 2007a) and may also be reduced by tissue oedema and inflammation (Dousset *et al.*, 1992; Gareau *et al.*, 2000). There have been no histopathological studies looking for a gradient of pathology in extra-lesional periventricular WM. Several mechanisms could underlie the periventricular MTR changes seen, perhaps in combination, but without knowing the underlying pathological substrate we can only speculate which are responsible. These are discussed in a later section (p.165).

Elucidating the responsible mechanism(s) may have significant implications for early MS treatment. For example, in established MS, neuropathological work has shown a cortical gradient in neuronal loss (Magliozzi *et al.*, 2010) where an MTR gradient has also been identified (Samson *et al.*, 2014). If a gradient in axonal loss were confirmed around the ventricles, one might infer that the *in vivo* periventricular MTR findings indicate a neurodegenerative process that should be targeted from the earliest clinical stages of MS.

There are a few study limitations worth noting. First, we used previously acquired MTR data with lower resolution (1x1x5mm) than that used in our recent study examining periventricular gradients in established MS (1x1x1mm, (Liu *et al.*, 2015)) and given this, partial volume effects were a greater concern. To minimize these, we restricted our analysis to two axial slices perpendicular to the lateral ventricular wall (Figure 3), so avoiding oblique CSF-WM boundaries within periventricular voxels, and through plane smoothing of periventricular MTR gradients (recalling that these were seen over the first 5 mm around the ventricles, and the axial slices were 5 mm thick). Despite this, the first two periventricular bands still contained CSF in the majority of participants, and so these bands were also excluded from subsequent analyses. Noting that the periventricular MTR gradient seen in previous work was steepest close to the ventricles (Liu *et al.*, 2015), it is likely that excluding these bands will have significantly reduced our sensitivity to gradients. In 10/81 participants with ON and 2/39 healthy controls, there was still CSF in the third band so these participants were also excluded from the analyses, further reducing the power of the study to detect periventricular gradients. While we were very careful to avoid partial volume effects between CSF and WM, partial volume between periventricular bands will tend to smooth MTR gradients, and so reduce sensitivity to disease effects. Similarly, restricting our analysis to two axial slices, while limiting the risk of MTR gradients being smoothed through plane, substantially reduced the volume of each band studied when compared to our previous study using 1x1x1mm MTR data; this too is likely to have reduced sensitivity to disease effects. To allow for brain atrophy, which could exacerbate this further, we included BPF as a covariate when looking for differences in MTR gradients between clinical subgroups, and found no material difference in the results. To provide context with established MTR metrics and confirm that the difference in MTR gradient between converters and non-converters was not simply driven by diffuse

tissue differences, we added NAWM and GM MTR as covariates and the MTR gradient remained a significant factor.

By five years, about ~55% of the ON group developed CDMS, while at the time of their MTR scan only ~10% had done so (Table 3). The pattern of group differences in periventricular MTR gradient were still apparent, albeit with less statistical significance, following exclusion of those converting before the MTR scan (see p.**Error! Bookmark not defined.**). As such, we think it is unlikely that the apparent predictive power of the periventricular MTR gradient for conversion to CDMS within 5 years is simply due to such a gradient being present in those who had already developed CDMS by the time of their MTR scan. Thirteen of the 71 people with ON studied at baseline did not have clinical follow-up. There were no significant differences in any baseline demographic features between those who were or were not followed up (see p.**Error! Bookmark not defined.**), so we believe this is unlikely to have biased our results in favour of detecting differences in periventricular MTR gradients between groups, but it may have reduced our sensitivity to them.

While we have assessed cross-sectional differences in MTR measures between the HC and ON groups, it would be of considerable interest to see how these differences evolve with time, and whether or not these changes relate more closely to clinical outcomes. Some longitudinal MTR data is available for the present cohorts (HC n = 18, ON n = 44), but the resolution of the 2D MTR scans (1 x 1 x 5mm) means that it is not possible to accurately align the same axial slices over time. When we looked for changes in periventricular MTR gradients over time without registering scans, we found no significant change over 5 years.

It is well recognised that a substantial number of people with MS may have significant cognitive deficits (Langdon, 2011). However, only about half (31/58) of those followed-up at 5 years underwent cognitive testing, of whom only 12 had developed clinically definite MS. Given this, it is perhaps unsurprising that we did not find a correlation between periventricular MTR gradients and cognitive impairment in this cohort, and this might be better examined in a group of people with progressive MS who are more likely to have cognitive impairment (Langdon, 2011).

The parent cohort's principal presenting CIS was ON, and for consistency we excluded three non-ON participants who would otherwise have been eligible for our study. In some cohorts, ON appears to carry a lower risk of conversion to CDMS when compared with other presentations (Tintore *et al.*, 2015) and it would be of interest to see if periventricular gradients differ dependent on the type of CIS.

In our assessment of the lesional periventricular gradient, we account for increasing band size by presenting the percentage of lesioned WM per band (Figure 10). However, this might not fully exclude an effect from band volume due to the periventricular predilection for lesions. Future work should list the volume per band.

While inner periventricular MTR gradients independently contributed to the prediction of conversion to CDMS and McDonald MS, there was substantial overlap in the range of values between groups (see p.99) and no clear threshold was found beyond which conversion to MS by 5 years was inevitable. As such the methods employed here for measuring periventricular MTR gradients are unlikely to be useful in clinical practice. It remains unclear whether

methodological optimisation will improve this capability, or whether – like lesional metrics – accurate individual prognostication using gradients is not possible. However, this does not negate the clinical relevance of the pathological processes underlying abnormal MTR gradients, which - independent of those leading to WM lesion formation - may be a potential target for treatments.

In conclusion, our findings show that an abnormal periventricular MTR gradient occurs soon after a CIS and is associated with subsequent conversion to MS and disability. The abnormal periventricular MTR gradient was not significantly affected by the presence of WM lesions, and therefore seems likely to arise from an at least partly independent mechanism. Histopathological studies are warranted to elucidate the nature of these MTR gradients.

Project 2: Periventricular and cortical gradients in progressive multiple sclerosis

We identified both periventricular and cortical MTR gradients in PPMS and replicated our previous findings of cortical and periventricular gradients in SPMS (Samson *et al.*, 2014; Liu *et al.*, 2015). The cortical and periventricular gradients did not differ significantly between the PPMS and SPMS groups. In the few subjects with longitudinal imaging, when compared with healthy controls, no significant changes in these gradients were observed over a median period of 2 years. When all people with MS were combined, significant associations were seen between periventricular and cortical gradient severity; and both gradients increased with increasing disability and disease duration.

The present results suggest that the processes underlying cortical and periventricular MTR gradients may be similar in PPMS and SPMS. The finding of a cortical gradient in PPMS in the present study but not previously (Samson *et al.*, 2014) appears to reflect the larger cohort (28 here versus 19 previously with PPMS; 51 versus 35 healthy controls). However, while the optimized processing pipeline better accounts for cortical folding, its ability to distinguish cortical gradients from whole cortical MTR effects is severely limited because cortical gradients are calculated from the only 2 cortical bands of MTR, which may explain why all cortical models lost significance when additionally covaried for mean CGM MTR.

The pathological substrate and pathogenic processes underlying these MTR gradients remain unknown, but are discussed in a later section (p.165).

The presence of a significant association between cortical and periventricular gradients in the RRMS group (n=56) but not the PPMS (n=28) or SPMS (n=35) groups may also reflect the smaller sample sizes, particularly given the significant association seen at the whole-group level when additionally covarying for clinical classification. The apparent absence of a change in gradients over time should also be interpreted with caution, given that only a small subset of the cohorts had serial MTR studies (12/51 healthy controls, 14/28 with PPMS and 15/35 with SPMS), and follow-up was limited to 1.6-2.3 years (Table 7). The correlations seen between disease duration and gradient severity were very weak (Table 9) though this and previous cross-sectional works have shown a steeper periventricular gradient in SPMS compared with RRMS (Liu *et al.*, 2015) collectively suggesting that gradients do worsen over time. Associations of cortical and periventricular MTR gradients with disability, as measured by EDSS scores, were also very modest. Only in SPMS did cortical MTR gradients weakly correlate with EDSS scores. Furthermore, spinal cord pathology was not assessed, which may be of greater clinical relevance in PP than SPMS (Losseff *et al.*, 1996); and EDSS scores exceeding 3.5 essentially reflect impaired mobility and do not capture cognitive or memory impairments (Paul, 2016), both of which may be associated with cortical pathology (Calabrese *et al.*, 2011). Further work using larger cohorts and spinal cord examination is needed to explore these issues.

In conclusion, as with SPMS, periventricular and cortical gradients are present in PPMS, and do not appear to differ substantially between these subtypes of progressive MS. Histopathological examination of the substrates underlying these gradients may provide useful insights into the processes leading to them.

Project 3: Periventricular gradient evolution following peripheral immunotherapy

The number of participants in this study is small, and larger studies are required to corroborate these preliminary findings. Notwithstanding this, we found that, untreated, the abnormal periventricular MTR gradient in RRMS increased over time. In contrast, in those patients who received alemtuzumab this gradient decreased (becoming less abnormal), and this was not explained by effects on WM lesion accrual nor brain atrophy. As alemtuzumab is undetectable in the CSF after treatment (Moreau *et al.*, 1994) and has no apparent effect on oligoclonal bands (Hill-Cawthorne *et al.*, 2012), a direct intrathecal action is unlikely to explain this result. The biological implications of these findings are discussed on p.175.

The baseline periventricular MTR gradient was significantly more abnormal in those patients who relapsed within 4 years of receiving alemtuzumab compared to those who did not relapse, while no such differences in baseline lesion number, brain parenchymal fraction nor whole brain NAWM MTR were found.

Limitations

Our study has limitations. The number of participants is too small for definitive conclusions: caution is required when interpreting the results with small subgroups and larger cohorts are needed to verify our findings. Such work might also examine the effect of other DMTs on the gradient's evolution and predictive capabilities: insufficient numbers of patients imaged with the same protocol precluded this here.

Baseline differences (particularly in relapse rate) reflect the opposing treatment strategies (high efficacy therapy versus no treatment). This may account for the higher baseline periventricular gradient seen in the alemtuzumab group. Despite this, and the adjustment for baseline relapse rate in all models, a significantly different rate of change in gradient was still observed between the groups. The untreated group were older than the alemtuzumab group, though again significant differences were seen despite adjusting models for baseline age. While a significant difference in periventricular gradient evolution was seen between untreated patients who relapsed versus those who did not, no difference in baseline gradient was seen (p.**Error! Bookmark not defined.**). Given such a difference was seen in a larger untreated cohort (Brown *et al.*, 2017), we suggest that this most likely reflects this cohort's smaller size and exclusion of those untreated patients that started a DMT before their final scan (further diminishing the cohort size and biasing the untreated group that relapsed to a milder clinical phenotype).

No longitudinal healthy control or non-MS neurological disease data was obtained using this protocol, so the natural effects of age on the periventricular MTR gradient, nor its disease specificity, can be determined. This also means that we cannot establish if the effects alemtuzumab exerts on the periventricular MTR gradient are specific to MS. The baseline relapse rate in the untreated cohort is high compared with patients currently receiving no DMTs in clinical practice, reflecting the low DMT uptake rates in the United Kingdom at the time of recruitment. To minimize partial volume effects we applied a stringent probabilistic segmentation threshold and removed the two bands closest to the CSF, where periventricular disease effects are maximal. Despite this – and the sample size, and adjustment for atrophy and lesional measures – a treatment effect was still observed. The lack of gadolinium

administration prevented us examining the effects of enhancing lesions at baseline, though in a larger study we found no difference in periventricular gradient between those with and without enhancing lesions (Brown *et al.*, 2017).

The baseline periventricular MTR gradient partially correlated with baseline mean whole brain NAWM MTR (r=-0.57-0.59), although given that the MTR gradient is derived from bands of NAWM MTR this is unsurprising. While both improved following treatment with alemtuzumab, their rate of change was not correlated. We could not distinguish independent changes in the periventricular gradient from changes in NAWM MTR, though we did find this when examining predictors of post-treatment relapses in the alemtuzumab group. Given the independent differences between these metrics in a larger study (Brown *et al.*, 2017), we suspect this reflects the small sample size here. The 3mm-thick T1 slices provide less accurate tissue segmentations than with scans used for volumetric measures (typically obtained at 1 x 1 x 1 mm resolution), and this will affect small structures (such as DGM) more than larger ones; this precluded examination of the effect of alemtuzumab on DGM periventricular and cortical MTR gradients. Despite any resultant noise, statistically significant changes in NAWM MTR gradient were still seen between the groups. It is unlikely that an improvement in the periventricular MTR gradient represents a ceiling effect (i.e. less abnormal regions have less scope for improvement) as the final post-alemtuzumab MTR in each band was still considerably lower than that seen in healthy controls (<38pu versus >40pu respectively (Pardini *et al.*, 2016)).

In conclusion, we have shown that the abnormal periventricular MTR gradient in multiple sclerosis increases with time but appears to be reversed following treatment with

alemtuzumab. The periventricular MTR gradient may predict therapeutic response. Larger corroboratory studies are now needed. The cause of the periventricular MTR gradient remains unknown, but growing evidence of its clinical relevance, responsiveness to treatment, and therefore its potential use as a trial outcome measure, make it increasingly important to understand the processes underlying it.

Integration of projects 1-3 into a rapidly-evolving picture of outside-in tissue abnormalities in MS

The work detailed in this thesis forms a small part of a growing delineation of outside-in tissue abnormalities within multiple sclerosis. Much work has been published contemporaneous to this PhD, so this section of the discussion will provide an updated summary and set our findings into the wider characterisation of outside-in tissue abnormalities, and what may underlie them. The evidence for outside-in gradients - neuropathological and imaging - will be summarised in WM and GM before potential causes and clinical relevance are discussed.

Normal-appearing white matter

The NAWM is not normal, yet abnormalities are not uniform. First, perilesional tissue is abnormal on MTR, for up to 4mm from the T2-defined lesion edge (Vrenken *et al.*, 2006). Second, in healthy controls WM MTR is highest adjacent to the lateral ventricles and decreases with distance from them; in all types of MS, NAWM MTR is lowest (most abnormal) at the ventricular edge and increases over the first ~5 mm before mirroring, at lower levels, patterns seen in healthy controls (Liu *et al.*, 2015; Brown *et al.*, 2017; Brown *et al.*, 2019a). This periventricular MTR gradient surrounds supratentorial and infratentorial ventricles (Pardini *et al.*, 2016) and has been replicated with DTI, most markedly in patients with oligoclonal bands (Pardini *et al.*, 2019).

The periventricular NAWM MTR gradient appears independent of lesions: the severity is the same in those with and without WM or enhancing lesions and remains visible after excluding up to 3mm of perilesional tissue to mitigate subtle MTR abnormalities; gradients and lesions

have differing distributions (gradients surround the fourth ventricle (despite low lesion density around the fourth ventricle)); and gradients occur within lesional tissues (Pardini *et al.*, 2016; Brown *et al.*, 2017; Pardini *et al.*, 2019). Outside-in MTR gradients are also seen in cervical cord WM (Kearney *et al.*, 2014). Taken together this suggests at least partially distinct mechanisms underlying lesion formation and those causing outside-in gradients).

Neither MTR nor DTI can distinguish myelin or neuronal loss and the pathologic substrate underlying periventricular WM gradients remains unexplored. Despite the low resolution, a PET study has found a periventricular gradient of microglial activation in NAWM and GM (Poirion *et al.*, 2017).

Normal-appearing grey matter (NAGM)

Extralesional cortical and thalamic GM show significant axonal loss compared to healthy controls (Cifelli *et al.*, 2002; Choi *et al.*, 2012; Bevan *et al.*, 2018). Neuronal loss appears relatively independent of demyelination (Magliozzi et al., 2010): no differences in axonal density were seen between demyelinating cortical lesions and NAGM (Klaver *et al.*, 2015). Cortical demyelination has typically been quantified in terms of demyelinating lesions, but extralesional reductions in myelin density are seen (Bevan *et al.*, 2018), in part reflecting areas of remyelination (Albert *et al.*, 2007).

Significantly greater neuronal loss in the outermost cortical layers is seen in some patients with SPMS (Magliozzi *et al.*, 2010) and PPMS (Choi *et al.*, 2012) that is related to the level of immune cell infiltration in the meninges. In SPMS an accompanying gradient of microglial activation is seen (Magliozzi *et al.*, 2010), though this has not been examined in PPMS.

Preliminary neuropathology studies in patients with progressive MS have recently found a thalamic "outside-in" gradient of neuronal loss and microglial activation, maximal close to the ependyma (Magliozzi *et al.*, 2018a). This gradient, present in lesional and normal-appearing thalamic tissues, was most marked in cases where meningeal B-cell follicles were found in other brain regions. This finding may mirror the "pial-in" pattern of subpial cortical injury, providing further evidence that intrathecal, compartmentalized inflammation is a major driver of cortical and subcortical GM MS damage (Magliozzi et al., 2010).

Notwithstanding the limited sensitivity to GM lesions, mean GM MTR is decreased in all disease stages, including after a CIS (Fernando *et al.*, 2005). Outside-in gradients in GM MTR are seen in all types of MS, both in the cortex (where the MTR is lowest (most abnormal) in comparison to healthy controls at the outer cortical surface (Samson *et al.*, 2014; Brown *et al.*, 2019a)), and the deep GM (where the MTR is lowest at the inner ventricular surface (Pardini *et al.*, 2016)). A corresponding gradient of thalamic atrophy, maximal at the CSF boundary and lessening with increasing distance from it, is visible at the earliest stage of paediatric MS (Fadda *et al.*, 2019) and is MS-specific (since it was not seen in children with monophasic demyelination). T2*, which inversely correlates with myelin and iron content, has also shown outside-in cortical gradients, visible from the first relapse (Mainero *et al.*, 2015).

Both periventricular and cortical MTR gradients are more severe in SPMS compared to RRMS (Samson *et al.*, 2014; Liu *et al.*, 2015) and worsen with increasing disease duration (Brown *et al.*, 2019a).

What causes outside-in gradients?

The cause of periventricular and cortical gradients – and whether or not they reflect the same processes – remains unclear. The correlations between the severity of (i) periventricular and cortical MTR gradients; (ii) periventricular DTI gradients and cortical lesion loads; and (iii) periventricular lesion loads and cortical atrophy may suggest a common cause (Jehna *et al.*, 2015; Brown *et al.*, 2019a; Pardini *et al.*, 2019). A spatially consistent feature could therefore be CSF. CSF from patients with MS (or a CIS) causes axonal damage and neuronal death in-vitro (Alcazar *et al.*, 2000; Vidaurre *et al.*, 2014), and when sampled at the time of a relapse induces oligodendrocyte apoptosis (Menard *et al.*, 1998).

CSF: intrathecal inflammation

Meningeal inflammation, lymphoid-like tissue formation and choroid plexus trafficking have all been invoked in the genesis of intrathecal inflammation; their surface-based effects on brain parenchyma must be mediated via CSF, as few if any immune cells are found in the surface layers.

Intrathecal inflammation: meningeal inflammation

While most pronounced in progressive disease, meningeal inflammation is seen histopathologically at all stages of relapse-onset and progressive MS (Magliozzi *et al.*, 2007; Lucchinetti *et al.*, 2011; Choi *et al.*, 2012). Such 'compartmentalised inflammation' may attract and retain further inflammatory cells, facilitating a pro-inflammatory microenvironment within this relatively sequestered compartment (Krumbholz *et al.*, 2006; Meinl *et al.*, 2008). Although lesions and surface-based gradients appear to reflect distinct mechanisms, identical antigen-experienced B-cell clones are found in meningeal aggregates

and WM perivascular spaces in progressive MS (Lovato *et al.*, 2011), suggesting a common origin and possibly a unifying cause of GM and WM lesions.

A strong correlation has recently been found between a common molecular pattern of intrathecal (CSF) inflammation able to predict cortical pathology (R^2 = 0.88), both at disease onset (where it correlated with cortical lesion number) and at post-mortem (where it correlated with the presence of meningeal inflammation and the percentage of demyelinated cortex). Magliozzi and colleagues found increased expression of proinflammatory cytokines (IFNγ, TNF, IL2 and IL22) and molecules promoting sustained B-cell activity and lymphoid neogenesis (CXCL13, CXCL10, LTα, IL6 and IL10) in the post-mortem meninges and correspondent CSF of SPMS patients with increased meningeal inflammation and GM demyelination (Magliozzi *et al.*, 2018b). Their data corroborate the hypothesis that meningeal inflammation, diffuse or organized in lymphoid-like structures, in one of the main sources of CSF inflammatory mediators (Gardner et al., 2013). Similar molecular patterns were identified in the CSF of naïve patients with recent-onset MS, and multivariate models including seven such cytokines explained 88% and 89% of the variance in cortical lesion number and volume respectively. Interestingly, this specific profile is MS-specific, not present in the other neurological diseases examined (inflammatory and non-inflammatory) and incorporates both inflammatory and non-inflammatory components which may explain the fact that in other conditions characterised by meningeal and CSF inflammation, subpial cortical demyelination was never observed (Magliozzi *et al.*, 2018b).

Studies of MS animal models also support a key role of meningeal inflammation in cortical demyelination and axonal loss. In experimental autoimmune encephalomyelitis (EAE), pathogenic T-cells enter the CSF, are re-stimulated by meningeal antigen-presenting cells, undergo clonal expansion and produce cytokines, in turn promoting T-cell infiltration across

pial vessels, parenchymal invasion in the (CSF-adjacent) cord WM and the clinical onset of disease (Bartholomaus *et al.*, 2009; Kivisakk *et al.*, 2009; Reboldi *et al.*, 2009). This pattern has been reproduced in cortical biopsies of patients presenting with an atypical CIS (Lucchinetti *et al.*, 2011). Periventricular and pericisternal leucocyte invasion is seen in the earliest stages of both EAE and peripheral (adjuvant-induced) inflammation (Schmitt *et al.*, 2012). The limitations of animal models are well-rehearsed: these animals do not have MS, only a model of inflammatory demyelination. Caution should therefore be exercised in translating animal findings to humans. However, injection of a combination of TNF and IFNγ into the subarachnoid space overlying the cortical GM can give rise to similar subpial pathology in rats with circulating anti-myelin antibodies (Gardner *et al*., 2013).

Until recently, MRI detection of meningeal inflammation relied on surrogates (principally cortical lesions) with poor sensitivity and very low inter-rater reliability (Geurts *et al.*, 2011; Seewann *et al.*, 2012). However, postcontrast T2 FLAIR has recently identified changes that may represent leptomeningeal enhancement in up to half of patients with MS, with the greatest frequency in those with SPMS, older age, longer disease duration and higher EDSS scores (Absinta *et al.*, 2015; Eisele *et al.*, 2015; Zivadinov *et al.*, 2017). Although only two patients proceeded to post-mortem examination (both with PPMS), areas of leptomeningeal enhancement on T2 FLAIR corresponded to regions of cortical demyelination, and meningeal inflammation (Absinta *et al.*, 2015). However, leptomeningeal enhancement is not specific for meningeal inflammation as subarachnoid veins, dural venous sinuses and basal meninges all enhance on postcontrast T2 FLAIR (Zurawski *et al.*, 2017). A small recent study at 7T found that LME correlated with cortical GM atrophy but not with neocortical lesions (Ighani *et al.*, 2019). Notwithstanding MRI's limited ability to detect GM lesions, this finding may suggest

that meningeal inflammation is more involved in MS neurodegenerative inflammatory processes, rather than focal lesion development.

Intrathecal inflammation: lymphoid tissues

The most striking form of meningeal inflammation – lymphoid tissue formation – is seen in about 40% of patients with SPMS at post-mortem (Magliozzi *et al.*, 2007), but has recently been reported in similar proportions of patients who died following their first MS presentation (Bevan *et al.*, 2018). Lymphoid-like tissues are topographically related to subpial cortical demyelinating lesions, but also occur alongside areas of reduced myelin density suggesting either partial demyelination or remyelination (Magliozzi *et al.*, 2010; Bevan *et al.*, 2018). In particular, the presence of lymphoid-like structures in the meninges of SPMS is closely associated with graded damage: elevated neuronal and astrocyte loss accompanied by increased microglia density have been measured close to the CSF/pia surface and decrease in the inner cortical layers close to the WM (Magliozzi *et al.*, 2010). The partial destruction of the glia limitans formed by the astrocyte end-feet on the pial surface may probably favour the diffusion of soluble cytotoxic, myelinotoxic and inflammatory factors from the circulating CSF towards the superficial cortical layers directly causing neurodegeneration or indirectly so (by activating resident microglia) (Calabrese *et al.*, 2015).

Further neuropathology studies seeking meningeal aggregates in PPMS cases - as well as exploring the substrates underlying gradients in periventricular brain regions - are now sorely needed. The absence of organized lymphoid-like structures in PPMS might reflect the lower numbers of tissue blocks examined from a smaller number of patients at post-mortem or that aggregates are not required for surface-based gradients in tissue damage to occur. Given aggregates typically occur in sulci, the lack of difference between mean sulcal and gyral

cortical MTR favours the latter explanation (Samson *et al.*, 2013). Up to now, lymphoid follicles have not been found in the spinal cord either despite a clear correlation between the severity of NAWM axonal loss and the degree of both NAWM microglial/macrophage activation and the density of meningeal T-cells (Androdias *et al.*, 2010).

Intrathecal inflammation: choroid plexus

An alternative (or perhaps additional) route for inflammatory cells to enter the CSF is via the choroid plexus. The concentration of the tight-junction protein claudin-3 (responsible for maintaining the blood-CSF barrier) is significantly lower in patients with MS than in healthy controls (Kooij *et al.*, 2014).

CSF: oxidative stress

The finding of elevated proinflammatory CSF cytokines suggested that cytokine-induced synaptic hyperexcitability, glutamate-dependent neurotoxicity or direct cytokine induced death receptor signalling caused neuronal death and dysfunction, again pointing to an inflammatory origin (Rossi *et al.*, 2012; Rossi *et al.*, 2014). Elevated ceramide levels, which impair mitochondrial function, decrease neuronal energy production and increase reactive oxygen species and free radical production, culminating in neuronal damage, have been found in MS CSF (Vidaurre *et al.*, 2014). In patients with progressive (but not relapsing-remitting) MS, ceramides additionally accentuate this process by decreasing glucose bioavailability, culminating in 'virtual hypoglycosis' in these patients' CSF which too leads to neurotoxicity (Wentling *et al.*, 2019). Ceramides are sphingolipids, and the elevated levels found in the CSF, particularly C24, are thought to reflect white matter destruction or exosome release from membranes of mature oligodendrocytes (Wentling *et al.*, 2019).

Factors beyond the CSF

The periventricular venous watershed predisposes the region to hypoperfusion and hypoxia, and from the earliest clinical stage of MS, periventricular hypoperfusion is greater in MS than in healthy controls (Andeweg, 1996; Dewar *et al.*, 2003; Varga *et al.*, 2009; Beggs, 2013). Such a watershed has not been demonstrated in the well-perfused cortex though.

Granular ependymitis is seen in some patients with MS at post-mortem, and is associated with 11% of (largely chronic or burnt-out) periventricular lesions (Adams *et al.*, 1987). A resultant soluble factor released into the CSF could conceivably cause both periventricular and cortical damage. The structural integrity of the cortical glia limitans is compromised in progressive MS (Magliozzi *et al.*, 2010), thus allowing greater diffusion of molecules into the underlying grey matter, but a similar compromise of the ependymal layer has yet to be investigated.

WM lesions nearly always form around veins, and the high venular density around the lateral ventricles likely accounts for WM lesions' periventricular predilection (Brownell and Hughes, 1962; Adams *et al.*, 1987; Narayanan *et al.*, 1997; Evangelou *et al.*, 2000). Lesions themselves are unlikely to directly explain the WM periventricular MTR gradient: lesions plus a two voxel-layer NAWM perilesional cuff were excluded in all projects (Liu *et al.*, 2015; Brown *et al.*, 2017; Brown *et al.*, 2019a; Brown *et al.*, 2019c), and extending this to a four voxel-layer cuff led to almost identical results (Liu *et al.*, 2015). Further, the periventricular gradient is visible in NAWM, deep GM and in lesional tissue itself and appeared similar in those with and without T2-visible or enhancing lesions (Liu *et al.*, 2015; Pardini *et al.*, 2016; Brown *et al.*, 2017).

A tract-mediated effect of lesions may also contribute to periventricular (but not cortical) gradients: adjacent to the lateral ventricles run multiple WM tracts (e.g. those in the corpus

callosum, and so it may be expected that the remote effects of axonal transection in lesions (Trapp *et al.*, 1998) will be more apparent in regions with high compared with low densities of parallel tracts. Again, as periventricular MTR gradients did not significantly differ between CIS patents who did and those who did not have additional brain lesions this is unlikely to explain periventricular gradients (Brown *et al.*, 2017).

Clinical relevance of surface-based gradients in MS

WM lesions have established diagnostic and prognostic utility. Following a CIS, the presence of characteristic T2-hyperintense WM lesions can fulfil the diagnosis of McDonald RRMS (Thompson *et al.*, 2017) and predict the likelihood of a further relapse (Fisniku *et al.*, 2008). Infratentorial lesions independently predict moderate disability (hazard ratio 6.3) (Minneboo *et al.*, 2004) while baseline enhancing lesions (and new supratentorial lesions within 1 year) independently predict cognitive impairment (Brownlee *et al.*, 2019).

Outside-in gradients occur early in MS (Samson *et al.*, 2016; Brown *et al.*, 2017; Fadda *et al.*, 2019). They may have clinical utility (though at present require offline image processing and require corroboration in larger cohorts using the optimised processing pipeline before considering use in trials or even clinical practice). The periventricular NAWM MTR gradient is seen within 5 months of a CIS and independently predicts a further relapse within 2 years (OR 61.7, p=0.02), dwarfing the predictive effect of T2 lesions (OR 8.5, p=0.07, (Brown *et al.*, 2017)). Furthermore, unlike any other radiological markers (Wattjes, 2015), it independently predicts on-treatment relapses following alemtuzumab (Brown *et al.*, 2019c), though larger studies are mandatory to corroborate this. Surface-based gradients in the cortex (Mainero *et al.*, 2015; Brown *et al.*, 2019a), periventricular WM (Brown *et al.*, 2017; Brown *et al.*, 2019a)

and spinal cord WM (Kearney *et al.*, 2014) all modestly correlate with disability. Pathological studies noted the most aggressive disease-course during life was associated with gradients of cortical neuronal loss and the most marked meningeal inflammation at post-mortem, and a pro-inflammatory CSF pattern which was detectable early in disease (Magliozzi *et al.*, 2007; Magliozzi *et al.*, 2018b).

Insights from treatment effects on surface-based pathology

Interpretation of the improvement in periventricular MTR gradients following alemtuzumab is speculative, as their underlying pathogenesis remains unknown (Brown *et al.*, 2019c). Axonal regeneration has not been reported to any substantial degree in the adult human brain, so an improvement in periventricular MTR gradients following alemtuzumab is therefore more likely to reflect resolution of periventricular inflammation, facilitation of remyelination or both. While identical antigen-experienced B-cell clones are found in meningeal aggregates and perilesional spaces in progressive multiple sclerosis (suggesting a common peripheral origin (Lovato *et al.*, 2011)), the periventricular MTR gradient seen in both NAWM and lesional tissue is, at least partially, independent of WM lesion formation (Brown *et al.*, 2017). Further, the distribution of WM lesions differs from that of the MTR gradient (Pardini *et al.*, 2016), suggesting there are two overlapping processes; one linked with lesion formation and another influencing the intensity of pathology within them. Alemtuzumab exerts its effects by depleting mature lymphocytes outside the BBB, not by entering the brain parenchyma (Moreau *et al.*, 1994), yet it effects a substantial reduction in new WM lesion formation. It is plausible that alemtuzumab also modulates lymphocyte populations entering the CSF space, so the subsequent amelioration of periventricular MTR gradients might reflect a reduction in intrathecal inflammation. The apparent ability to predict treatment response

might therefore reflect the degree of intrathecal inflammation, and - given the MTR gradient showed continued improvement two years after the last dose of alemtuzumab - aggressive peripheral immunodepletion may have an enduring effect on it. Alemtuzumab may additionally facilitate endogenous repair through the production of a beneficial factor (neurotrophins, for example, are increased following alemtuzumab (Jones *et al.*, 2010)).

Trials of intrathecal rituximab (an anti-CD20 B-cell depleting immunotherapy) in progressive MS have found only transient improvements in intrathecal B-cell numbers, markers of CNS—tissue embedded B-cells (sCD21) and cytokines released by lymphoid follicles (including CXCL-13) – despite sustained peripheral B-cell depletion - and no material improvements in clinical outcomes (Komori *et al.*, 2016; Bergman *et al.*, 2018; Bhargava *et al.*, 2019). One trial used leptomeningeal enhancement as a surrogate for meningeal inflammation which remained unaffected by two courses of intrathecal rituximab (Bhargava *et al.*, 2019). The disappointing results may in part reflect the methodology - small sample sizes (n=8-23), short follow-up (6-24 months) and small numbers of treatments (2-3 cycles) – or the participants' prolonged disease duration (19-24 years), noting that in the relapsing phase early treatment is associated with better clinical outcomes (for example (Brown *et al.*, 2019b)). Alternatively, intrathecal rituximab may not be a viable strategy for reducing meningeal inflammation. Lower CSF-complement levels and insufficient antibody-mediated natural killer cell-mediated cytotoxicity may mean that intrathecal rituximab cannot deplete intrathecal B-cells sufficiently. The high levels of B-cell survival factors (BAFF for example (Magliozzi *et al.*, 2004)) in areas of meningeal inflammation might also prevent sufficient B-cell depletion by rituximab. Or, the persistence of other cell populations may continue to drive tissue damage and thus disability. The lack of standardised biomarkers of meningeal inflammation hamper

such studies. However, longer and larger studies on patients with shorter disease duration comparing the effect of intravenous rituximab (B-cell depleting), intrathecal rituximab (B-cell depleting), intravenous natalizumab (T-cell depleting) and intravenous alemtuzumab (B and T-cell depleting) on putative imaging biomarkers of meningeal inflammation (periventricular gradients, subpial lesion numbers and leptomeningeal enhancement) and on molecular biomarkers (e.g. CSF CXCL13) might help illuminate the effect of currently available therapies.

In addition, a recent phase IIb trial of GNbAC1 (an agent targeting a component of the human endogenous retrovirus type W, linked with inflammation and inhibition of remyelination) has interpreted improvements in periventricular MTR gradients as possible remyelination (Curtin *et al.*, 2012; Hartung *et al.*, 2017), though this may, in part or whole, be an anti-inflammatory effect.

There is now a clear imperative to understand the cellular substrates and molecular mechanisms underlying periventricular MTR gradients and to explore the effects of different therapies on them.

Project 4: The effect of disease-modifying therapies on conversion to secondary progressive multiple sclerosis

In this observational cohort study that used prospectively-collected clinical data, initial treatment with fingolimod, alemtuzumab or natalizumab was associated with a significantly lower risk of conversion to SPMS compared to initial treatment with glatiramer acetate or interferon beta. The risk of conversion was significantly lower for early compared to late treatment: either in the case of starting glatiramer acetate or interferon beta within 5 years of disease onset versus later commencement, or when escalating from glatiramer acetate or interferon beta to fingolimod, alemtuzumab or natalizumab within 5 years of disease onset versus later escalation.

These results suggest that initial treatment with glatiramer acetate or interferon beta is associated with reduced conversion to SPMS compared to untreated patients. There is no consensus in the literature. Intention-to-treat analysis of the study conducted by the IFNβ Multiple Sclerosis Study Group found no difference in conversion rates between interferon and placebo 16 years later, though many placebo-treated patients subsequently received DMTs (Ebers *et al.*, 2010). Six of seven observational studies reported favourable associations between glatiramer acetate or interferon beta and SPMS conversion, both individually (Trojano *et al.*, 2007; Goodin *et al.*, 2011; Patrucco *et al.*, 2012; Drulovic *et al.*, 2013; Tedeholm *et al.*, 2013; Bergamaschi *et al.*, 2016) and in a meta-analysis (Signori *et al.*, 2016). The remaining observational study from British Columbia – the only one to circumvent immortal time bias (Suissa, 2008) through treating interferon exposure as a time-dependent variable (ensuring time before interferon treatment contributed to the untreated follow-up time) –

found no relationship between interferon exposure and SPMS conversion (Zhang *et al.*, 2015). These observational studies – all published before an objective SPMS definition became available – have highly heterogeneous methods including variable (or inaccessible) SPMS definitions, inconsistent exclusion of relapse-related disability-increases; and variable strategies for mitigating indication bias (arising from non-random treatment exposure), attrition bias (reflecting between-group differences in follow-up duration), detection bias (from differing EDSS frequency during follow-up) and immortal-time bias. In observational study designs, propensity score-based estimators better reflect true differences than nonexperimental estimators, such as multivariable regression or latent variable selection models, providing an overlap exists between the compared groups (Dehejia RH, 1999). In this analysis, matching with a caliper was employed, which is more robust in scenarios with restricted sample size and strong treatment-selection processes than unrestricted propensity score-based methods such as inverse probability of treatment weighting or optimal full matching (Austin, 2011; Lunt, 2014). All models were adjusted for EDSS frequency to mitigate detection bias and setwise censoring of follow-up duration was used to mitigate attrition bias. To address the issue of immortal-time bias (Suissa, 2008) disease-modifying therapy was treated as a time-dependent variable. The risk of SPMS conversion increases with disease duration (Weinshenker *et al.*, 1989), which should be considered in evaluations of SPMS conversion rates in different treatment scenarios (Table 14, Figure 18). For instance, subgroups with longer disease duration at baseline (e.g. here natalizumab) are expected to be associated with a relatively greater SPMS conversion rate than those with shorter disease duration at baseline (e.g. here alemtuzumab or fingolimod).

This study has several limitations. First, given its observational design, the study is unable to ascribe causality and cannot distinguish between prevention and delay of conversion to SPMS. The longest comparison however showed a favourable association of early (versus later) glatiramer acetate or interferon beta, enduring to the end of follow-up 17 years after baseline (median disease duration 20 years; Figure 19). Second, the absence of EDSS functional score subcomponents precluded using the SPMS definition with the highest combination of sensitivity, specificity and accuracy; the definition used in this study, requiring total EDSS only, has previously been shown to be associated with a 1% loss of accuracy and 6% reduction in sensitivity (Lorscheider *et al.*, 2016). Third, the differing baseline demographics of each DMT cohort (Table 14) required differing matched untreated cohorts with differing follow-up durations; their relative therapeutic effects should therefore not be compared between analyses (Figure 18). A particular problem with the fingolimod/untreated comparison was the inability to eliminate informed censoring bias because fingolimod-treated patients subsequently escalated to monoclonal antibody treatment (due to on-treatment disease activity) were excluded (Figure 18). Such informed censoring does not affect the comparison between untreated patients and monoclonal antibodies (as patients cannot be escalated from these highly-effective therapies (Kalincik *et al.*, 2017a)) nor the untreated comparisons with glatiramer acetate or interferon beta (where the inclusion criteria ensured more potent therapies were not generally available during the studied epoch). Fourth, the glatiramer acetate or interferon beta cohorts therefore came from an earlier period, leading to 10-11 years median difference in the baseline dates of the glatiramer acetate or interferon beta versus untreated analyses, and 13 years median difference in the glatiramer acetate or interferon beta versus fingolimod, alemtuzumab or natalizumab analysis. It is possible that unmeasured changes in care between time epochs - more specialist

nurses, better symptomatic management, lower thresholds for escalating therapy for example - may have contributed to differences in SPMS conversion rates in these particular analyses. However, all other analyses (with contemporaneous groups (≤5 years difference, Table 14)) also support early and aggressive DMT use. The ability to match contemporaneous untreated patients to those commencing fingolimod, alemtuzumab or natalizumab (Table 14) took advantage of the United Kingdom's lower DMT uptake rates. The generalisability of the untreated group to other geographic regions cannot be guaranteed. Fifth, a large number of patients were excluded due to ineligibility (Figure 17). At least 65 patients were excluded through stopping their DMT within 6 months due to inefficacy. Though a modest number, their exclusion may have biased the remaining patients presented for matching towards a relatively milder disease. Those excluded due to missing data were slightly older with higher baseline EDSS scores (Table 26). While the exclusion criteria have made the results more robust, the resultant unmatched cohorts are, by definition, unrepresentative of the whole unfiltered cohort. Despite the stringent matching criteria 63-97% of treated eligible patients were successfully matched, and beyond lower baseline relapse rates, the matched cohorts (Table 14) are similar to those in the original placebo-controlled phase III trials of these therapies (Group, 1993; Comi *et al.*, 2001; Polman *et al.*, 2006). Sixth, some factors were unavailable across all cohorts (for example smoking status; lesion number or brain volume on MRI; drug adherence; or the presence of oligoclonal bands in cerebrospinal fluid), precluding their inclusion in matching models. If these variables differed systematically between the compared groups, and are associated with the risk of SPMS conversion, then they might have acted as confounders. Through the use of an objective SPMS definition, any positive bias of outcomes by the clinician instigating the intervention or escalation should have been mitigated. Seventh, the assessment of disability (and therefore SPMS conversion) relied on

the EDSS. Although the most widely-used disability measure, it has high inter-rater variability at lower scores, limited sensitivity to cognitive impairment and – at scores over 3.5 – is largely determined by ambulation (Meyer-Moock *et al.*, 2014). To mitigate inter-rater variability, this published definition of SPMS requires EDSS step 4 attainment and confirmation of EDSS increases on two occasions, at least 3 months apart. Eighth, the numbers of patients available in some analyses was quite small. Despite this, clinically and statistically significant differences between the groups were observed. Ninth, while relatively few patients contribute to the final periods of follow-up in Figure 18 and Figure 19, the groups universally diverge long before this and the statistics are heavily weighted towards the left of each figure. Tenth, while death due to non-MS causes may represent a competing risk, we were unable to include this in the presented models due to incomplete reporting. Eleventh, this study did not assess the risks associated with DMTs, and so the association between initial fingolimod, alemtuzumab or natalizumab use and lower risk of SPMS conversion – which is consistent with these therapies' greater effect on relapse rates and disability metrics (Coles *et al.*, 2008; Cohen *et al.*, 2010; Spelman *et al.*, 2016) - must be considered in light of their greater risks, administration and monitoring schedules, and initial costs during the DMT selection process.

Chapter 7: Conclusions

Outside-in gradients in lesional and normal-appearing tissues are seen in all types of MS and may have some predictive capabilities. The underlying process(es) appear at least partially distinct from those underlying lesion formation. We now need to know the molecular and histopathological substrates underlying MRI-visible periventricular gradients, in particular whether or not it is pathologically equivalent to the neurodegenerative gradient already seen in cortical GM. Additionally, to explore whether they are requisite for outside-in gradients, lymphoid-like aggregates should be sought in the brains of patients with PPMS, and in the spinal cord of all patients with MS (in both settings MRI and histopathological evidence of gradients are seen). Demonstrating subpial pathology following subarachnoid cytokine injection in non-EAE animal models might support the aetiological role of inflammation and may provide a chronic model to study the effects of therapeutics.

At present, meningeal inflammation represents the best explanation for cortical gradients. As this does not explain gradients seen in WM lesions and periventricular tissues, a CSF-mediated process – secondary to meningeal inflammation or primarily degenerative - would offer a plausible link. The precise unifying CSF factor is as yet unidentified. Potential biomarker candidates - cortical lesions, leptomeningeal enhancement, gradients and CSF profiling – require optimisation, standardisation, comparison (including with existing outcome measures) and a systematic examination of their response to therapies.

Among patients with RRMS, initial treatment with fingolimod, natalizumab or alemtuzumab was associated with a lower risk of conversion to SPMS compared to initial treatment with glatiramer acetate or interferon beta over a median 5.8 years of follow-up. Lower conversion to SPMS was also associated with earlier DMT commencement or escalation compared to later commencement or escalation. These findings, considered along with these therapies' risks, may help inform decisions about DMT selection. But other critical questions surrounding DMT use remain unanswered. How early to commence DMTs; whether to 'treat-to-target' (suppressing both clinical evidence of inflammation (e.g. relapses) and paraclinical evidence (e.g. silent MRI lesions). I hope to explore both questions using observational data as a post-doctoral researcher. Whether early intensive therapy is more effective than escalation therapy; how to sequence DMTs; and whether (and when) to stop DMTs are critical yet unresolved questions: clinical trials and international observational studies will be key.

Acknowledgements

I thank all the patients who participated in the imaging cohort studies, the CAMMS223 trial and those that consented for their clinical data to be contributed to MSBase.

I gratefully acknowledge funding from the Grand Charity of the Freemasons (via a Next Generation Fellowship) and the MSBase Foundation Fellowship.

I am indebted to Matteo Pardini for taking me under his wing upon my arrival to the NMR Research Unit at Queen Square and patiently introducing me to the skills and knowledge required. Dr Ferran Prados Carrasco's IT knowledge, pipeline optimisation and scripting capabilities have made for higher quality data, in a fraction of the time. The scientific rigour and friendships formed with both colleagues has been one of the PhD's greatest gains.

Tomas Kalincik facilitated my transition from a hopelessly inept scripter and statistical novice into a vaguely competent researcher and ignited a lasting passion for translating real-world data into clinically meaningful research.

The concept of periventricular gradients must be solely credited to Declan Chard. From welcoming me into this exciting field, to tolerating my frequent errors and misunderstandings, and providing unwavering encouragement and scientific rigour, I am profoundly grateful.

Eight years ago, Alasdair Coles, bravely, welcomed me into Cambridge neuroscience. Beyond facilitating stints in world-class laboratories and restaurants, he has allowed me the space to develop my own ideas, buoyed me when I've made mistakes, and, somehow, provided immeasurable support, tutelage and tolerance throughout the process.

My wife Claire has made all this possible.

References

Absinta M, Vuolo L, Rao A, Nair G, Sati P, Cortese IC*, et al.* Gadolinium-based MRI characterization of leptomeningeal inflammation in multiple sclerosis. Neurology 2015; 85(1): 18-28.

Adams CW, Abdulla YH, Torres EM, Poston RN. Periventricular lesions in multiple sclerosis: their perivenous origin and relationship to granular ependymitis. Neuropathol Appl Neurobiol 1987; 13(2): 141-52.

Albert M, Antel J, Bruck W, Stadelmann C. Extensive cortical remyelination in patients with chronic multiple sclerosis. Brain pathology (Zurich, Switzerland) 2007; 17(2): 129-38.

Alcazar A, Regidor I, Masjuan J, Salinas M, Alvarez-Cermeno JC. Axonal damage induced by cerebrospinal fluid from patients with relapsing-remitting multiple sclerosis. Journal of neuroimmunology 2000; 104(1): 58-67.

Andeweg J. The anatomy of collateral venous flow from the brain and its value in aetiological interpretation of intracranial pathology. Neuroradiology 1996; 38(7): 621-8.

Androdias G, Reynolds R, Chanal M, Ritleng C, Confavreux C, Nataf S. Meningeal T cells associate with diffuse axonal loss in multiple sclerosis spinal cords. Annals of neurology 2010; 68(4): 465-76.

Ascherio A, Munger KL, White R, Kochert K, Simon KC, Polman CH*, et al.* Vitamin D as an early predictor of multiple sclerosis activity and progression. JAMA neurology 2014; 71(3): 306-14.

Austin PC. Optimal caliper widths for propensity-score matching when estimating differences in means and differences in proportions in observational studies. Pharm Stat 2011; 10(2): 150-61.

Baarnhielm M, Hedstrom AK, Kockum I, Sundqvist E, Gustafsson SA, Hillert J*, et al.* Sunlight is associated with decreased multiple sclerosis risk: no interaction with human leukocyte antigen-DRB1*15. European journal of neurology : the official journal of the European Federation of Neurological Societies 2012; 19(7): 955-62.

Barker GJ, Schreiber WG, Gass A, Ranjeva JP, Campi A, van Waesberghe JH*, et al.* A standardised method for measuring magnetisation transfer ratio on MR imagers from different manufacturers--the EuroMT sequence. Magma (New York, NY) 2005; 18(2): 76-80.

Barker GJ, Tofts PS, Gass A. An interleaved sequence for accurate and reproducible clinical measurement of magnetization transfer ratio. Magnetic resonance imaging 1996; 14(4): 403-11.

Barkhof F, Bruck W, De Groot CJ, Bergers E, Hulshof S, Geurts J*, et al.* Remyelinated lesions in multiple sclerosis: magnetic resonance image appearance. Archives of neurology 2003; 60(8): 1073-81.

Barkhof F, Filippi M, Miller DH, Scheltens P, Campi A, Polman CH*, et al.* Comparison of MRI criteria at first presentation to predict conversion to clinically definite multiple sclerosis. Brain : a journal of neurology 1997; 120 (Pt 11): 2059-69.

Bartholomaus I, Kawakami N, Odoardi F, Schlager C, Miljkovic D, Ellwart JW*, et al.* Effector T cell interactions with meningeal vascular structures in nascent autoimmune CNS lesions. Nature 2009; 462(7269): 94-8.

Basser PJ, Pierpaoli C. Microstructural and physiological features of tissues elucidated by quantitative-diffusion-tensor MRI. J Magn Reson B 1996; 111(3): 209-19.

Becklund BR, Severson KS, Vang SV, DeLuca HF. UV radiation suppresses experimental autoimmune encephalomyelitis independent of vitamin D production. Proceedings of the National Academy of Sciences of the United States of America 2010; 107(14): 6418-23.
Beggs CB. Venous hemodynamics in neurological disorders: an analytical review with hydrodynamic analysis. BMC medicine 2013; 11: 142.
Bergamaschi R, Quaglini S, Tavazzi E, Amato MP, Paolicelli D, Zipoli V*, et al.* Immunomodulatory therapies delay disease progression in multiple sclerosis. Multiple sclerosis (Houndmills, Basingstoke, England) 2016; 22(13): 1732-40.
Bergman J, Burman J, Gilthorpe JD, Zetterberg H, Jiltsova E, Bergenheim T*, et al.* Intrathecal treatment trial of rituximab in progressive MS: An open-label phase 1b study. Neurology 2018; 91(20): e1893-e901.
Bermel RA, Bakshi R. The measurement and clinical relevance of brain atrophy in multiple sclerosis. The Lancet Neurology 2006; 5(2): 158-70.
Bevan RJ, Evans R, Griffiths L, Watkins LM, Rees MI, Magliozzi R*, et al.* Meningeal inflammation and cortical demyelination in acute multiple sclerosis. Annals of neurology 2018; 84(6): 829-42.
Bhargava P, Wicken C, Smith MD, Strowd RE, Cortese I, Reich DS*, et al.* Trial of intrathecal rituximab in progressive multiple sclerosis patients with evidence of leptomeningeal contrast enhancement. Mult Scler Relat Disord 2019; 30: 136-40.
Bitsch A, Kuhlmann T, Stadelmann C, Lassmann H, Lucchinetti C, Bruck W. A longitudinal MRI study of histopathologically defined hypointense multiple sclerosis lesions. Annals of neurology 2001; 49(6): 793-6.
Bjartmar C, Kidd G, Mork S, Rudick R, Trapp BD. Neurological disability correlates with spinal cord axonal loss and reduced N-acetyl aspartate in chronic multiple sclerosis patients. Annals of neurology 2000; 48(6): 893-901.
Bo L, Vedeler CA, Nyland HI, Trapp BD, Mork SJ. Subpial demyelination in the cerebral cortex of multiple sclerosis patients. Journal of neuropathology and experimental neurology 2003; 62(7): 723-32.
Bodini B, Veronese M, Garcia-Lorenzo D, Battaglini M, Poirion E, Chardain A*, et al.* Dynamic imaging of individual remyelination profiles in multiple sclerosis. Annals of neurology 2016.
Brown JW, Chard DT. The role of MRI in the evaluation of secondary progressive multiple sclerosis. Expert review of neurotherapeutics 2016; 16(2): 157-71.
Brown JW, Pardini M, Brownlee WJ, Fernando K, Samson RS, Prados Carrasco F*, et al.* An abnormal periventricular magnetization transfer ratio gradient occurs early in multiple sclerosis. Brain : a journal of neurology 2017; 140(Pt 2): 387-98.
Brown JWL, Chowdhury A, Kanber B, Prados Carrasco F, Eshaghi A, Sudre CH*, et al.* Magnetisation transfer ratio abnormalities in primary and secondary progressive multiple sclerosis. Multiple sclerosis (Houndmills, Basingstoke, England) 2019a: 1352458519841810.
Brown JWL, Coles A, Horakova D, Havrdova E, Izquierdo G, Prat A*, et al.* Association of Initial Disease-Modifying Therapy With Later Conversion to Secondary Progressive Multiple Sclerosis. JAMA 2019b; 321(2): 175-87.
Brown JWL, Prados Carrasco F, Eshaghi A, Sudre CH, Button T, Pardini M*, et al.* Periventricular magnetisation transfer ratio abnormalities in multiple sclerosis improve after alemtuzumab. Multiple sclerosis (Houndmills, Basingstoke, England) 2019c: 1352458519852093.
Brownell B, Hughes JT. The distribution of plaques in the cerebrum in multiple sclerosis. Journal of neurology, neurosurgery, and psychiatry 1962; 25: 315-20.

Brownlee WJ, Altmann DR, Prados F, Miszkiel KA, Eshaghi A, Gandini Wheeler-Kingshott CAM*, et al.* Early imaging predictors of long-term outcomes in relapse-onset multiple sclerosis. Brain : a journal of neurology 2019; 142(8): 2276-87.
Brownlee WJ, Hardy TA, Fazekas F, Miller DH. Diagnosis of multiple sclerosis: progress and challenges. Lancet 2017; 389(10076): 1336-46.
Brownlee WJ, Swanton JK, Altmann DR, Ciccarelli O, Miller DH. Earlier and more frequent diagnosis of multiple sclerosis using the McDonald criteria. Journal of neurology, neurosurgery, and psychiatry 2015; 86(5): 584-5.
Button T, Altmann D, Tozer D, Dalton C, Hunter K, Compston A*, et al.* Magnetization transfer imaging in multiple sclerosis treated with alemtuzumab. Multiple sclerosis (Houndmills, Basingstoke, England) 2013; 19(2): 241-4.
Butzkueven H, Chapman J, Cristiano E, Grand'Maison F, Hoffmann M, Izquierdo G*, et al.* MSBase: an international, online registry and platform for collaborative outcomes research in multiple sclerosis. Multiple sclerosis (Houndmills, Basingstoke, England) 2006; 12(6): 769-74.
Cadavid D, Balcer L, Galetta S, Aktas O, Ziemssen T, Vanopdenbosch L*, et al.* Safety and efficacy of opicinumab in acute optic neuritis (RENEW): a randomised, placebo-controlled, phase 2 trial. The Lancet Neurology 2017; 16(3): 189-99.
Cadavid D, Mellion M, Hupperts R, Edwards KR, Calabresi PA, Drulovic J*, et al.* Safety and efficacy of opicinumab in patients with relapsing multiple sclerosis (SYNERGY): a randomised, placebo-controlled, phase 2 trial. The Lancet Neurology 2019; 18(9): 845-56.
Calabrese M, De Stefano N, Atzori M, Bernardi V, Mattisi I, Barachino L*, et al.* Detection of cortical inflammatory lesions by double inversion recovery magnetic resonance imaging in patients with multiple sclerosis. Archives of neurology 2007; 64(10): 1416-22.
Calabrese M, Magliozzi R, Ciccarelli O, Geurts JJ, Reynolds R, Martin R. Exploring the origins of grey matter damage in multiple sclerosis. Nat Rev Neurosci 2015; 16(3): 147-58.
Calabrese M, Rinaldi F, Grossi P, Gallo P. Cortical pathology and cognitive impairment in multiple sclerosis. Expert review of neurotherapeutics 2011; 11(3): 425-32.
Calabrese M, Rocca MA, Atzori M, Mattisi I, Favaretto A, Perini P*, et al.* A 3-year magnetic resonance imaging study of cortical lesions in relapse-onset multiple sclerosis. Annals of neurology 2010; 67(3): 376-83.
Campbell GR, Ziabreva I, Reeve AK, Krishnan KJ, Reynolds R, Howell O*, et al.* Mitochondrial DNA deletions and neurodegeneration in multiple sclerosis. Annals of neurology 2011; 69(3): 481-92.
Cardoso MJ, Modat M, Wolz R, Melbourne A, Cash D, Rueckert D*, et al.* Geodesic Information Flows: Spatially-Variant Graphs and Their Application to Segmentation and Fusion. IEEE Trans Med Imaging 2015; 34(9): 1976-88.
Carotenuto AG, B.; Dervenoulas, G.; Wilson, H.; Veronese, M.; Chappell, Z. A hybrid [18F]florbetapir-PET/MR imaging study to assess in vivo demyelination in multiple sclerosis. Multiple Sclerosis Journal 2018; 24(Issue 2_suppl, ECTRIMS 2018,): 614.
Catana C. Principles of Simultaneous PET/MR Imaging. Magn Reson Imaging Clin N Am 2017; 25(2): 231-43.
Chang A, Tourtellotte WW, Rudick R, Trapp BD. Premyelinating oligodendrocytes in chronic lesions of multiple sclerosis. N Engl J Med 2002; 346(3): 165-73.
Chard DT, Griffin CM, Parker GJ, Kapoor R, Thompson AJ, Miller DH. Brain atrophy in clinically early relapsing-remitting multiple sclerosis. Brain : a journal of neurology 2002; 125(Pt 2): 327-37.

Chard DT, Jackson JS, Miller DH, Wheeler-Kingshott CA. Reducing the impact of white matter lesions on automated measures of brain gray and white matter volumes. Journal of magnetic resonance imaging : JMRI 2010; 32(1): 223-8.
Chataway J, Schuerer N, Alsanousi A, Chan D, MacManus D, Hunter K*, et al.* Effect of high-dose simvastatin on brain atrophy and disability in secondary progressive multiple sclerosis (MS-STAT): a randomised, placebo-controlled, phase 2 trial. Lancet 2014; 383(9936): 2213-21.
Chen JT, Easley K, Schneider C, Nakamura K, Kidd GJ, Chang A*, et al.* Clinically feasible MTR is sensitive to cortical demyelination in MS. Neurology 2013; 80(3): 246-52.
Choi SR, Howell OW, Carassiti D, Magliozzi R, Gveric D, Muraro PA*, et al.* Meningeal inflammation plays a role in the pathology of primary progressive multiple sclerosis. Brain : a journal of neurology 2012; 135(Pt 10): 2925-37.
Cifelli A, Arridge M, Jezzard P, Esiri MM, Palace J, Matthews PM. Thalamic neurodegeneration in multiple sclerosis. Annals of neurology 2002; 52(5): 650-3.
Cohen J. Statistical power analysis for the behavioral sciences 2ed: Hillsdale, NJ; Erlbaum; 1988.
Cohen JA, Barkhof F, Comi G, Hartung HP, Khatri BO, Montalban X*, et al.* Oral fingolimod or intramuscular interferon for relapsing multiple sclerosis. N Engl J Med 2010; 362(5): 402-15.
Coles AJ, Compston DA, Selmaj KW, Lake SL, Moran S, Margolin DH*, et al.* Alemtuzumab vs. interferon beta-1a in early multiple sclerosis. N Engl J Med 2008; 359(17): 1786-801.
Coles AJ, Cox A, Le Page E, Jones J, Trip SA, Deans J*, et al.* The window of therapeutic opportunity in multiple sclerosis: evidence from monoclonal antibody therapy. Journal of neurology 2006; 253(1): 98-108.
Comi G, Filippi M, Wolinsky JS. European/Canadian multicenter, double-blind, randomized, placebo-controlled study of the effects of glatiramer acetate on magnetic resonance imaging--measured disease activity and burden in patients with relapsing multiple sclerosis. European/Canadian Glatiramer Acetate Study Group. Annals of neurology 2001; 49(3): 290-7.
Compston A, Coles A. Multiple sclerosis. Lancet 2002; 359(9313): 1221-31.
Confavreux C, Vukusic S, Adeleine P. Early clinical predictors and progression of irreversible disability in multiple sclerosis: an amnesic process. Brain : a journal of neurology 2003; 126(Pt 4): 770-82.
Confavreux C, Vukusic S, Moreau T, Adeleine P. Relapses and progression of disability in multiple sclerosis. N Engl J Med 2000; 343(20): 1430-8.
Correale J, Gaitan MI, Ysrraelit MC, Fiol MP. Progressive multiple sclerosis: from pathogenic mechanisms to treatment. Brain : a journal of neurology 2017; 140(3): 527-46.
Curtin F, Lang AB, Perron H, Laumonier M, Vidal V, Porchet HC*, et al.* GNbAC1, a humanized monoclonal antibody against the envelope protein of multiple sclerosis-associated endogenous retrovirus: a first-in-humans randomized clinical study. Clinical therapeutics 2012; 34(12): 2268-78.
Cutter GR, Baier ML, Rudick RA, Cookfair DL, Fischer JS, Petkau J*, et al.* Development of a multiple sclerosis functional composite as a clinical trial outcome measure. Brain : a journal of neurology 1999; 122 (Pt 5): 871-82.
Dale AM, Fischl B, Sereno MI. Cortical surface-based analysis. I. Segmentation and surface reconstruction. NeuroImage 1999; 9(2): 179-94.
Dalton CM, Chard DT, Davies GR, Miszkiel KA, Altmann DR, Fernando K*, et al.* Early development of multiple sclerosis is associated with progressive grey matter atrophy in

patients presenting with clinically isolated syndromes. Brain : a journal of neurology 2004; 127(Pt 5): 1101-7.
Dalton CM, Miszkiel KA, O'Connor PW, Plant GT, Rice GP, Miller DH. Ventricular enlargement in MS: one-year change at various stages of disease. Neurology 2006; 66(5): 693-8.
Davies AL, Desai RA, Bloomfield PS, McIntosh PR, Chapple KJ, Linington C*, et al.* Neurological deficits caused by tissue hypoxia in neuroinflammatory disease. Annals of neurology 2013; 74(6): 815-25.
Davies GR, Altmann DR, Hadjiprocopis A, Rashid W, Chard DT, Griffin CM*, et al.* Increasing normal-appearing grey and white matter magnetisation transfer ratio abnormality in early relapsing-remitting multiple sclerosis. Journal of neurology 2005; 252(9): 1037-44.
de la Fuente AG, Errea O, van Wijngaarden P, Gonzalez GA, Kerninon C, Jarjour AA*, et al.* Vitamin D receptor-retinoid X receptor heterodimer signaling regulates oligodendrocyte progenitor cell differentiation. J Cell Biol 2015; 211(5): 975-85.
De Stefano N, Matthews PM, Filippi M, Agosta F, De Luca M, Bartolozzi ML*, et al.* Evidence of early cortical atrophy in MS: relevance to white matter changes and disability. Neurology 2003; 60(7): 1157-62.
De Stefano N, Matthews PM, Fu L, Narayanan S, Stanley J, Francis GS*, et al.* Axonal damage correlates with disability in patients with relapsing-remitting multiple sclerosis. Results of a longitudinal magnetic resonance spectroscopy study. Brain : a journal of neurology 1998; 121 (Pt 8): 1469-77.
Dehejia RH WS. Causal effects in nonexperimental studies: Re-evaluating the evaluation of training programs. Journal of the American Statistical Association 1999; 94: 1053-62.
Deoni SC, Rutt BK, Arun T, Pierpaoli C, Jones DK. Gleaning multicomponent T1 and T2 information from steady-state imaging data. Magnetic resonance in medicine : official journal of the Society of Magnetic Resonance in Medicine / Society of Magnetic Resonance in Medicine 2008; 60(6): 1372-87.
Dewar D, Underhill SM, Goldberg MP. Oligodendrocytes and ischemic brain injury. Journal of cerebral blood flow and metabolism : official journal of the International Society of Cerebral Blood Flow and Metabolism 2003; 23(3): 263-74.
Dousset V, Grossman RI, Ramer KN, Schnall MD, Young LH, Gonzalez-Scarano F*, et al.* Experimental allergic encephalomyelitis and multiple sclerosis: lesion characterization with magnetization transfer imaging. Radiology 1992; 182(2): 483-91.
Drulovic J, Kostic J, Mesaros S, Dujmovic Basuroski I, Stojsavljevic N, Kisic-Tepavcevic D*, et al.* Interferon-beta and disability progression in relapsing-remitting multiple sclerosis. Clinical neurology and neurosurgery 2013; 115 Suppl 1: S65-9.
Ebers GC, Traboulsee A, Li D, Langdon D, Reder AT, Goodin DS*, et al.* Analysis of clinical outcomes according to original treatment groups 16 years after the pivotal IFNB-1b trial. Journal of neurology, neurosurgery, and psychiatry 2010; 81(8): 907-12.
Edgar JM, McLaughlin M, Yool D, Zhang SC, Fowler JH, Montague P*, et al.* Oligodendroglial modulation of fast axonal transport in a mouse model of hereditary spastic paraplegia. J Cell Biol 2004; 166(1): 121-31.
Eisele P, Griebe M, Szabo K, Wolf ME, Alonso A, Engelhardt B*, et al.* Investigation of leptomeningeal enhancement in MS: a postcontrast FLAIR MRI study. Neurology 2015; 84(8): 770-5.
Evangelou N, DeLuca GC, Owens T, Esiri MM. Pathological study of spinal cord atrophy in multiple sclerosis suggests limited role of local lesions. Brain : a journal of neurology 2005; 128(Pt 1): 29-34.

Evangelou N, Esiri MM, Smith S, Palace J, Matthews PM. Quantitative pathological evidence for axonal loss in normal appearing white matter in multiple sclerosis. Annals of neurology 2000; 47(3): 391-5.
Fadda G, Brown RA, Magliozzi R, Aubert-Broche B, O'Mahony J, Shinohara RT*, et al.* A surface-in gradient of thalamic damage evolves in pediatric multiple sclerosis. Annals of neurology 2019; 85(3): 340-51.
Fancy SP, Baranzini SE, Zhao C, Yuk DI, Irvine KA, Kaing S*, et al.* Dysregulation of the Wnt pathway inhibits timely myelination and remyelination in the mammalian CNS. Genes Dev 2009; 23(13): 1571-85.
Farh KK, Marson A, Zhu J, Kleinewietfeld M, Housley WJ, Beik S*, et al.* Genetic and epigenetic fine mapping of causal autoimmune disease variants. Nature 2015; 518(7539): 337-43.
Fedorov A, Beichel R, Kalpathy-Cramer J, Finet J, Fillion-Robin JC, Pujol S*, et al.* 3D Slicer as an image computing platform for the Quantitative Imaging Network. Magnetic resonance imaging 2012; 30(9): 1323-41.
Felts PA, Woolston AM, Fernando HB, Asquith S, Gregson NA, Mizzi OJ*, et al.* Inflammation and primary demyelination induced by the intraspinal injection of lipopolysaccharide. Brain : a journal of neurology 2005; 128(Pt 7): 1649-66.
Ferguson B, Matyszak MK, Esiri MM, Perry VH. Axonal damage in acute multiple sclerosis lesions. Brain : a journal of neurology 1997; 120 (Pt 3): 393-9.
Fernando KT, Tozer DJ, Miszkiel KA, Gordon RM, Swanton JK, Dalton CM*, et al.* Magnetization transfer histograms in clinically isolated syndromes suggestive of multiple sclerosis. Brain : a journal of neurology 2005; 128(Pt 12): 2911-25.
Filippi M, Rocca MA. MRI evidence for multiple sclerosis as a diffuse disease of the central nervous system. Journal of neurology 2005; 252 Suppl 5: v16-24.
Fischer JS, Rudick RA, Cutter GR, Reingold SC. The Multiple Sclerosis Functional Composite Measure (MSFC): an integrated approach to MS clinical outcome assessment. National MS Society Clinical Outcomes Assessment Task Force. Multiple sclerosis (Houndmills, Basingstoke, England) 1999; 5(4): 244-50.
Fischer MT, Sharma R, Lim JL, Haider L, Frischer JM, Drexhage J*, et al.* NADPH oxidase expression in active multiple sclerosis lesions in relation to oxidative tissue damage and mitochondrial injury. Brain : a journal of neurology 2012; 135(Pt 3): 886-99.
Fischer MT, Wimmer I, Hoftberger R, Gerlach S, Haider L, Zrzavy T*, et al.* Disease-specific molecular events in cortical multiple sclerosis lesions. Brain : a journal of neurology 2013; 136(Pt 6): 1799-815.
Fisher E, Lee JC, Nakamura K, Rudick RA. Gray matter atrophy in multiple sclerosis: a longitudinal study. Annals of neurology 2008; 64(3): 255-65.
Fisniku LK, Brex PA, Altmann DR, Miszkiel KA, Benton CE, Lanyon R*, et al.* Disability and T2 MRI lesions: a 20-year follow-up of patients with relapse onset of multiple sclerosis. Brain : a journal of neurology 2008; 131(Pt 3): 808-17.
Fog T. Topographic distribution of plaques in the spinal cord in multiple sclerosis. Archives of neurology 1950; 63: 382-414.
Franklin RJ. Why does remyelination fail in multiple sclerosis? Nat Rev Neurosci 2002; 3(9): 705-14.
Franklin RJ, Ffrench-Constant C. Remyelination in the CNS: from biology to therapy. Nat Rev Neurosci 2008; 9(11): 839-55.
Franklin RJ, ffrench-Constant C, Edgar JM, Smith KJ. Neuroprotection and repair in multiple sclerosis. Nature reviews Neurology 2012; 8(11): 624-34.

Freedman MS, Selchen D, Arnold DL, Prat A, Banwell B, Yeung M*, et al.* Treatment optimization in MS: Canadian MS Working Group updated recommendations. The Canadian journal of neurological sciences Le journal canadien des sciences neurologiques 2013; 40(3): 307-23.
Friese MA, Jakobsen KB, Friis L, Etzensperger R, Craner MJ, McMahon RM*, et al.* Opposing effects of HLA class I molecules in tuning autoreactive CD8+ T cells in multiple sclerosis. Nature medicine 2008; 14(11): 1227-35.
Frischer JM, Bramow S, Dal-Bianco A, Lucchinetti CF, Rauschka H, Schmidbauer M*, et al.* The relation between inflammation and neurodegeneration in multiple sclerosis brains. Brain : a journal of neurology 2009; 132(Pt 5): 1175-89.
Gale CR, Martyn CN. Migrant studies in multiple sclerosis. Prog Neurobiol 1995; 47(4-5): 425-48.
Gareau PJ, Rutt BK, Karlik SJ, Mitchell JR. Magnetization transfer and multicomponent T2 relaxation measurements with histopathologic correlation in an experimental model of MS. Journal of magnetic resonance imaging : JMRI 2000; 11(6): 586-95.
Gayou A, Brochet B, Dousset V. Transitional progressive multiple sclerosis: a clinical and imaging study. Journal of neurology, neurosurgery, and psychiatry 1997; 63(3): 396-8.
Geurts JJ, Bo L, Pouwels PJ, Castelijns JA, Polman CH, Barkhof F. Cortical lesions in multiple sclerosis: combined postmortem MR imaging and histopathology. AJNR American journal of neuroradiology 2005a; 26(3): 572-7.
Geurts JJ, Pouwels PJ, Uitdehaag BM, Polman CH, Barkhof F, Castelijns JA. Intracortical lesions in multiple sclerosis: improved detection with 3D double inversion-recovery MR imaging. Radiology 2005b; 236(1): 254-60.
Geurts JJ, Roosendaal SD, Calabrese M, Ciccarelli O, Agosta F, Chard DT*, et al.* Consensus recommendations for MS cortical lesion scoring using double inversion recovery MRI. Neurology 2011; 76(5): 418-24.
Giacomini PS, Levesque IR, Ribeiro L, Narayanan S, Francis SJ, Pike GB*, et al.* Measuring demyelination and remyelination in acute multiple sclerosis lesion voxels. Archives of neurology 2009; 66(3): 375-81.
Goodin DS, Jones J, Li D, Traboulsee A, Reder AT, Beckmann K*, et al.* Establishing long-term efficacy in chronic disease: use of recursive partitioning and propensity score adjustment to estimate outcome in MS. PloS one 2011; 6(11): e22444.
Goodkin DE, Cookfair D, Wende K, Bourdette D, Pullicino P, Scherokman B*, et al.* Inter- and intrarater scoring agreement using grades 1.0 to 3.5 of the Kurtzke Expanded Disability Status Scale (EDSS). Multiple Sclerosis Collaborative Research Group. Neurology 1992; 42(4): 859-63.
Grabner G, Janke AL, Budge MM, Smith D, Pruessner J, Collins DL. Symmetric atlasing and model based segmentation: an application to the hippocampus in older adults. Medical image computing and computer-assisted intervention : MICCAI International Conference on Medical Image Computing and Computer-Assisted Intervention 2006; 9(Pt 2): 58-66.
Gray E, Thomas TL, Betmouni S, Scolding N, Love S. Elevated myeloperoxidase activity in white matter in multiple sclerosis. Neurosci Lett 2008; 444(2): 195-8.
Green AJ, Gelfand JM, Cree BA, Bevan C, Boscardin WJ, Mei F*, et al.* Clemastine fumarate as a remyelinating therapy for multiple sclerosis (ReBUILD): a randomised, controlled, double-blind, crossover trial. Lancet 2017; 390(10111): 2481-9.

Gregersen JW, Kranc KR, Ke X, Svendsen P, Madsen LS, Thomsen AR*, et al.* Functional epistasis on a common MHC haplotype associated with multiple sclerosis. Nature 2006; 443(7111): 574-7.
Gregory SG, Schmidt S, Seth P, Oksenberg JR, Hart J, Prokop A*, et al.* Interleukin 7 receptor alpha chain (IL7R) shows allelic and functional association with multiple sclerosis. Nat Genet 2007; 39(9): 1083-91.
Group TIMSS. Interferon beta-1b is effective in relapsing-remitting multiple sclerosis. I. Clinical results of a multicenter, randomized, double-blind, placebo-controlled trial. The IFNB Multiple Sclerosis Study Group. Neurology 1993; 43(4): 655-61.
Haider L, Simeonidou C, Steinberger G, Hametner S, Grigoriadis N, Deretzi G*, et al.* Multiple sclerosis deep grey matter: the relation between demyelination, neurodegeneration, inflammation and iron. Journal of neurology, neurosurgery, and psychiatry 2014; 85(12): 1386-95.
Haider L, Zrzavy T, Hametner S, Hoftberger R, Bagnato F, Grabner G*, et al.* The topograpy of demyelination and neurodegeneration in the multiple sclerosis brain. Brain : a journal of neurology 2016; 139(Pt 3): 807-15.
Hallgren B, Sourander P. The effect of age on the non-haemin iron in the human brain. J Neurochem 1958; 3(1): 41-51.
Hametner S, Wimmer I, Haider L, Pfeifenbring S, Bruck W, Lassmann H. Iron and neurodegeneration in the multiple sclerosis brain. Annals of neurology 2013; 74(6): 848-61.
Harkiolaki M, Holmes SL, Svendsen P, Gregersen JW, Jensen LT, McMahon R*, et al.* T cell-mediated autoimmune disease due to low-affinity crossreactivity to common microbial peptides. Immunity 2009; 30(3): 348-57.
Hartmann FJ, Khademi M, Aram J, Ammann S, Kockum I, Constantinescu C*, et al.* Multiple sclerosis-associated IL2RA polymorphism controls GM-CSF production in human TH cells. Nat Commun 2014; 5: 5056.
Hartung H, Curtin F, Schneble H, Pochet H, Glanzman R, Lambert E*, et al.* Week 24 results from a Phase IIb trial of GNbAC1 in patients with relapsing remitting multiple sclerosis (CHANGE-MS; Clinical trial assessing the HERV-W Env antagonist GNbAC1 for Efficacy in MS). Multiple Sclerosis Journal 2017; 23(3_suppl): 980.
Hayton T, Furby J, Smith KJ, Altmann DR, Brenner R, Chataway J*, et al.* Clinical and imaging correlates of the multiple sclerosis impact scale in secondary progressive multiple sclerosis. Journal of neurology 2012; 259(2): 237-45.
He A, Spelman T, Jokubaitis V, Havrdova E, Horakova D, Trojano M*, et al.* Comparison of switch to fingolimod or interferon beta/glatiramer acetate in active multiple sclerosis. JAMA neurology 2015; 72(4): 405-13.
Hedstrom AK, Alfredsson L, Lundkvist Ryner M, Fogdell-Hahn A, Hillert J, Olsson T. Smokers run increased risk of developing anti-natalizumab antibodies. Multiple sclerosis (Houndmills, Basingstoke, England) 2014a; 20(8): 1081-5.
Hedstrom AK, Lima Bomfim I, Barcellos L, Gianfrancesco M, Schaefer C, Kockum I*, et al.* Interaction between adolescent obesity and HLA risk genes in the etiology of multiple sclerosis. Neurology 2014b; 82(10): 865-72.
Hedstrom AK, Ryner M, Fink K, Fogdell-Hahn A, Alfredsson L, Olsson T*, et al.* Smoking and risk of treatment-induced neutralizing antibodies to interferon beta-1a. Multiple sclerosis (Houndmills, Basingstoke, England) 2014c; 20(4): 445-50.
Henkelman RM, Stanisz GJ, Graham SJ. Magnetization transfer in MRI: a review. NMR in biomedicine 2001; 14(2): 57-64.

Hernan MA, Olek MJ, Ascherio A. Cigarette smoking and incidence of multiple sclerosis. Am J Epidemiol 2001; 154(1): 69-74.
Herranz E, Louapre C, Treaba CA, Govindarajan ST, Ouellette R, Mangeat G*, et al.* Profiles of cortical inflammation in multiple sclerosis by (11)C-PBR28 MR-PET and 7 Tesla imaging. Multiple sclerosis (Houndmills, Basingstoke, England) 2019: 1352458519867320.
Hickman SI, Barker GJ, Molyneux PD, Miller DH. Technical note: the comparison of hypointense lesions from 'pseudo-T1' and T1-weighted images in secondary progressive multiple sclerosis. Multiple sclerosis (Houndmills, Basingstoke, England) 2002; 8(5): 433-5.
Hill-Cawthorne GA, Button T, Tuohy O, Jones JL, May K, Somerfield J*, et al.* Long term lymphocyte reconstitution after alemtuzumab treatment of multiple sclerosis. Journal of neurology, neurosurgery, and psychiatry 2012; 83(3): 298-304.
Hobart J, Freeman J, Thompson A. Kurtzke scales revisited: the application of psychometric methods to clinical intuition. Brain : a journal of neurology 2000; 123 (Pt 5): 1027-40.
Hochmeister S, Grundtner R, Bauer J, Engelhardt B, Lyck R, Gordon G*, et al.* Dysferlin is a new marker for leaky brain blood vessels in multiple sclerosis. Journal of neuropathology and experimental neurology 2006; 65(9): 855-65.
Holland CM, Charil A, Csapo I, Liptak Z, Ichise M, Khoury SJ*, et al.* The relationship between normal cerebral perfusion patterns and white matter lesion distribution in 1,249 patients with multiple sclerosis. Journal of neuroimaging : official journal of the American Society of Neuroimaging 2012; 22(2): 129-36.
Horsfield MA, Sala S, Neema M, Absinta M, Bakshi A, Sormani MP*, et al.* Rapid semi-automatic segmentation of the spinal cord from magnetic resonance images: application in multiple sclerosis. NeuroImage 2010; 50(2): 446-55.
Howell OW, Reeves CA, Nicholas R, Carassiti D, Radotra B, Gentleman SM*, et al.* Meningeal inflammation is widespread and linked to cortical pathology in multiple sclerosis. Brain : a journal of neurology 2011; 134(Pt 9): 2755-71.
Huang JK, Jarjour AA, Nait Oumesmar B, Kerninon C, Williams A, Krezel W*, et al.* Retinoid X receptor gamma signaling accelerates CNS remyelination. Nat Neurosci 2011; 14(1): 45-53.
Ighani M, Jonas S, Izbudak I, Choi S, Lema-Dopico A, Hua J*, et al.* No association between cortical lesions and leptomeningeal enhancement on 7-Tesla MRI in multiple sclerosis. Multiple sclerosis (Houndmills, Basingstoke, England) 2019: 1352458519876037.
Ingram G, Colley E, Ben-Shlomo Y, Cossburn M, Hirst CL, Pickersgill TP*, et al.* Validity of patient-derived disability and clinical data in multiple sclerosis. Multiple sclerosis (Houndmills, Basingstoke, England) 2010; 16(4): 472-9.
International Multiple Sclerosis Genetics C, Beecham AH, Patsopoulos NA, Xifara DK, Davis MF, Kemppinen A*, et al.* Analysis of immune-related loci identifies 48 new susceptibility variants for multiple sclerosis. Nat Genet 2013; 45(11): 1353-60.
International Multiple Sclerosis Genetics C, Bush WS, Sawcer SJ, de Jager PL, Oksenberg JR, McCauley JL*, et al.* Evidence for polygenic susceptibility to multiple sclerosis--the shape of things to come. Am J Hum Genet 2010; 86(4): 621-5.
International Multiple Sclerosis Genetics C, Wellcome Trust Case Control C, Sawcer S, Hellenthal G, Pirinen M, Spencer CC*, et al.* Genetic risk and a primary role for cell-mediated immune mechanisms in multiple sclerosis. Nature 2011; 476(7359): 214-9.
Jeffery ND, Blakemore WF. Locomotor deficits induced by experimental spinal cord demyelination are abolished by spontaneous remyelination. Brain : a journal of neurology 1997; 120 (Pt 1): 27-37.

Jehna M, Pirpamer L, Khalil M, Fuchs S, Ropele S, Langkammer C*, et al.* Periventricular lesions correlate with cortical thinning in multiple sclerosis. Annals of neurology 2015; 78(4): 530-9.
Jones JL, Anderson JM, Phuah CL, Fox EJ, Selmaj K, Margolin D*, et al.* Improvement in disability after alemtuzumab treatment of multiple sclerosis is associated with neuroprotective autoimmunity. Brain : a journal of neurology 2010; 133(Pt 8): 2232-47.
Kalincik T, Brown JW, Robertson N, Willis M, Scolding N, Rice CM*, et al.* Treatment effectiveness of alemtuzumab compared with natalizumab, fingolimod, and interferon beta in relapsing-remitting multiple sclerosis: a cohort study. The Lancet Neurology 2017a.
Kalincik T, Jokubaitis V, Spelman T, Horakova D, Havrdova E, Trojano M*, et al.* Cladribine versus fingolimod, natalizumab and interferon beta for multiple sclerosis. Multiple sclerosis (Houndmills, Basingstoke, England) 2017b: 1352458517728812.
Kampman MT, Steffensen LH, Mellgren SI, Jorgensen L. Effect of vitamin D3 supplementation on relapses, disease progression, and measures of function in persons with multiple sclerosis: exploratory outcomes from a double-blind randomised controlled trial. Multiple sclerosis (Houndmills, Basingstoke, England) 2012; 18(8): 1144-51.
Kanda T, Ishii K, Kawaguchi H, Kitajima K, Takenaka D. High signal intensity in the dentate nucleus and globus pallidus on unenhanced T1-weighted MR images: relationship with increasing cumulative dose of a gadolinium-based contrast material. Radiology 2014; 270(3): 834-41.
Kapoor R, Furby J, Hayton T, Smith KJ, Altmann DR, Brenner R*, et al.* Lamotrigine for neuroprotection in secondary progressive multiple sclerosis: a randomised, double-blind, placebo-controlled, parallel-group trial. The Lancet Neurology 2010; 9(7): 681-8.
Kearney H, Yiannakas MC, Samson RS, Wheeler-Kingshott CA, Ciccarelli O, Miller DH. Investigation of magnetization transfer ratio-derived pial and subpial abnormalities in the multiple sclerosis spinal cord. Brain : a journal of neurology 2014; 137(Pt 9): 2456-68.
Kilsdonk ID, Jonkman LE, Klaver R, van Veluw SJ, Zwanenburg JJ, Kuijer JP*, et al.* Increased cortical grey matter lesion detection in multiple sclerosis with 7 T MRI: a post-mortem verification study. Brain : a journal of neurology 2016; 139(Pt 5): 1472-81.
Kivisakk P, Imitola J, Rasmussen S, Elyaman W, Zhu B, Ransohoff RM*, et al.* Localizing central nervous system immune surveillance: meningeal antigen-presenting cells activate T cells during experimental autoimmune encephalomyelitis. Annals of neurology 2009; 65(4): 457-69.
Klaver R, Popescu V, Voorn P, Galis-de Graaf Y, van der Valk P, de Vries HE*, et al.* Neuronal and axonal loss in normal-appearing gray matter and subpial lesions in multiple sclerosis. Journal of neuropathology and experimental neurology 2015; 74(5): 453-8.
Kollia K, Maderwald S, Putzki N, Schlamann M, Theysohn JM, Kraff O*, et al.* First clinical study on ultra-high-field MR imaging in patients with multiple sclerosis: comparison of 1.5T and 7T. AJNR American journal of neuroradiology 2009; 30(4): 699-702.
Komori M, Lin YC, Cortese I, Blake A, Ohayon J, Cherup J*, et al.* Insufficient disease inhibition by intrathecal rituximab in progressive multiple sclerosis. Ann Clin Transl Neurol 2016; 3(3): 166-79.
Kooij G, Kopplin K, Blasig R, Stuiver M, Koning N, Goverse G*, et al.* Disturbed function of the blood-cerebrospinal fluid barrier aggravates neuro-inflammation. Acta Neuropathol 2014; 128(2): 267-77.
Kramer-Albers EM, Bretz N, Tenzer S, Winterstein C, Mobius W, Berger H*, et al.* Oligodendrocytes secrete exosomes containing major myelin and stress-protective proteins: Trophic support for axons? Proteomics Clin Appl 2007; 1(11): 1446-61.

Kreidstein ML, Giguere D, Freiberg A. MRI interaction with tattoo pigments: case report, pathophysiology, and management. Plast Reconstr Surg 1997; 99(6): 1717-20.
Kremenchutzky M, Rice GP, Baskerville J, Wingerchuk DM, Ebers GC. The natural history of multiple sclerosis: a geographically based study 9: observations on the progressive phase of the disease. Brain : a journal of neurology 2006; 129(Pt 3): 584-94.
Kremer D, Kury P, Dutta R. Promoting remyelination in multiple sclerosis: current drugs and future prospects. Multiple sclerosis (Houndmills, Basingstoke, England) 2015; 21(5): 541-9.
Krumbholz M, Theil D, Cepok S, Hemmer B, Kivisakk P, Ransohoff RM*, et al.* Chemokines in multiple sclerosis: CXCL12 and CXCL13 up-regulation is differentially linked to CNS immune cell recruitment. Brain : a journal of neurology 2006; 129(Pt 1): 200-11.
Kuchling J, Ramien C, Bozin I, Dorr J, Harms L, Rosche B*, et al.* Identical lesion morphology in primary progressive and relapsing-remitting MS--an ultrahigh field MRI study. Multiple sclerosis (Houndmills, Basingstoke, England) 2014; 20(14): 1866-71.
Kuhlmann T, Lingfeld G, Bitsch A, Schuchardt J, Bruck W. Acute axonal damage in multiple sclerosis is most extensive in early disease stages and decreases over time. Brain : a journal of neurology 2002; 125(Pt 10): 2202-12.
Kurtzke JF. Rating neurologic impairment in multiple sclerosis: an expanded disability status scale (EDSS). Neurology 1983; 33(11): 1444-52.
Kutzelnigg A, Lucchinetti CF, Stadelmann C, Bruck W, Rauschka H, Bergmann M*, et al.* Cortical demyelination and diffuse white matter injury in multiple sclerosis. Brain : a journal of neurology 2005; 128(Pt 11): 2705-12.
Langdon DW. Cognition in multiple sclerosis. Current opinion in neurology 2011; 24(3): 244-9.
Laule C, Leung E, Lis DK, Traboulsee AL, Paty DW, MacKay AL*, et al.* Myelin water imaging in multiple sclerosis: quantitative correlations with histopathology. Multiple sclerosis (Houndmills, Basingstoke, England) 2006; 12(6): 747-53.
Levin LI, Munger KL, O'Reilly EJ, Falk KI, Ascherio A. Primary infection with the Epstein-Barr virus and risk of multiple sclerosis. Annals of neurology 2010; 67(6): 824-30.
Linington C, Bradl M, Lassmann H, Brunner C, Vass K. Augmentation of demyelination in rat acute allergic encephalomyelitis by circulating mouse monoclonal antibodies directed against a myelin/oligodendrocyte glycoprotein. Am J Pathol 1988; 130(3): 443-54.
Liu W, Nair G, Vuolo L, Bakshi A, Massoud R, Reich DS*, et al.* In vivo imaging of spinal cord atrophy in neuroinflammatory diseases. Annals of neurology 2014; 76(3): 370-8.
Liu Z, Pardini M, Yaldizli O, Sethi V, Muhlert N, Wheeler-Kingshott CA*, et al.* Magnetization transfer ratio measures in normal-appearing white matter show periventricular gradient abnormalities in multiple sclerosis. Brain : a journal of neurology 2015; 138(Pt 5): 1239-46.
Lorscheider J, Buzzard K, Jokubaitis V, Spelman T, Havrdova E, Horakova D*, et al.* Defining secondary progressive multiple sclerosis. Brain : a journal of neurology 2016; 139(Pt 9): 2395-405.
Losseff NA, Webb SL, O'Riordan JI, Page R, Wang L, Barker GJ*, et al.* Spinal cord atrophy and disability in multiple sclerosis. A new reproducible and sensitive MRI method with potential to monitor disease progression. Brain : a journal of neurology 1996; 119 (Pt 3): 701-8.
Lovato L, Willis SN, Rodig SJ, Caron T, Almendinger SE, Howell OW*, et al.* Related B cell clones populate the meninges and parenchyma of patients with multiple sclerosis. Brain : a journal of neurology 2011; 134(Pt 2): 534-41.

Lublin FD, Reingold SC. Defining the clinical course of multiple sclerosis: results of an international survey. National Multiple Sclerosis Society (USA) Advisory Committee on Clinical Trials of New Agents in Multiple Sclerosis. Neurology 1996; 46(4): 907-11.
Lublin FD, Reingold SC, Cohen JA, Cutter GR, Sorensen PS, Thompson AJ*, et al.* Defining the clinical course of multiple sclerosis: the 2013 revisions. Neurology 2014; 83(3): 278-86.
Lucas RM, Byrne SN, Correale J, Ilschner S, Hart PH. Ultraviolet radiation, vitamin D and multiple sclerosis. Neurodegener Dis Manag 2015; 5(5): 413-24.
Lucchinetti C, Bruck W, Parisi J, Scheithauer B, Rodriguez M, Lassmann H. Heterogeneity of multiple sclerosis lesions: implications for the pathogenesis of demyelination. Annals of neurology 2000; 47(6): 707-17.
Lucchinetti CF, Popescu BF, Bunyan RF, Moll NM, Roemer SF, Lassmann H*, et al.* Inflammatory cortical demyelination in early multiple sclerosis. N Engl J Med 2011; 365(23): 2188-97.
Lumeng CN, Bodzin JL, Saltiel AR. Obesity induces a phenotypic switch in adipose tissue macrophage polarization. J Clin Invest 2007; 117(1): 175-84.
Lunt M. Selecting an appropriate caliper can be essential for achieving good balance with propensity score matching. Am J Epidemiol 2014; 179(2): 226-35.
MacKay A, Whittall K, Adler J, Li D, Paty D, Graeb D. In vivo visualization of myelin water in brain by magnetic resonance. Magnetic resonance in medicine : official journal of the Society of Magnetic Resonance in Medicine / Society of Magnetic Resonance in Medicine 1994; 31(6): 673-7.
Magliozzi R, Columba-Cabezas S, Serafini B, Aloisi F. Intracerebral expression of CXCL13 and BAFF is accompanied by formation of lymphoid follicle-like structures in the meninges of mice with relapsing experimental autoimmune encephalomyelitis. Journal of neuroimmunology 2004; 148(1-2): 11-23.
Magliozzi R, Fadda G, Bar-Or A, Brown R, Mazziotti V, Nicholas R*, et al.* Substantial 'subependymal-in' gradient of thalamic damage in progressive multiple sclerosis. Multiple Sclerosis Journal 2018a; 24(S2): 94-5.
Magliozzi R, Howell O, Vora A, Serafini B, Nicholas R, Puopolo M*, et al.* Meningeal B-cell follicles in secondary progressive multiple sclerosis associate with early onset of disease and severe cortical pathology. Brain : a journal of neurology 2007; 130(Pt 4): 1089-104.
Magliozzi R, Howell OW, Nicholas R, Cruciani C, Castellaro M, Romualdi C*, et al.* Inflammatory intrathecal profiles and cortical damage in multiple sclerosis. Annals of neurology 2018b; 83(4): 739-55.
Magliozzi R, Howell OW, Reeves C, Roncaroli F, Nicholas R, Serafini B*, et al.* A Gradient of neuronal loss and meningeal inflammation in multiple sclerosis. Annals of neurology 2010; 68(4): 477-93.
Mahad DH, Trapp BD, Lassmann H. Pathological mechanisms in progressive multiple sclerosis. The Lancet Neurology 2015; 14(2): 183-93.
Mainero C, Benner T, Radding A, van der Kouwe A, Jensen R, Rosen BR*, et al.* In vivo imaging of cortical pathology in multiple sclerosis using ultra-high field MRI. Neurology 2009; 73(12): 941-8.
Mainero C, Louapre C, Govindarajan ST, Gianni C, Nielsen AS, Cohen-Adad J*, et al.* A gradient in cortical pathology in multiple sclerosis by in vivo quantitative 7 T imaging. Brain : a journal of neurology 2015; 138(Pt 4): 932-45.
Makhani N, Banwell B, Tellier R, Yea C, McGovern S, O'Mahony J*, et al.* Viral exposures and MS outcome in a prospective cohort of children with acquired demyelination. Multiple sclerosis (Houndmills, Basingstoke, England) 2016; 22(3): 385-8.

Maldjian JA, Laurienti PJ, Kraft RA, Burdette JH. An automated method for neuroanatomic and cytoarchitectonic atlas-based interrogation of fMRI data sets. NeuroImage 2003; 19(3): 1233-9.
Manouchehrinia A, Tench CR, Maxted J, Bibani RH, Britton J, Constantinescu CS. Tobacco smoking and disability progression in multiple sclerosis: United Kingdom cohort study. Brain : a journal of neurology 2013; 136(Pt 7): 2298-304.
Martyn CN, Cruddas M, Compston DA. Symptomatic Epstein-Barr virus infection and multiple sclerosis. Journal of neurology, neurosurgery, and psychiatry 1993; 56(2): 167-8.
Matarese G, Carrieri PB, La Cava A, Perna F, Sanna V, De Rosa V*, et al.* Leptin increase in multiple sclerosis associates with reduced number of CD4(+)CD25+ regulatory T cells. Proceedings of the National Academy of Sciences of the United States of America 2005; 102(14): 5150-5.
McDonald RJ, McDonald JS, Kallmes DF, Jentoft ME, Murray DL, Thielen KR*, et al.* Intracranial Gadolinium Deposition after Contrast-enhanced MR Imaging. Radiology 2015; 275(3): 772-82.
Meinl E, Krumbholz M, Derfuss T, Junker A, Hohlfeld R. Compartmentalization of inflammation in the CNS: a major mechanism driving progressive multiple sclerosis. Journal of the neurological sciences 2008; 274(1-2): 42-4.
Menard A, Pierig R, Pelletier J, Bensa P, Belliveau J, Mandrand B*, et al.* Detection of a gliotoxic activity in the cerebrospinal fluid from multiple sclerosis patients. Neurosci Lett 1998; 245(1): 49-52.
Meyer-Moock S, Feng YS, Maeurer M, Dippel FW, Kohlmann T. Systematic literature review and validity evaluation of the Expanded Disability Status Scale (EDSS) and the Multiple Sclerosis Functional Composite (MSFC) in patients with multiple sclerosis. BMC neurology 2014; 14: 58.
Mi S, Hu B, Hahm K, Luo Y, Kam Hui ES, Yuan Q*, et al.* LINGO-1 antagonist promotes spinal cord remyelination and axonal integrity in MOG-induced experimental autoimmune encephalomyelitis. Nature medicine 2007; 13(10): 1228-33.
Mi S, Miller RH, Lee X, Scott ML, Shulag-Morskaya S, Shao Z*, et al.* LINGO-1 negatively regulates myelination by oligodendrocytes. Nat Neurosci 2005; 8(6): 745-51.
Miller DH, Grossman RI, Reingold SC, McFarland HF. The role of magnetic resonance techniques in understanding and managing multiple sclerosis. Brain : a journal of neurology 1998; 121 (Pt 1): 3-24.
Miller DM, Weinstock-Guttman B, Bethoux F, Lee JC, Beck G, Block V*, et al.* A meta-analysis of methylprednisolone in recovery from multiple sclerosis exacerbations. Multiple sclerosis (Houndmills, Basingstoke, England) 2000; 6(4): 267-73.
Minneboo A, Barkhof F, Polman CH, Uitdehaag BM, Knol DL, Castelijns JA. Infratentorial lesions predict long-term disability in patients with initial findings suggestive of multiple sclerosis. Archives of neurology 2004; 61(2): 217-21.
Modat M, Cash DM, Daga P, Winston GP, Duncan JS, Ourselin S. Global image registration using a symmetric block-matching approach. J Med Imaging (Bellingham) 2014; 1(2): 024003.
Modat M, Ridgway GR, Taylor ZA, Lehmann M, Barnes J, Hawkes DJ*, et al.* Fast free-form deformation using graphics processing units. Comput Methods Programs Biomed 2010; 98(3): 278-84.
Montalban X, Hauser SL, Kappos L, Arnold DL, Bar-Or A, Comi G*, et al.* Ocrelizumab versus Placebo in Primary Progressive Multiple Sclerosis. N Engl J Med 2017; 376(3): 209-20.

Moreau T, Thorpe J, Miller D, Moseley I, Hale G, Waldmann H*, et al.* Preliminary evidence from magnetic resonance imaging for reduction in disease activity after lymphocyte depletion in multiple sclerosis. Lancet 1994; 344(8918): 298-301.
Muhlert N, Sethi V, Schneider T, Daga P, Cipolotti L, Haroon HA*, et al.* Diffusion MRI-based cortical complexity alterations associated with executive function in multiple sclerosis. Journal of magnetic resonance imaging : JMRI 2013; 38(1): 54-63.
Munger KL, Levin LI, Hollis BW, Howard NS, Ascherio A. Serum 25-hydroxyvitamin D levels and risk of multiple sclerosis. JAMA 2006; 296(23): 2832-8.
Muris AH, Smolders J, Rolf L, Thewissen M, Hupperts R, Damoiseaux J*, et al.* Immune regulatory effects of high dose vitamin D3 supplementation in a randomized controlled trial in relapsing remitting multiple sclerosis patients receiving IFNbeta; the SOLARIUM study. Journal of neuroimmunology 2016; 300: 47-56.
Narayanan S, Fu L, Pioro E, De Stefano N, Collins DL, Francis GS*, et al.* Imaging of axonal damage in multiple sclerosis: spatial distribution of magnetic resonance imaging lesions. Annals of neurology 1997; 41(3): 385-91.
Nave KA. Myelination and the trophic support of long axons. Nat Rev Neurosci 2010; 11(4): 275-83.
Nguyen TD, Wisnieff C, Cooper MA, Kumar D, Raj A, Spincemaille P*, et al.* T2 prep three-dimensional spiral imaging with efficient whole brain coverage for myelin water quantification at 1.5 tesla. Magnetic resonance in medicine : official journal of the Society of Magnetic Resonance in Medicine / Society of Magnetic Resonance in Medicine 2012; 67(3): 614-21.
Niehaus A, Shi J, Grzenkowski M, Diers-Fenger M, Archelos J, Hartung HP*, et al.* Patients with active relapsing-remitting multiple sclerosis synthesize antibodies recognizing oligodendrocyte progenitor cell surface protein: implications for remyelination. Annals of neurology 2000; 48(3): 362-71.
Nielsen TR, Rostgaard K, Askling J, Steffensen R, Oturai A, Jersild C*, et al.* Effects of infectious mononucleosis and HLA-DRB1*15 in multiple sclerosis. Multiple sclerosis (Houndmills, Basingstoke, England) 2009; 15(4): 431-6.
Noseworthy JH, Vandervoort MK, Wong CJ, Ebers GC. Interrater variability with the Expanded Disability Status Scale (EDSS) and Functional Systems (FS) in a multiple sclerosis clinical trial. The Canadian Cooperation MS Study Group. Neurology 1990; 40(6): 971-5.
Novotny GE. Formation of cytoplasm-containing vesicles from double-walled coated invaginations containing oligodendrocytic cytoplasm at the axon-myelin sheath interface in adult mammalian central nervous system. Acta Anat (Basel) 1984; 119(2): 106-12.
Ourselin S, Roche A, Subsol G, Pennec X, Ayache N. Reconstructing a 3D structure from serial histological sections. Image Vis Comput 2001; 19: 25-31.
Pardini M, Gualco L, Bommarito G, Roccatagliata L, Schiavi S, Solaro C*, et al.* CSF oligoclonal bands and normal appearing white matter periventricular damage in patients with clinically isolated syndrome suggestive of MS. Mult Scler Relat Disord 2019; 31: 93-6.
Pardini M, Sudre CH, Prados F, Yaldizli O, Sethi V, Muhlert N*, et al.* Relationship of grey and white matter abnormalities with distance from the surface of the brain in multiple sclerosis. Journal of neurology, neurosurgery, and psychiatry 2016.
Patani R, Balaratnam M, Vora A, Reynolds R. Remyelination can be extensive in multiple sclerosis despite a long disease course. Neuropathol Appl Neurobiol 2007; 33(3): 277-87.

Patrikios P, Stadelmann C, Kutzelnigg A, Rauschka H, Schmidbauer M, Laursen H*, et al.* Remyelination is extensive in a subset of multiple sclerosis patients. Brain : a journal of neurology 2006; 129(Pt 12): 3165-72.
Patrucco L, Rojas JI, Cristiano E. Assessing the value of spinal cord lesions in predicting development of multiple sclerosis in patients with clinically isolated syndromes. Journal of neurology 2012; 259(7): 1317-20.
Paul F. Pathology and MRI: exploring cognitive impairment in MS. Acta neurologica Scandinavica 2016; 134 Suppl 200: 24-33.
Perez-Miralles F, Sastre-Garriga J, Tintore M, Arrambide G, Nos C, Perkal H*, et al.* Clinical impact of early brain atrophy in clinically isolated syndromes. Multiple sclerosis (Houndmills, Basingstoke, England) 2013; 19(14): 1878-86.
Poirion E, Bodini B, Benoit C, Tonietto M, Bera G, Giannesini C*, et al.* A gradient of periventricular microglial activation suggests a CSF-derived neurodegenerative component in MS. Multiple Sclerosis Journal 2017; 23(3_suppl): 80.
Polman CH, O'Connor PW, Havrdova E, Hutchinson M, Kappos L, Miller DH*, et al.* A randomized, placebo-controlled trial of natalizumab for relapsing multiple sclerosis. N Engl J Med 2006; 354(9): 899-910.
Polman CH, Reingold SC, Banwell B, Clanet M, Cohen JA, Filippi M*, et al.* Diagnostic criteria for multiple sclerosis: 2010 revisions to the McDonald criteria. Annals of neurology 2011; 69(2): 292-302.
Popescu V, Ran NC, Barkhof F, Chard DT, Wheeler-Kingshott CA, Vrenken H. Accurate GM atrophy quantification in MS using lesion-filling with co-registered 2D lesion masks. NeuroImage Clinical 2014; 4: 366-73.
Poser CM, Paty DW, Scheinberg L, McDonald WI, Davis FA, Ebers GC*, et al.* New diagnostic criteria for multiple sclerosis: guidelines for research protocols. Annals of neurology 1983; 13(3): 227-31.
Prados F, Cardoso MJ, Kanber B, Ciccarelli O, Kapoor R, Gandini Wheeler-Kingshott CA*, et al.* A multi-time-point modality-agnostic patch-based method for lesion filling in multiple sclerosis. NeuroImage 2016; 139: 376-84.
Prasloski T, Rauscher A, MacKay AL, Hodgson M, Vavasour IM, Laule C*, et al.* Rapid whole cerebrum myelin water imaging using a 3D GRASE sequence. NeuroImage 2012; 63(1): 533-9.
Preisner A, Albrecht S, Cui QL, Hucke S, Ghelman J, Hartmann C*, et al.* Non-steroidal anti-inflammatory drug indometacin enhances endogenous remyelination. Acta Neuropathol 2015.
Preziosa P, Rocca MA, Filippi M. PET is necessary to make the next step forward in understanding MS pathophysiology - No. Multiple sclerosis (Houndmills, Basingstoke, England) 2019; 25(8): 1088-90.
Prineas JW, Kwon EE, Cho ES, Sharer LR, Barnett MH, Oleszak EL*, et al.* Immunopathology of secondary-progressive multiple sclerosis. Annals of neurology 2001; 50(5): 646-57.
Ramanujam R, Hedstrom AK, Manouchehrinia A, Alfredsson L, Olsson T, Bottai M*, et al.* Effect of Smoking Cessation on Multiple Sclerosis Prognosis. JAMA neurology 2015; 72(10): 1117-23.
Rana S, Rogers LJ, Halliday GM. Systemic low-dose UVB inhibits CD8 T cells and skin inflammation by alternative and novel mechanisms. Am J Pathol 2011; 178(6): 2783-91.
Rassen JA, Shelat AA, Myers J, Glynn RJ, Rothman KJ, Schneeweiss S. One-to-many propensity score matching in cohort studies. Pharmacoepidemiol Drug Saf 2012; 21 Suppl 2: 69-80.

Reboldi A, Coisne C, Baumjohann D, Benvenuto F, Bottinelli D, Lira S*, et al.* C-C chemokine receptor 6-regulated entry of TH-17 cells into the CNS through the choroid plexus is required for the initiation of EAE. Nat Immunol 2009; 10(5): 514-23.
Revesz T, Kidd D, Thompson AJ, Barnard RO, McDonald WI. A comparison of the pathology of primary and secondary progressive multiple sclerosis. Brain : a journal of neurology 1994; 117 (Pt 4): 759-65.
Rissanen E, Tuisku J, Rokka J, Paavilainen T, Parkkola R, Rinne JO*, et al.* In Vivo Detection of Diffuse Inflammation in Secondary Progressive Multiple Sclerosis Using PET Imaging and the Radioligand (1)(1)C-PK11195. Journal of nuclear medicine : official publication, Society of Nuclear Medicine 2014; 55(6): 939-44.
Rossi S, Furlan R, De Chiara V, Motta C, Studer V, Mori F*, et al.* Interleukin-1beta causes synaptic hyperexcitability in multiple sclerosis. Annals of neurology 2012; 71(1): 76-83.
Rossi S, Motta C, Studer V, Barbieri F, Buttari F, Bergami A*, et al.* Tumor necrosis factor is elevated in progressive multiple sclerosis and causes excitotoxic neurodegeneration. Multiple sclerosis (Houndmills, Basingstoke, England) 2014; 20(3): 304-12.
Samaraweera AP, Clarke MA, Whitehead A, Falah Y, Driver ID, Dineen RA*, et al.* The Central Vein Sign in Multiple Sclerosis Lesions Is Present Irrespective of the T2* Sequence at 3 T. Journal of neuroimaging : official journal of the American Society of Neuroimaging 2017; 27(1): 114-21.
Samson RS, Brownlee WJ, Cardoso M, J. , Brown JWL, Pardini M, F. PC*, et al.* Outer and inner cortical MTR abnormalities in clinically isolated syndromes. Multiple Sclerosis Journal 2016; 22(3 (Supp)): 30.
Samson RS, Cardoso MJ, Muhlert N, Sethi V, Wheeler-Kingshott CA, Ron M*, et al.* Investigation of outer cortical magnetisation transfer ratio abnormalities in multiple sclerosis clinical subgroups. Multiple sclerosis (Houndmills, Basingstoke, England) 2014; 20(10): 1322-30.
Samson RS, Muhlert N, Sethi V, Wheeler-Kingshott CA, Ron MA, Miller DH*, et al.* Sulcal and gyral crown cortical grey matter involvement in multiple sclerosis: A magnetisation transfer ratio study. Mult Scler Relat Disord 2013; 2(3): 204-12.
Sand IK, Krieger S, Farrell C, Miller AE. Diagnostic uncertainty during the transition to secondary progressive multiple sclerosis. Multiple sclerosis (Houndmills, Basingstoke, England) 2014; 20(12): 1654-7.
Sandberg L, Bistrom M, Salzer J, Vagberg M, Svenningsson A, Sundstrom P. Vitamin D and axonal injury in multiple sclerosis. Multiple sclerosis (Houndmills, Basingstoke, England) 2016; 22(8): 1027-31.
Saxena A, Bauer J, Scheikl T, Zappulla J, Audebert M, Desbois S*, et al.* Cutting edge: Multiple sclerosis-like lesions induced by effector CD8 T cells recognizing a sequestered antigen on oligodendrocytes. J Immunol 2008; 181(3): 1617-21.
Scalfari A, Neuhaus A, Daumer M, Muraro PA, Ebers GC. Onset of secondary progressive phase and long-term evolution of multiple sclerosis. Journal of neurology, neurosurgery, and psychiatry 2014; 85(1): 67-75.
Schmierer K, Parkes HG, So PW, An SF, Brandner S, Ordidge RJ*, et al.* High field (9.4 Tesla) magnetic resonance imaging of cortical grey matter lesions in multiple sclerosis. Brain : a journal of neurology 2010; 133(Pt 3): 858-67.
Schmierer K, Scaravilli F, Altmann DR, Barker GJ, Miller DH. Magnetization transfer ratio and myelin in postmortem multiple sclerosis brain. Annals of neurology 2004; 56(3): 407-15.

Schmierer K, Tozer DJ, Scaravilli F, Altmann DR, Barker GJ, Tofts PS*, et al.* Quantitative magnetization transfer imaging in postmortem multiple sclerosis brain. Journal of magnetic resonance imaging : JMRI 2007a; 26(1): 41-51.
Schmierer K, Wheeler-Kingshott CA, Boulby PA, Scaravilli F, Altmann DR, Barker GJ*, et al.* Diffusion tensor imaging of post mortem multiple sclerosis brain. NeuroImage 2007b; 35(2): 467-77.
Schmitt C, Strazielle N, Ghersi-Egea JF. Brain leukocyte infiltration initiated by peripheral inflammation or experimental autoimmune encephalomyelitis occurs through pathways connected to the CSF-filled compartments of the forebrain and midbrain. J Neuroinflammation 2012; 9: 187.
Schoenfeld D. Chi-squared goodness-of-fit tests for the proportional hazards regression model. Biometrika 1980; 67(1): 145-53.
Seewann A, Kooi EJ, Roosendaal SD, Pouwels PJ, Wattjes MP, van der Valk P*, et al.* Postmortem verification of MS cortical lesion detection with 3D DIR. Neurology 2012; 78(5): 302-8.
Sethi V, Muhlert N, Ron M, Golay X, Wheeler-Kingshott CA, Miller DH*, et al.* MS cortical lesions on DIR: not quite what they seem? PloS one 2013; 8(11): e78879.
Signori A, Gallo F, Bovis F, Di Tullio N, Maietta I, Sormani MP. Long-term impact of interferon or Glatiramer acetate in multiple sclerosis: A systematic review and meta-analysis. Mult Scler Relat Disord 2016; 6: 57-63.
Silver N, Lai M, Symms M, Barker G, McDonald I, Miller D. Serial gadolinium-enhanced and magnetization transfer imaging to investigate the relationship between the duration of blood-brain barrier disruption and extent of demyelination in new multiple sclerosis lesions. Journal of neurology 1999; 246(8): 728-30.
Simpson S, Jr., Blizzard L, Otahal P, Van der Mei I, Taylor B. Latitude is significantly associated with the prevalence of multiple sclerosis: a meta-analysis. Journal of neurology, neurosurgery, and psychiatry 2011; 82(10): 1132-41.
Smith KJ, Blakemore WF, McDonald WI. Central remyelination restores secure conduction. Nature 1979; 280(5721): 395-6.
Smith SM, Zhang Y, Jenkinson M, Chen J, Matthews PM, Federico A*, et al.* Accurate, robust, and automated longitudinal and cross-sectional brain change analysis. NeuroImage 2002; 17(1): 479-89.
Soilu-Hanninen M, Aivo J, Lindstrom BM, Elovaara I, Sumelahti ML, Farkkila M*, et al.* A randomised, double blind, placebo controlled trial with vitamin D3 as an add on treatment to interferon beta-1b in patients with multiple sclerosis. Journal of neurology, neurosurgery, and psychiatry 2012; 83(5): 565-71.
Sormani MP, Bruzzi P. MRI lesions as a surrogate for relapses in multiple sclerosis: a meta-analysis of randomised trials. The Lancet Neurology 2013; 12(7): 669-76.
Spelman T, Kalincik T, Jokubaitis V, Zhang A, Pellegrini F, Wiendl H*, et al.* Comparative efficacy of first-line natalizumab vs IFN-beta or glatiramer acetate in relapsing MS. Neurol Clin Pract 2016; 6(2): 102-15.
Spencer PS, Thomas PK. Ultrastructural studies of the dying-back process. II. The sequestration and removal by Schwann cells and oligodendrocytes of organelles from normal and diseases axons. J Neurocytol 1974; 3(6): 763-83.
Stankoff B, Freeman L, Aigrot MS, Chardain A, Dolle F, Williams A*, et al.* Imaging central nervous system myelin by positron emission tomography in multiple sclerosis using [methyl-

(1)(1)C]-2-(4'-methylaminophenyl)- 6-hydroxybenzothiazole. Annals of neurology 2011; 69(4): 673-80.
Stankoff B, Poirion E, Tonietto M, Bodini B. Exploring the heterogeneity of MS lesions using positron emission tomography: a reappraisal of their contribution to disability. Brain pathology (Zurich, Switzerland) 2018; 28(5): 723-34.
Suissa S. Immortal time bias in pharmaco-epidemiology. Am J Epidemiol 2008; 167(4): 492-9.
Swingler RJ, Compston DA. The prevalence of multiple sclerosis in south east Wales. Journal of neurology, neurosurgery, and psychiatry 1988; 51(12): 1520-4.
Tedeholm H, Lycke J, Skoog B, Lisovskaja V, Hillert J, Dahle C*, et al.* Time to secondary progression in patients with multiple sclerosis who were treated with first generation immunomodulating drugs. Multiple sclerosis (Houndmills, Basingstoke, England) 2013; 19(6): 765-74.
Thompson AJ, Banwell BL, Barkhof F, Carroll WM, Coetzee T, Comi G*, et al.* Diagnosis of multiple sclerosis: 2017 revisions of the McDonald criteria. The Lancet Neurology 2017.
Tintore M, Rovira A, Rio J, Otero-Romero S, Arrambide G, Tur C*, et al.* Defining high, medium and low impact prognostic factors for developing multiple sclerosis. Brain : a journal of neurology 2015; 138(Pt 7): 1863-74.
Trapp BD, Peterson J, Ransohoff RM, Rudick R, Mork S, Bo L. Axonal transection in the lesions of multiple sclerosis. N Engl J Med 1998; 338(5): 278-85.
Trojano M, Pellegrini F, Fuiani A, Paolicelli D, Zipoli V, Zimatore GB*, et al.* New natural history of interferon-beta-treated relapsing multiple sclerosis. Annals of neurology 2007; 61(4): 300-6.
Tronel C, Largeau B, Santiago Ribeiro MJ, Guilloteau D, Dupont AC, Arlicot N. Molecular Targets for PET Imaging of Activated Microglia: The Current Situation and Future Expectations. International journal of molecular sciences 2017; 18(4).
Tuohy O, Costelloe L, Hill-Cawthorne G, Bjornson I, Harding K, Robertson N*, et al.* Alemtuzumab treatment of multiple sclerosis: long-term safety and efficacy. Journal of neurology, neurosurgery, and psychiatry 2015; 86(2): 208-15.
van Walderveen MA, Kamphorst W, Scheltens P, van Waesberghe JH, Ravid R, Valk J*, et al.* Histopathologic correlate of hypointense lesions on T1-weighted spin-echo MRI in multiple sclerosis. Neurology 1998; 50(5): 1282-8.
Varga AW, Johnson G, Babb JS, Herbert J, Grossman RI, Inglese M. White matter hemodynamic abnormalities precede sub-cortical gray matter changes in multiple sclerosis. Journal of the neurological sciences 2009; 282(1-2): 28-33.
Vargas WS, Monohan E, Pandya S, Raj A, Vartanian T, Nguyen TD*, et al.* Measuring longitudinal myelin water fraction in new multiple sclerosis lesions. NeuroImage Clinical 2015; 9: 369-75.
Vidaurre OG, Haines JD, Katz Sand I, Adula KP, Huynh JL, McGraw CA*, et al.* Cerebrospinal fluid ceramides from patients with multiple sclerosis impair neuronal bioenergetics. Brain : a journal of neurology 2014; 137(Pt 8): 2271-86.
Viglietta V, Baecher-Allan C, Weiner HL, Hafler DA. Loss of functional suppression by CD4+CD25+ regulatory T cells in patients with multiple sclerosis. J Exp Med 2004; 199(7): 971-9.
Vrenken H, Geurts JJ, Knol DL, Polman CH, Castelijns JA, Pouwels PJ*, et al.* Normal-appearing white matter changes vary with distance to lesions in multiple sclerosis. AJNR American journal of neuroradiology 2006; 27(9): 2005-11.

Vukusic S, Confavreux C. Prognostic factors for progression of disability in the secondary progressive phase of multiple sclerosis. Journal of the neurological sciences 2003; 206(2): 135-7.
Wattjes MR, A; Miller, D; Yousry TA; Sormani, MP; de Stefano, N; Tintoré, M; Auger, C; Tur, C; Filippi, M; Rocca, MA; Fazekas, F; Kappos, L; Polman, C; Barkhof, F; Montalban, X. Evidence-based guidelines: MAGNIMS consensus guidelines on the use of MRI in multiple sclerosis—establishing disease prognosis and monitoring patients. Nature Reviews Neurology 2015; 11: 597–606.
Weinshenker BG, Bass B, Rice GP, Noseworthy J, Carriere W, Baskerville J*, et al.* The natural history of multiple sclerosis: a geographically based study. I. Clinical course and disability. Brain : a journal of neurology 1989; 112 (Pt 1): 133-46.
Weinshenker BG, O'Brien PC, Petterson TM, Noseworthy JH, Lucchinetti CF, Dodick DW*, et al.* A randomized trial of plasma exchange in acute central nervous system inflammatory demyelinating disease. Annals of neurology 1999; 46(6): 878-86.
Weinshenker BG, Rice GP, Noseworthy JH, Carriere W, Baskerville J, Ebers GC. The natural history of multiple sclerosis: a geographically based study. 4. Applications to planning and interpretation of clinical therapeutic trials. Brain : a journal of neurology 1991; 114 (Pt 2): 1057-67.
Wentling M, Lopez-Gomez C, Park HJ, Amatruda M, Ntranos A, Aramini J*, et al.* A metabolic perspective on CSF-mediated neurodegeneration in multiple sclerosis. Brain : a journal of neurology 2019.
Wilkins A, Majed H, Layfield R, Compston A, Chandran S. Oligodendrocytes promote neuronal survival and axonal length by distinct intracellular mechanisms: a novel role for oligodendrocyte-derived glial cell line-derived neurotrophic factor. The Journal of neuroscience : the official journal of the Society for Neuroscience 2003; 23(12): 4967-74.
Willis MD, Harding KE, Pickersgill TP, Wardle M, Pearson OR, Scolding NJ*, et al.* Alemtuzumab for multiple sclerosis: Long term follow-up in a multi-centre cohort. Multiple sclerosis (Houndmills, Basingstoke, England) 2016; 22(9): 1215-23.
Witt A, Brady ST. Unwrapping new layers of complexity in axon/glial relationships. Glia 2000; 29(2): 112-7.
Wolswijk G. Chronic stage multiple sclerosis lesions contain a relatively quiescent population of oligodendrocyte precursor cells. The Journal of neuroscience : the official journal of the Society for Neuroscience 1998; 18(2): 601-9.
Wortsman J, Matsuoka LY, Chen TC, Lu Z, Holick MF. Decreased bioavailability of vitamin D in obesity. Am J Clin Nutr 2000; 72(3): 690-3.
Wujek JR, Bjartmar C, Richer E, Ransohoff RM, Yu M, Tuohy VK*, et al.* Axon loss in the spinal cord determines permanent neurological disability in an animal model of multiple sclerosis. Journal of neuropathology and experimental neurology 2002; 61(1): 23-32.
Yezzi AJ, Jr., Prince JL. An Eulerian PDE approach for computing tissue thickness. IEEE Trans Med Imaging 2003; 22(10): 1332-9.
Zajicek JP, Wing M, Scolding NJ, Compston DA. Interactions between oligodendrocytes and microglia. A major role for complement and tumour necrosis factor in oligodendrocyte adherence and killing. Brain : a journal of neurology 1992; 115 (Pt 6): 1611-31.
Zhang T, Shirani A, Zhao Y, Karim ME, Gustafson P, Petkau J*, et al.* Beta-interferon exposure and onset of secondary progressive multiple sclerosis. European journal of neurology : the official journal of the European Federation of Neurological Societies 2015; 22(6): 990-1000.

Zivadinov R, Ramasamy DP, Vaneckova M, Gandhi S, Chandra A, Hagemeier J*, et al.* Leptomeningeal contrast enhancement is associated with progression of cortical atrophy in MS: A retrospective, pilot, observational longitudinal study. Multiple sclerosis (Houndmills, Basingstoke, England) 2017; 23(10): 1336-45.
Zuk O, Hechter E, Sunyaev SR, Lander ES. The mystery of missing heritability: Genetic interactions create phantom heritability. Proceedings of the National Academy of Sciences of the United States of America 2012; 109(4): 1193-8.
Zurawski J, Lassmann H, Bakshi R. Use of Magnetic Resonance Imaging to Visualize Leptomeningeal Inflammation in Patients With Multiple Sclerosis: A Review. JAMA neurology 2017; 74(1): 100-9.